Ollscoil Chathair Bhaile Átha Cliath
Dublin City University

Unlocking the Stability of Multi-Component Pharmaceutical Forms

Robert Fox MCHEM

Thesis submitted for the award of PhD

Prof. Andrew Kellett and Prof. Damien Thompson (University of Limerick)

Faculty of Science and Health

School of Chemical Sciences

Dublin City University

Ireland

April 2025

Declaration

I hereby certify that this material, which I now submit for assessment on the programme of study leading to the award of Doctor of Philosophy is entirely my own work, and that I have exercised reasonable care to ensure that the work is original, and does not to the best of my knowledge breach any law of copyright, and has not been taken from the work of others save and to the extent that such work has been cited and acknowledged within the text of my work

Signed Robert Fox Student ID 19214434 Date 22nd April 2025

Acknowledgements

I would like to express my sincere gratitude to all those who contributed to and supported me throughout this journey. I extend my deepest thanks to Professor Andrew Kellett and Professor Damien Thompson for warmly welcoming me into their research groups and providing invaluable guidance.

I am also grateful to the Kellett group for their kindness and willingness to assist me, despite the shift in research focus from their usual work. A special thank you to Dr Reabetswe Zwane who offered me a warm welcome at the start of my PhD journey.

Finally, I'd could have not written this thesis without my family who supported me throughout this entire project and supported me through COVID.

Scientific outputs

Peer reviewed publications

- E. Kiely, R. Zwane, R. Fox, A. M. Reilly, S. Guerin, CrystEngComm, 2021, **23**, 5697-5710
- A. Gibney, R. E. F. de Paiva, V. Singh, R. Fox, D. Thompson, J. Hennessy, C. Slator, C. J. McKenzie, P. Johansson, V. McKee, F. Westerlund, and A. Kellett, Angewandte Chemie, 2023, **135**, e202305759
- R. Fox, J. Klug, D. Thomson, A. Reilly, Journal of Computational Chemistry, 2024, **45**, 2465-2475

Presentations

- Shannon Region Postgraduate Research Conference, Virtual, May 2021 Benchmarking multicomponent solid forms.
- DCU Chemistry Research Symposium, Virtual, June 2021 'Benchmarking multicomponent solid forms'.

Posters

- DCU Chemistry Research Day Poster April 2022, DCU 'Benchmarking Multicomponent solid forms'.
- Institute of Chemistry of Ireland Chemistry Colloquium June 2022, UCD 'Stability of Co-crystals a Density Functional Theory study'.
- 33rd European Crystallographic Meeting August 2022 Versailles 'Stability of Co-crystals: Density Functional Theory study'.

Contents

Abbreviations

AMN	Artificial metallonuclease
API	Active pharmaceutical ingredient
ATM	Axilrod-Teller-Muto
B3LYP	Becke 3-parameter Lee-Yang-Parr
B.E.	Binding energy
B.J.	Becke-Johnson dampening
BLYP	Becke-Lee-Yang-Parr
BSIE	Basis set incompleteness error
BSSE	Basis set superposition error
CASTEP	Cambridge Serial Total Energy Package
CCDC	Cambridge crystal data centre
CD	Circular dichroism
CP	Counterpoise correction
CPCM	Conductor-like polarizable continuum model
CSD	Crystal structure database
CSP	Crystal structure prediction
ctDNA	Calf thymus DNA
CuAAC	Cu(I)-catalysed azide-alkyne cycloaddition
DDD	Dickerson-Drew Dodecamer
DFT	Density functional theory
DFTB	Density functional tight binding
DFTB-D	Dispersion corrected density functional tight binding
DFT-D	Dispersion corrected density functional theory.
EMSA	Electrophoretic mobility shift assays
ESI-MS	electrospray ionization mass spectroscopy
EtBr	Ethidium bromide
FDA	Food and drug administration’s
gCP	Geometry counterpoise correction
GGA	Generalised gradient approximation
HOMO	Highest occupied molecular orbital
K_{app}	Apparent binding constant
K_b	Binding constant
LCAO	Linear combination of atomic orbitals
LDA	Local density approximation
LUMO	Lowest unoccupied molecular orbital
MAE	Mean absolute error
MAPE	Mean absolute percentage error
MBD	Many-bodied dispersion
MD	Molecular dynamics
MG	Methyl green
MST	Microscale thermophoresis
OLYP	Optimised-Lee-Yang-Parr
PAW	Projector augmented wave
PBE	Purdew-Burke- Ernzerhof
RESP	Restrained Electrostatic Potential

RMS	Root mean squared
RMSD	Root mean squared deviation
ROS	Reactive oxygen species
SCF	Self-consistent field
SOD	Super oxide dismutase
SPAAC	strain-promoted azide-alkyne cycloaddition
SSB	Single strand break
T_g	Glass transition temperature
T_m	Thermal melting point
TS	Tkatchenko-Scheffler
TZVP	Triple zeta valence potential
def2-TZVP	Second default triple zeta valence potential
vdW	van der Waals

Equations

Figures

Tables

Unlocking the Stability of Multi-Component Pharmaceutical Forms

Robert Fox

Abstract

The field of computational chemistry is constantly developing new predictive methods to guide experiments. Co-crystals are a promising development for improving the properties of active molecules, which is an exciting prospect specifically for the pharmaceutical field in formulating active pharmaceutical ingredients (API). To minimise computational cost, quantum mechanical models based on density functional theory (DFT) can be supported where appropriate with faster semi-empirical density functional tight binding (DFTB). These types of models can be used to predict the enthalpy of formation of the co-crystal structures. My results show that the full DFT methodologies predict the enthalpy of formation well for a broad range of co-crystals, with the DFTB methods giving high-throughput predictions for simple co-crystals but failing for larger, more complex APIs.

Another area of intensive research in multi-component pharmaceutical forms is the development of anti-cancer artificial metallonucleases (AMNs) that can be used to recognise and damage nucleic acids. This is aided by the metal centre which promotes oxidative processes chiefly responsible for cleavage activity. Thus, ensuring coordination of the metals in their parent AMN scaffolds is imperative for them to function correctly. Click chemistry is a recently discovered modular process to produce various AMNs with differing terminal groups. The goal here is to produce various polynuclear AMN structures, as these have previously been found to have a greater activity than mononuclear congeners, resulting in greater DNA damaging effects. This thesis aims to predict metal ion binding properties based on a wide range of scaffolds. The pendant groups can influence the strength of the metal to scaffold binding. DFT calculations are used to predict the effect of a broad range of molecular groups in place of the hetero-aromatic donors and explore how this can improve the metal binding in molecular scaffolds.

Chapter 1 Introduction

1.1 An Introduction to molecular solids

Molecular solids are uncharged structures with a broad array of properties, allowing them to be used in many fields, such as applications in pharmaceuticals, inks and insecticides.[1–3] Generally, they have a low melting point, are soluble in water or organic solvents, and are soft and easily mailable.[4] One prominent use of molecular solids is within the pharmaceutical sector, and a few examples of these include *Ritonavir®,* used for the treatment of HIV,[5] *Tegretol®,*[6] used for the treatment of bipolar disorder and epilepsy,[6] along with more household medications such as *paracetamol*[7] and *aspirin.*[6] Their widespread use demonstrates an ability to have predictable and controllable material properties such as solubility, dissolution rate, morphology, and tabletting characteristics.[8] These properties can be influenced through the intermolecular interactions, and solid forms can be chosen or engineered depending on the applications for which they are used.[9]

The solid form packing is how the molecules are organised within the solid. The crystal packing plays a factor in the properties of the solid form as different intermolecular interaction mapping will influence the physical properties.[5] The supramolecular packing in the crystal is governed by non-covalent interactions. These could be van der Waals interactions, dipole-dipole interactions or hydrogen bonds.[10]

Molecular solids may be packed in either an amorphous or crystalline manner.[11] These packing arrangements are defined through the repeating arrangement of the molecules within the solid form, known as the long-range order or periodicity.[10] Crystalline materials show high long-range order,[12,13] whereas amorphous materials do not. Amorphous materials may exhibit structural order locally, however not enough to have crystalline properties.[14,15] One example of how these material properties differ is the melting point, with amorphous materials having a broad glass transition temperature, T_g, where the material melting will spread through a broad temperature range. In contrast, a crystalline material has a sharp melting point.[11]

Within the crystalline form, these large repeating units are broken down into smaller sections called the unit cell, which, when pieced together, can fill the solid's entire space, leaving no gaps.[11] These unit cells can be broken down into 14 distinct

classes of Bravais lattice.[11,16] The method with which the material is crystalised alters the crystalline size and shape by directing the crystallisation pathway.[16] This is particularly important when there are multiple ways the molecules can be arranged within the unit cell, recognised as polymorphism. This phenomenon is critical due to the role of the crystal structure on the physical properties of the material, as it could alter these properties, reducing the efficacy of the resulting product with the potential to reduce the bioavailability and reactivity of the crystal structure along with other physical properties, solubility, stability, dissolution rate, bioavailability, and tabletability.[10,17] The bioavailability is the rate that the body can absorb a drug substance,[18] while tabletability represents the ability of a powdered material to be transformed into a tablet of a specific strength under the effect of compaction pressure.[19]

Amorphous materials, as previously stated, do not have long-range order.[11] These materials may have crystal structures which have the potential to form despite not being energetically favourable due to these crystal structures not resulting in a significant energetic saving.[11] Amorphous packing arrangements results from molecules with poor packing abilities, or molecules possessing many internal degrees of freedom which reduce their ability to pack in a crystalline manner.[15] Along with these molecular features, these systems can also be produced by drying hydrate crystals. Here, the amorphous materials may form through water inclusions, and where water is removed from a hydrate structure, holes which form around the water molecule are left.[20] Due to the amorphous packing being higher energy, this allows for the material to have a higher solubility.[3] Amorphous materials are also known to flow and deform through plastic deformation. The ability to flow and deform allows amorphous materials to have better tabletting abilities.[3] Conformational flexibility is the ease at which the molecule can rotate into different orientations. When a molecule has a high level of conformational flexibility, it becomes easier to form amorphous solid forms as it is easier to produce different molecular orientations so that it is harder to crystallise.[15] Below the T_g, the material may have a brittle state, and above this, the material will be in a rubbery state due to the molecular mobility being increased as the glass temperature is reached.[12]

Materials may be also classified as semi-crystalline, whereby structures show repetition within one or two dimensions within the unit cell with repetition not shown

in all three dimensions.[11] Some polymers show long-range order in two dimensions, and most fibrous materials demonstrate long-range order in one dimension along the fibrous axis.[11] This is due to the long chains' inability to move close enough to form these periodic arrangements; examples of such semi-crystalline materials include poly(lactic acid) and polyethene glycol.[11]

1.2 Intermolecular interactions

Crystalline structures form due to strong intermolecular interactions, such as hydrogen bonding, dipole–dipole and van der Waals interactions. Through the rational modulation of these interactions, these intermolecular forces can be used to develop the properties of the solid form so that it may have, for example, a higher solubility or more mechanically stable structure.[21] Crystalline materials are used in many fields due to their controllable and predictable nature, with uses in adhesives,[22] pharmaceuticals,[20] agriculture[23] and dyes.[1] These structures have a long shelf life due to the highly stable nature of the crystalline.

Intermolecular interactions depend on electronegativity.[10] Electronegativity is the ability of an element or species to attract electrons towards itself. The highly electronegative atoms can form partial charges, which are the basis of intermolecular interactions. Hydrogen bonds form strong intermolecular interactions between two dipoles due to the high electronegativity.[24] Highly electronegative atoms which are used to form hydrogen bonds are oxygen, nitrogen and fluorine commonly used within functional groups such as aldehydes, ketones, amines and amides.[24] These are complimented by electropositive atoms which have a tendency to donate electrons and form cations which form hydrogen bonds with the more electronegative atoms due to the charge difference examples of highly electropositive elements are the alkali metals with the heaviest being cesium.[25] Thus, hydrogen bonding can be broken down into 'structural units within a molecule that can be assembled using known synthetic operations',[26] which can be either hydrogen bond donor/acceptor regions. These regions have a high or low electron density. Functional groups containing both, such as amines and carboxylic acid, can be homosynthons, which allow for self-association with the formation of hydrogen bonds between two identical functional groups.[27]

Van der Waals interactions are the weakest intermolecular interactions formed through the induction of partial charges due to the polarisability of atoms within the molecule.[28] Polarisability is defined through the ease with which the electron distribution is distorted; the polarisability increases with a greater quantity of electrons and larger molecules due to the electrons being less localised due to the nucleus not holding the electron density as firmly.[4] These interactions can be attractive or repulsive forces, thus influencing the packing of the material.

The differences in strength between the hydrogen bonds and van der Waals interactions makes hydrogen bonds the primary director of crystal packing, with hydrogen bonding having the strongest interactions with a typical binding strength of 20 kJ mol^{-1}, while van der Waals interactions occur with a typical binding strength of 2 kJ mol^{-1}.[29] For comparison, ionic bonds that form between charged species are stronger than covalent bonds, with typical strength of ~250 kJ mol^{-1}.[29]

There are crystalline-packed systems with more than one distinct species known as multi-component solid forms.[30] These multi-component crystal structures are used in many fields, such as fertilisers,[23] pigments[1] and medicines.[31] The versatility of these multi-component solid forms is due to the ability to improve the properties of the parent molecule. The multi-component solid forms can be divided into three subclasses: solvates, hydrates and co-crystals.[30] These co-crystal structures show development in the improvement of the physical properties of the active molecule however are believed to have a higher propensity of polymorphism.[32]

As previously mentioned, the packing of solid forms is vital for the properties of solid forms. The intermolecular interactions may form in multiple ways, meaning that different packing arrangements produce stable crystal structures, known as polymorphism. These packing arrangements may have different physical properties, affecting the crystal structure's final use.[33] Abbott Laboratories initially released the drug *Ritonavir*® in 1996.[5] A second polymorph was crystallised in 1998 with a lower lattice energy polymorph than the marketed form meaning this was a more stable crystal structure as a result of the hydrogen bond formation whereas the form I uses a β-sheet structure.[34] This second polymorph had a significantly lower solubility reported to be <50% compared to the initial marketed form.[5] Identification of this new polymorph halted the production of the drug, which was expensive and time-

consuming with an estimated loss of $250 million after its reintroduction in 1999.[34] The initial form was unable to be isolated as a result of the seeding of the second form.[6]

The subclass of co-crystals contains two or more uncharged molecules that are solid at ambient conditions; these molecules comprise the co-crystal and are known as the co-formers.[30] Co-crystals are used in various areas depending on how the active ingredient. Solvates and hydrates are multicomponent crystals where one co-former is not solid under ambient conditions, and within the hydrate form, water is incorporated into the crystal structure. These solvates and hydrates form hydrogen bonds within the crystal structure. Co-formers with a low molecular weight tend to form these solvates and hydrates readily due to the small molecular weight allowing for the incorporation of the solvent within the crystal structure.[7]

Molecules can also display chirality, where the molecules are the same within 2D space; however, they are nonsuperimposable as they are mirror images of themselves; separately, these are known as enantiomers. Chirality is important within the pharmaceutical chemistry due to the one enantiomer potentially having little to no physiological effects.[35] Another side effect maybe undesired or toxic effect within the body as the racemate maybe metabolised differently.[35] A historical example taken from 1950s is that of thalidomide, a molecule initially intended as a morning sickness treatment and a sedative.[36] However, it was later removed from the market when it was found that one enantiomer is a teratogen causing severe congenital disabilities. The drug has since been repurposed where one of the enantiomers is now used to treat leprosy.[36] It is now essential to identify all enantiomers that are produced and characterise their biological activity.

1.3 Properties of solid forms

Solid forms have important influences on physical properties, including stability and solubility. The physical properties are highly dependent upon the packing of the solid form.

The stability of the solid forms is dependent upon how it is packed. The packing of polymorphs can be thermodynamically unfavourable compared to other packing arrangements.[37] Thermodynamically unfavourable packing means the crystal

structure can convert to the more thermodynamically favourable packing arrangement. The potential for thermodynamically unfavourable packing means that if all crystal forms are not identified, there may be unexpected crystal structures which have unseen physical properties. As was shown in the drug *Ritonavir*® where the initially crystallised form produced by Abbott laboratory received a patent. However, when form-II was crystallised, this was found to be a more stable form with the originally patented form was unable to be formed. With ongoing work still discovering yet more polymorphs of this drug being found with a third anhydrous *Ritonavir*® polymorph being reported in 2022 as confirmed through thermal methods.[38] These structures had drastically different solubility and bioavailability. Other examples include *Rotigotine*®*,* this is the active ingredient in *Neupro*®*,* that is used in the treatment of Parkinson's disease. However, in 2008 identified a second polymorph was identified with a solubility 8 times lower than the initially marketed form. Later, crystal structure prediction work identified a third polymorph with a lower relative stability than the initially marketed form.[39]

The conformational changes within the molecule can cause alterations in the intermolecular forces, which result in dislocations; these are linear defects that result in long-range weaknesses in the crystal structure.[40,41] The dislocations can potentially cause crystallisation to occur with different conformational isomers, referred to as conformational polymorphism.[33] The differing conformational isomers will have different stabilities due to the different intramolecular forces acting upon the molecule; one prominent example is cyclohexane, which typically crystallises in the 'chair' form to minimise the ring strain.[33]

The solid form also governs the solubility of the final product. The solubility varies depending upon the polymorph produced. The change in the solubility will differ due to changes to the intermolecular interactions that must be broken to separate the material into discrete molecules to dissolve the material.[42] The use of different solvents can adjust the polymorph produced.[43] Within the pharmaceutical sector, solubility is important with a large proportion of potential drug products failing clinical trials as a result of the poor aqueous solubility.[44]

1.4 Co-crystals

Since multicomponent solid forms comprise one or more materials under ambient conditions (either solid or liquid), it is due to this classification that hydrates and solvates lie in the multicomponent crystal classification. These are two common examples of multi-component solid forms that are typically formed with smaller molecules.[27] These hydrates and solvates contain active ingredients and co-formers, which may be water or other solvents called pseudo-polymorphic forms. [27,45] Some hydrates can form quickly, such as with the molecule carbamazepine, which converts from the anhydrous crystalline form to the dihydrate crystalline form within one hour of being suspended in water. [46]

In contrast to form co-crystals, all components must be solids under ambient conditions. From a structural perspective, co-crystal design is highly focused on hydrogen bonding, so they rely on functional groups such as carboxylic acid and amine as hydrogen-bonding synthons. [9] The multiple molecules that make up a co-crystal aid the thermodynamic stability of the co-crystal through intermolecular interactions. The added stability will alter and adapt the physicochemical and pharmacokinetic properties such as the dissolution rate, [47] density and melting point. [16] These co-crystals have often shown to have an apparent improvement in solubility from the single molecule forms. In some cases, the solubility is up to 1000 times more soluble than the single molecule, as reported with danazol-4-hydroxybenzoic acid and danazol-vanillin co-crystal. [48] This is especially important as 40% of approved drug substances and 90% of developmental drugs have poor solubility.[49] One example of a phenomenon that pharmacokinetics can exhibit is referred to as 'springs and parachutes'; [50] this is where the 'springs' are a higher energy drug form to take the drug solubility past its solubility limit where no further drug substance can be dissolved. Then, agents such as surfactants are used to maintain the high concentration.[50] Co-crystals can be used for various applications, from use in pharmaceuticals improving the solubility and bioavailability of the active pharmaceutical ingredient (API),[6] to use in semiconductors used to tune the band gap.[51]

There are a few co-crystal pharmaceuticals, such as the marketed drug *Suglat®,* which is a co-crystal of *ipragliflozin* and *L-proline* that is used as a treatment for type

2 diabetes; this co-crystallisation prevents the formation of the hydrate form of the *ipragliflozin* which can form during storage and reduce the solubility of the *ipragliflozin*.[52] These co-crystals have also been shown to be more photostable with a variety of drug products being brought to market, such as progesterone co-crystallised with *Phloroglucinol*[53] and vitamin D3 co-crystallised with vitamin D2,[54] resulting in a stable crystal structure not easily degraded during storage by exposure to light. Co-crystallisation can also improve bioavailability whereby the active pharmaceutical ingredient is absorbed by the body at an improved rate. An elegant example of this effect was demonstrated by the co-crystallisation of baicalein with caffeine where a four-fold improvement in the bioavailability of baicalein compared to the single component crystal form was achieved.[55]

Co-crystals can affect the conduction ability of a crystal structure this is achieved by changes to the band gap this is the difference between valence band and conduction band. The valence band is the build-up of occupied orbitals when sufficient energy is provided an electron can move up to the higher energy conduction band, this conduction band is the build-up of unoccupied orbitals allowing for the movement of charge through a material.[51] This band gap defines the conductivity of a material; this means that if there is a substantial gap, this material is an insulator, and if this gap is low enough, the material can be considered a conductor. In contrast, semiconductors are structures which the electrons can move into the conduction band from the valence band but a higher energy requirement is needed. A band gap between 1-5 eV is considered a semiconductor as if a sufficient electric field is imparted, the electron may move up to the conduction band.[56] With the use of co-formers it can be possible to create a reduced band gap.[51] Co-crystals can also be used to produce piezoelectric and ferroelectric compounds.[57,58] Piezoelectric compounds produce an electric current when stress is applied,[57] and ferroelectrics produce spontaneous electric currents above a specific temperature, referred to as the Curie temperature.[58] The Curie temperature can be raised through co-crystallisation – for example an elevated Curie temperature of 68˚C was reported for a co-crystal of acenaphthene and 2,3,5,6-tetrafluoro-7,7,8,8-tetracyanoquinodimethane.[58]

1.5 Computational work on co-crystal forms

Crystal structure prediction (CSP) can be used to predict the packing of the molecules within the crystal structure to get the lowest energy structures that match with stable and metastable polymorphs.[59] These ultimately become significantly more challenging when predicting structures of multicomponent crystals due to the need to predict the component orientation and the increased number of potential structures that need to be considered.[60]

Blind CSP tests are carried out approximately every 5 years to identify progress within the CSP field, as the latest modelling codes are tasked with predicting the crystal structure just from the molecular structures. In the last three blind tests three multicomponent structures have been incorporated, two co-crystal structures and one salt structure,[61–63] with the current blind test incorporating a further co-crystal structure with two different stoichiometries along with an organic, multi-component salt system. In the sixth blind test, the co-crystal studied was a multi component system of 3,5-dinitrobenzoic acid and 2,8-dimethyl-6*H*,12*H*-5,11-methanodibenzo[*b,f*][1,5]diazocine, and showed similar structural comparison result to the previous blind tests where the difference between the experimental structure and the predicted structures measured using root mean squared deviation (RMSD) ranged from 0.124 Å to 0.464 Å.[62] In the fourth blind test, the RMSD ranged from 0.075 Å to 0.536 Å.[64]

There have been attempts to model co-crystal stability using the lattice enthalpies to predict how stable these structures are. One density functional theory model predicted that most co-crystals would be thermodynamically stable, predicting 95% of co-crystals to be a thermodynamically favourable process.[65] However, this model only used a single basis set (see **section 3.3** below). a larger range of basis sets may predict the formation of co-crystal structures more accurately and correctly identify all observed crystal structures as physically plausible. When studying co-crystals, it is important to consider dispersive forces and the role that these play in co-crystal stability.[66] Free-energy calculations including entropic temperature effects may help identify co-crystal structures that potentially show kinetic stability as opposed to thermodynamic stability. Along with this, there have been attempts to

produce neural networks that inform the formation of co-crystals; one method reported ≥97% accuracy[67].

All these methods will struggle with a broader co-crystal set due to the primary focus within the crystal engineering field being biased towards hydrogen bonding. Models are generally based on, or trained, using structures available in the CCDC; however, these will undergo the same biases that purely experimental trial and error and/or "pen and paper" design approach entails in that these experimental structures will be more hydrogen bonding focused with the training set not having the co-crystal structures that failed to be produced. Hence, these models based purely on known structures will not have the diversity of the knowledge that is necessary to produce a machine learning to predict the formation of co-crystals accurately purely from scratch, purely from just libraries of single molecules.[67]

Chapter 2 Research Objectives

A primary goal of this work is to predict co-crystals stability using computational models with equations that underpin the calculation of the dispersive forces and further computational models presented within this thesis described in **Chapter 3**.

Presented in **Chapter 4** is the foundational work which assesses the ability of the current computational models to predict the enthalpy of the formation of co-crystal structures. The large computational dataset expands significantly on previous work that only incorporated a single exchange functional and dispersion correction combination.[65] The work presented here incorporates three exchange functional and dispersion correction combinations, one uncorrected method and three high throughput computational methods. The survey of multiple methods establishes the robustness of the computational method and informs model choices for future studies, highlighting the importance of including dispersion effects, relative insensitivity of results to functional, and prudent choice of fast semi-empirical methods for simple crystals but a necessity for full density functional theory (DFT) models for more complex systems.

Within **Chapter 5**, the strength of short-range metal–ligand interactions were established within metal complexes, initially utilising simple model complexes building up to larger artificial metallonucleases (AMNs) with multiple copper centres. The metal–ligand interactions play an essential role in the geometry of these complexes through the influence of the ligand field between the metal ion and the terminal thiophene donor. The strength with which the metal ion is bound to the organic ligand plays a vital role in stability prediction to avoid loss of the metal centre which is vital for the DNA damage. The non-covalent binding of these molecules to the DNA structure was then predicted using classical models, which were validated using biophysical analytical methods, with the aim to determine the site specificity of binding influences the potential DNA damaging ability of the molecules.

Chapter 6 builds on the methodology developed in **Chapter 5** with the more further copper AMN structures. This work expands the range of terminal donor groups within the AMN structure to assess the influence of the specific metal ion donors on the binding affinity between the ligand and the copper ion. This aims to identify key structural features which promote copper binding to the organic scaffold and enhance the drug-DNA interactions. To test the AMN potential, the models identify

the region with which the AMN binds to the DNA using molecular dynamics methodology, which is validated using biophysical methods to probe the mechanism through which the series of AMNs damage DNA.

Chapter 3 Computational Methodology

Parts of this chapter have been published within the journal Crystal Engineering Communication

E. Kiely, R. Zwane, R. Fox, A. M. Reilly, S. Guerin, CrystEngComm, 2021, **23**, 5697-5710

3.1 Schrödinger equation

The solution of the time-independent Schrödinger equation (**Equation 3-1**) is the lowest energy structure of a system, but it becomes a Many Body Problem that is impossible to solve analytically for systems more complex than a single-electron system, for example, hydrogenic atom H_2^+. However, iterative solutions become possible following several approximations, including the Born-Oppenheimer approximation and Hartree approximation, along with the anti-symmetry principle.[68]

The Born-Oppenheimer approximation separates the electronic and nuclear motion. Due to the nucleus being significantly heavier than the electrons, the nucleus can be viewed as stationary. This approximation calculates the total energy for a fixed set of atomic positions by separating electronic and nuclear wavefunctions.[69]

$$\hat{\mathrm{H}}\Psi(r_N) = E\Psi(r_N)$$

Equation 3-1 Time independent Schrödinger equation

The functionals connect the total energy, E, for a molecule or solid to the electron density. In an N electron system, the wavefunction, Ψ, has $3N$ coordinates; these are in the -x, $-y$ and $-z$ axis.

Subsequently, the Hartree approximation assumes that the electrons are not interacting and that the wave function of multiple electrons is a product of the wave function of one electron.[70] The electrons are assumed to have a smooth distribution of negative charge density, $\rho(r')$. So, the potential energy of an electron in the field would be referred to as within **Equation 3-2**[68] with r and r' is the two electron position.

$$V_{elec}(r) = -e\int dr'\rho(r')\frac{1}{|r-r'|}$$

Equation 3-2 Potential energy of an electron in a field

Finally, the anti-symmetry principle states that a multi-electron must be antisymmetric with respect to the interchange of the coordinate x (both space and spin) of any two electrons so no two electrons may not occupy the same spin orbital.[71]

3.1.1 Hartree-Fock

The Hartree-Fock method is a way to calculate the ground state energy of a structure with complex wave functions.[72] These electrons are described within a matrix where the total electron wavefunction is derived from **Equation 3-3** through the anti-symmetrised product.[73] Within this matrix each electron is indistinguishable.[73] Here each component within the matrix is a single particle spin orbital where each component is a function of the electron spatial orbital, $\psi_i^{\sigma}(r_j)$, and the spin variable, $\alpha_i(\sigma_j)$.[74] This determinant is later normalised for the number of electrons within the matrix, **Equation 3-3**. Within this method, the average electronic repulsion between the electrons is found leading to it being, somewhat neglected.[75] Thus, the electrons are assumed to be non-interacting.[74] The determinant of this matrix gets the one-electron wave function, which allows for energy minimisation of the system.[76] The orbitals used are 'guessed' through an iterative process using this method; the 'guessed' orbital is used to find the next until these orbital energy levels until these orbital energy levels change by less than a predetermined threshold.[73]

$$\Phi = \frac{1}{(N!)^{\frac{1}{2}}} \begin{vmatrix} \phi_1(r_1,\sigma_1) & \phi_1(r_2,\sigma_2) & \phi_1(r_3,\sigma_3) & \cdots & \phi_1(r_N,\sigma_N) \\ \phi_2(r_1,\sigma_1) & \phi_2(r_2,\sigma_2) & \phi_2(r_3,\sigma_3) & \cdots & \phi_2(r_N,\sigma_N) \\ \phi_3(r_1,\sigma_1) & \phi_3(r_2,\sigma_2) & \phi_3(r_3,\sigma_3) & \cdots & \phi_2(r_N,\sigma_N) \\ \vdots & \vdots & \vdots & \ddots & \\ \phi_N(r_1,\sigma_1) & \phi_N(r_2,\sigma_2) & \phi_N(r_3,\sigma_3) & & \phi_N(r_N,\sigma_N) \end{vmatrix}$$

Equation 3-3 Matrix used to calculate Slater determinant

3.2 Density Functional Theory

While the Hartree-Fock method utilises the electrons wave functions to allow for the energy minimisation calculations, this still limits the size of possible systems that can be ran due to the scale of the calculations required. However, in 1964, the Hohenberg and Kohn theorems were published.[77] This theorem states that the electron density determines the ground state electrical energy.[77] Density functional theory views the electron cloud as a function of the density as opposed to previous methods, which utilise the wavefunctions, though this method narrows the

calculation into a one-body density for the entire system.[78] The total energy calculation can be broken down into **Equation 3-4**,[79] where the kinetic energy is expressed in E_K, the electron-nucleus potential is expressed in E_{eN}, the electron-electron potential is expressed, as E_{ee}, finally the spin-effects are taken into account using the exchange-correlation functional, $E_{XC}[\rho]$.

$$E[\rho] = E_K + E_{eN} + E_{ee} + E_{XC}[\rho]$$

Equation 3-4 Equation for calculation of the total energy

The density is constructed using orbitals, calculated with the Kohn-Sham equations,[79] which contain the exchange-correlation functional. These equations are solved iteratively. The exchange-correlation functional can take multiple forms, ranging from local density approximations (the first developed in 1965)[77] to generalised gradient approximations and hybrid functionals. These have undergone multiple developments, allowing for increased computational power and more physically realistic calculations.

3.2.1 Local density approximations

The local density approximation (LDA) approach to modelling the electron density assumes that the electron density is spatially uniform with equal exchange-correlation energy within the electron gas; this is expected to be a good approximation with a slow variation in the electron density.[78]

This model tends to perform well with covalent, metallic and ionic bonds, with the predicted energies being similar to the experimental values with a tendency to predict over-binding, however, LDA's do not accurately predict long-range forces such as hydrogen bonding and van der Waals interactions as a result of density fluctuations not being properly accounted for within this approximation.[80]

3.2.2 Generalised gradient approximations

The generalised gradient approximation (GGA) method of modelling the electron density expands on the LDA by clarifying that the electron density will not be homogeneous and will have a gradient. This assumption has shown improvements in the total energies, atomization energies, energy barriers and structural energy

differences.[81] Illustrated as the LDA functional has a mean absolute deviation of 20 kJ/mol, whereas the GGA functionals have been shown to have a mean absolute deviation of 10 kJ/mol.[82] Expanding on this meta-GGA's further incorporate kinetic energy along with the electron density and density gradient,[83] and are reasonably accurate for near-equilibrium and compressed ground-state properties of matter.[83] Despite improvements to the bonding and long-range forces, this method still does not fully describe the long-range forces close to chemical accuracy.

Commonly used GGA exchange-correlation functionals include the functional devised by Perdew-Burke-Ernzerhof (PBE),[81] Becke-Lee-Yang-Parr (BLYP),[84] Lee-Yang-Parr functional incorporating OPTX (OLYP)[85,86] and BP86.[87]

3.2.3 Hybrid functionals

The hybrid functionals improve on the chemical accuracy of both the GGA and meta-GGA functionals through the inclusion of exact exchange terms; these may be through the inclusion of empirical data as in the case with the B3LYP term which is a development of the BLYP exchange-correlation function and includes three parameters fitted by experimental data. An alternative hybrid functional is the PBE0 model, a development on the PBE generalised gradient approximation that mixes 75% of the PBE energy with 25% of the Hartree-Fock energy.[88]

3.3 Geometry counterpoise correction with basis set

Basis set superposition error can occur when a complex's energy is not consistent with the experimental data, often because the van der Waals interactions are predicted to be overbound.[89] The basis set superposition error involves artificially shortening the intermolecular distances, followed by the artificial strengthening of the intermolecular interactions.[9] This means that the bond strength is artificially inflated, this becomes more prominent for smaller basis sets due to the energy of each unit within the associated complex being lowered by the basis set of the monomer unit being less converged than the basis set for the complex unit, this artificially increases the stability of the complex unit.[90] This error is not to be confused with the error produced when the basis set is incomplete, known as "Basis set Incompleteness error" (BSIE).[91] Basis set superposition error (BSSE) can be

corrected using Boys and Bernardi counterpoise correction (CP).[92,93] The uncorrected interaction between monomers would be computed as (for dimers):

$$\Delta E_{int} = E_{AB}^{AB}(AB) - E_{A}^{A}(A) - E_{B}^{B}(B)$$

Equation 3-5 Equation for uncorrected dimer interactions

Where the basis used is denoted by the superscript, and the subscript denotes the geometry. There is an approximation for the calculations that the geometries do not change as the monomers approach. However, these CP corrections have not been applied to transition states despite presumably the transition state still undergoing these BSSE. The correction is not applied because the CP correction was initially intended for molecules in fixed geometries and was intended as a single-point correction.[90] These CP-corrected surfaces significantly improved the geometry-optimised transition state for smaller basis sets, producing comparable results to the larger ones.[90]

3.4 Plane-wave DFT

Plane-wave DFT is a commonplace method for calculations with solid-state applications, with crystal structures being an ideal candidate for these applications due to the periodic boundary resulting from the unit cell.[94] Plane-wave DFT utilises the Kohn-Sham equations; these can be divided into valance and core electrons. These core electrons are viewed as frozen due to the strength of the attractive force applied by the nucleus, these electrons only impart 2% of the structural energy so these calculations can be simplified to reduce the computational resources required for these calculations.[95] These core electrons are not involved in bonding whereas the valence electrons are modelled using pseudopotentials, these are simplified descriptions of electronic nuclear interactions, this reduces the computational cost while maintaining accuracy.[96] These valence electrons can be modelled in two different ways using pseudopotentials these being ultra-soft [97] and norm-conserving pseudopotentials.[98] These allow for lower-cost calculations as the core electrons are pre-calculated, while preserving the accuracy of the calculations.[99]

Pseudopotentials are used to model the valence electron wavefunction. The goal of these is to create pseudopotentials which are both smooth and accurate. When applying a ultrasoft pseudo potential this aims to maximise the smoothness this

minimises the Fourier space used to describe the valence properties of the wavefunction this increase in smoothness allows for fewer planewaves which are necessary.[97] Whereas the norm-conserving pseudo potentials achieve a higher accuracy by sacrificing the smoothness of the pseudopotential.[100] When using the hybrid exchange functionals ultrasoft pseudo potentials are unable to be implemented due to mismatched accuracy between the ultrasoft pseudopotential and the hybrid exchange correlation energies.[101]

These plane-wave DFT calculations utilise Bloch's theorem to allow for energetic calculation of crystalline structure. Bloch's theorem states that when nuclei are arranged in a periodic manner, the resulting potential must also be periodic, leading to a periodic electron density. As a result, the magnitude of the wavefunction should be periodic with the phase being unknown making it quasi-periodic.[102] This theorem enables the study of electronic behaviour in reciprocal space, where these periodic structures. The magnitude and phase of the wave function is measured within reciprocal space with the spacing of these measurements denoted using k-point sampling.[72] Through the use of specific symmetry elements these calculations can be simplified as this reduces the number; these can further simplify the calculations.[103]

These methods might not be implemented correctly, so projector augmented waves (PAW) pseudopotentials are implemented for heavier atoms. These transform the wave function and reconstruct the all-electron orbitals from the pseudo orbitals.[104]

3.5 Density Functional Tight binding

Due to the computational expense of DFT models, calculating energies for large, chemically complex structures quickly become unfeasible. To bridge the gap between semi-empirical models and density functional theory (DFT) models a tight binding form of the Kohn-Sham operator can be implemented which offers a lower memory DFT method.[105] The Density Functional Tight Binding (DFTB) model allows for the energetic calculation of larger crystal structures and the modelling of quantum mechanical and molecular mechanical methods to be applied over longer time scales. DFTB treats valence electrons using a linear combination of atomic orbital (LCAO).[105–107] Additionally, these LCAO's treat the electrons with a minimal

atomic basis set with a two-centre approximation of the Hamiltonian operator represented in a LCAO basis and overlap matrix elements for each atomic pair.[108]

The most recent model, DFTB3+ is formed by expanding the energy functional in a Taylor series up to the third order.[105] This expansion is centred around the density fluctuations, calculated through density fluctuations taken through the reference density and how the density fluctuations alter the reference density.[105,109]

These methods can be parameterised to describe various bonding elements better, including Becke-Johnson, the Boese and the H5 parameterisation. The dampening parameters determine the proportion of dispersion correction included in the total energy at a short range.[110]

The Boese parameterisation method prioritises the unit cell geometry by minimising the cell volume's mean absolute error (MAE) over the default Becke-Johnson parameterisation. This reported improvements when using the Boese parameterisation when testing against the X23 benchmark set. This test set incorporates 23 experimentally generated organic single component crystal structures which were either bound with a broad range of binding mode ranging from mostly van der Waals bonded systems, such as Adamantane and Anthracene crystal structure, to mostly Hydrogen bonded systems, such as Oxalic acid and Acetic acid.[111,112] Initially the experimental lattice energy was compared against DFT generated lattice energy these showed comparable energies between the experimental and computational energetics. Later testing the experimental structures against structures generated through the implementation of DFTB with the Becke-Johnson parameterisation indicating a MAE of 48.0 $Å^3$, whereas the Boese parameterisation indicated a closer similarity to the experimentally generated geometries with a MAE of 24.5 $Å^3$.[108] However, when looking at the lattice energies the Becke-Johnson has closer resemblance to the experimental values with a MAE of 12.8 kJ/mol whereas when implementing the Boese parameterisation this indicated a MAE of 33.4 kJ/mol.[108]

The H5 method aims to improve the description of hydrogen bonding by the DFTB method due to the DFTB method typically underestimate the hydrogen bonding strength due to lower interaction energy between the electron donor and a hydrogen within a hydrogen bond as a result of limited atom polarizability and monopole

approximation within the DFTB method.[113] This is important due to the prevalence of hydrogen bonds within the crystal structure. This H5 correction is only applied at distances where hydrogen bonding can occur with the polarizability and multipolar components becoming important in the short range.[113] This parameterisation showed energetic improvements to the studied benchmark set with a Root mean Squared Error (RMSE) of 3.52 kJ/mol when ran with a geometry optimisation whereas compared against DFTB-D3 with comparable methods which showed a RMSE of 4.94 kJ/mol.[113]

3.6 Dispersion correction

Dispersion correction within DFT is important as exchange functionals have difficulty reproducing long-range behaviour, even those parameterised for long-range behaviour.[114] This is because approximations such as the generalized gradient approximation within the exchange functionals,[115] meaning the potential energy surface without these dispersion corrections could lack the crystal packing effects.[116] These are affected by the Van der Waals forces that are better estimated through the dispersion correction as this follows a simple formula where the displacement energy is added to the exchange-correlation function so as not to be included in the initial DFT calculations.

A vital aspect of the dispersion correction is the dampening, with methods lacking adequate dampening failing to give consistent results.[117] The dampening function within the dispersion correction determines the range at which the dispersion correction acts[118] and the steepness of the cut-off of the dispersion correction.[119] The dampening function means that the dispersion effects approach one at long distances, meaning it is purely dispersion. However, as the distance between the dipoles shortens, the dispersion correction gets dampened, eventually reaching zero.[120] This means there is no dispersion at the shorter distances as this is where the exchange functionals are optimised. The dampening effects are intended to reduce the double counting effects.[121]

The dispersion correction can be calculated in several ways; this tends to be a pairwise, three-body, or many-body approach. The pairwise approach, which is

taken with dispersion corrections schemes, such as Grimme -D2[122,123] and Tkatchenko-Scheffler (TS)[124], these methods summate over the C_6R^{-6} potential where R is the atomic distance and the C_6 is the dispersion coefficient. For the Grimme –D2 method, these are multiplied by a global scaling factor.[122] where the TS scheme calculates the pairwise dispersion energy using this formula:[125,126]

$$E_{disp} = -\frac{1}{2}\sum_{i \neq j} f_{damp}\frac{\left(R_{ij}, R_{ij}^{0}\right)C_{6ij}}{R_{ij}^{6}}$$

Equation 3-6 Pairwise dispersion correction calculation

In this case, f_{damp} is the dampening function, R_{ij} is the distance between atoms i and j, and R_{ij}^{0} is the sum of the Van der Waals equilibrium radii. These methods diverge as the DFT-D2 method developed by Grimme utilises the atom-type model, whereas the TS model utilises the atomic volume, this use of the atomic volume allows the rough approximation of the many-body effects.[127] An example of the three-bodied approach used in Grimme's- D3 correction scheme. The simplest way to employ a three-body approach is to utilise a non-additive third-order Axilrod-Teller-Muto (ATM) term:[128]

$$E_{disp} = \frac{C_9^{ABC}(3\ cos\ cos\ \theta_a cos\ \theta_b cos\theta_c + 1)}{(R_{AB}R_{BC}R_{CA})^3}$$

Equation 3-7 Non-additive third order ATM term

Where θ are the internal angles formed by R_{AB}, R_{BC} and R_{CA}, this uses a C_9 triple dipole constant that can be approximated in two possible ways, either through integrating the average dipole polarizability at an imaginary frequency for all three atoms dispersion coefficient.[129] This three-body treatment has been found to contribute minimally to the overall dispersion energy, with one paper saying that the three-body treatment contributes <5-10% of the dispersion energy,[130] and another paper stating that the three-body effect contributes 7.2% of the lattice energy[131].

As used in the many-body dispersion scheme (MBD), which builds on the pairwise TS approach and addresses the nature of long-range energy, it is many-bodied in nature.[125] The main drawback of the MBD scheme is the higher computational cost,[127] which is because this method involves having to calculate both pairwise and three-body dispersion energy utilising the formula:[117]

$$E_{disp} = \frac{1}{2}\sum_{IJ}^{atoms} E^{(2)}(R_I, R_J) + \frac{1}{6}\sum_{IJK}^{atom} E^{(3)}(R_I, R_J, R_K) + \cdots$$

Equation 3-8 Equation for three-bodied dispersion correction

$E^{(2)}$ is a pairwise, and $E^{(3)}$ is three body energies. These were covered earlier in both pairwise and triple-body dispersion coefficients. Which is extended up to N atoms up to the Nth order, coupled with a self-consistent screening to reduce the error.[132]

Chapter 4 DFT-based predictions of co-crystal formation: a benchmark study of 28 assemblies comparing five methods from high-throughput to advanced models.

This work has been published in the Journal for Computational Chemistry.

R. Fox, J. Klug, D. Thomson, A. Reilly, Journal of Computational Chemistry, 2024, **45**, 2465-2475

4.1 Introduction

Co-crystals are formed when two or more neutral molecules co-assemble in a single lattice.[65] Typically, a functional molecule and a second non-solvent molecule, termed the co-former, are crystallised in a stoichiometric ratio, with ordered supramolecular packing of the two components.[21,30] Other separate classes of multicomponent solid forms include hydrates with water, solvates with organic solvents, salts with charged compounds,[133] and racemic mixtures of chiral enantiomers.[31] Originally discovered by Wöhler in 1844 when quinhydrone was crystallised with quinone,[134] known co-crystals have experienced significant and rapid growth over the last 30 years.[134] This growth in the number of co-crystals is due to their ability to improve solubility, mechanical properties, density and bioavailability[135] by molecular and crystal engineering. Co-crystals have provided useful materials solutions in fields ranging from pharmaceuticals[50] to semiconductors[51] and other value-added chemicals.[23] The potential to improve the solubility of active pharmaceutical ingredients (API) using co-crystals significantly impacts the pharmaceutical sector because 40% of approved APIs and 90% of developmental drugs have poor solubility.[49] Another important issue for the (bio)pharma sector is the poor permeability of APIs.[136] For example, co-crystals formulated with permeation enhancing co-formers enable the delivery of peptides and related small molecule drugs.[137]

Molecules in a crystal structure can be arranged in multiple ways within the lattice, creating polymorphism. Polymorphism complicates the rational engineering of co-crystals, especially when polymorphs are near iso-energetic but have different properties, meaning multiple polymorphs can be produced under standard synthesis conditions. A well-known example is the HIV drug ritonavir, marketed under the brand name *Norvir*®, which morphed into a lower solubility structure over time. This was discovered two years after its release to the market when *Norvir*® capsules started failing dissolution tests, and the drug was removed from the market.[5]

Previous work has shown that co-crystals are thermodynamically stable, with 95% of the co-crystals studied having favourable negative lattice enthalpy.[65] This was established through dispersion-inclusive density functional theory (DFT-D)

calculations incorporating a van der Waals correction to the main exchange-correlation function to predict the lattice enthalpy. Uncorrected DFT can accurately predict simple salts, hydrates and solvates, and hydrogen-bonded assemblies but becomes less useful for co-crystals and crystals with significant van der Waals (vdW) contacts. Previous work predicted the mean absolute percentage error (MAPE) ranging from 97% presented by the B3LYP to 49% by the B971 exchange functional for crystals with significant vdW contacts in contrast to the much lower values for hydrogen bonded systems ranging from 18% using the HCTH407 exchange functional to 3% with B971.[138] The difference between the measured and calculated lattice energies emphasises the importance of incorporating dispersion corrections for more accurate description of the interactions between non-polar and weakly polar molecular groups.[127] Another example of the importance of dispersion corrections was the discovery of the previously unknown polymorph of aspirin, which was found using computational models with dispersion interactions and experiments.[139]

Dispersion corrections can scale to progressively longer-range and computationally more demanding calculations, with options to calculate over pairwise, three-body or many-body interactions.[112,117,127,129,140,141] Here, we have assessed the predictive power of different DFT-based methods to identify and quantify the stabilities of a broad range of co-crystals spanning four different functional molecules, namely, oxalic acid, 4,4'-bipyridine, aspirin and paracetamol, with multiple co-formers. Oxalic acid and 4,4'-bipyridine were selected due to the simplicity of their molecular structures, with primarily hydrogen bonding or van der Waals intermolecular interaction in their single crystal form, respectively. The more complex co-crystals containing the well-known active pharmaceutical ingredients (APIs), aspirin or paracetamol as the functional molecule were selected to test the limits of the predictive power of the various dispersion correction methods, including the pairwise Tkatchenko-Scheffler (TS)[124] dispersion correction and the Many-Body dispersion (MBD) schemes.[132,142]

One way to reduce the computational cost of DFT calculations and develop high throughput screens is to introduce approximations to the Kohn-Sham DFT model, and one of these approximations is density functional based tight binding (DFTB).[143] In DFTB, a minimal atomic basis set is used, and the exchange correlation energy

derived from the Kohn-sham DFT is expanded to a third-order Taylor series to calculate the total energy.[105] This allows faster calculations on more complex crystals but comes with reduced accuracy that may or may not significantly reduce the predictive power of the calculations.

4.2 Methods

4.2.1 Co-crystal selection

We systematically survey organic co-crystals of four selected molecules (oxalic acid, 4,4'-bipyridine, paracetamol, and aspirin) of increasing complexity to benchmark the computational methods, where paracetamol and aspirin are two well-characterised single component crystals. The co-crystal sets and their individual component crystals were mined from the Cambridge Structural Database (CSD)[144] using the ConQuest code, limiting the atom list to C, H, N, O, F, S and Cl. When duplicate structures were available, the lowest temperature structure was selected to better complement the 0 K DFT calculation. A limitation on the number of atoms in the unit cell was used to make the calculations feasible for the PBE0 hybrid exchange-correlation functional[145] that mixes the Perdew–Burke–Ernzerhof (PBE)[81] exchange energy and Hartree–Fock exchange energy in a set 3:1 ratio, along with the full PBE correlation energy. We investigate five oxalic acid co-crystals, thirteen 4,4'-bipyridine co-crystals, six paracetamol co-crystals and four aspirin co-crystals, with a broad range of commonly used, readily available co-formers (**Tables 4-1** and **4-2**) more information on the Conquest search on the supplementary information (**Appendix A**).

4.2.2 Computational methods

All the selected experimental co-crystal and single component crystal structures were optimised using planewave DFT as implemented in the CASTEP (CAmbridge Serial Total Energy Package) code.[146] The PBE exchange-correlation functional[81] was used for both standard DFT and dispersion-inclusive DFT, along with the PBE0 variant, and we compared the predictive power of DFT[122] utilising two different dispersion corrections, the Tkatchenko-Scheffler (TS)[124] and the Many-Body dispersion (MBD) schemes.[132,142]

In general, the dispersion interactions are incorporated in a second step following calculation of the base exchange-correlation functional energy.[127] The popular TS dispersion correction method uses a simple pairwise summation of the dispersion energy (**Equation 4-1**):[147]

$$E_{disp} = -\frac{1}{2}\sum_{A,B}\frac{C_{6AB}}{r_{AB}^{6}} f_{damp}(r_{AB})$$

Equation 4-1 Summation of dispersion energy using popular TS dispersion correction

Where r_{AB}^{6} is the interatomic distance between atoms A and B, and $f_{damp}(r_{AB})$ is the dampening function. With this method, the C_{6AB} uses the relationship between polarizability and volume, allowing it to factor in the chemical environment.

The many-body dispersion method attempts to calculate the many-body effects beyond two-body effects. This many-body energy is included within the long-range correlation energy.[127] This method has previously reported an improvement in the MAPE from 9% with PBE-TS to 5% with the PBE-MBD when using the S22 database.[132] The MBD model reduces the computational expense through the incorporation of the random phase approximation this enables the computational cost of both dispersion corrections being negligible in comparison to the exchange functional contributions.[125]

The unit cells were optimised with a cut-off energy of 900 eV, using an electronic energy tolerance of $1x10^{-7}$ eV per atom and geometry energy tolerance of $5x10^{-7}$ eV per atom to generate final structures with all forces below $5x10^{-3}$ eV $Å^{-1}$. A tight k-point spacing of 0.06 $Å^{-1}$ was used together with ultra-soft pseudopotentials (USP) to describe the electronic structure.[97]

To test the effect of the functional choice apart from the dispersion corrections, we performed some high-level single point energy PBE0-MBD calculations on the optimised PBE-MBD structures.

The crystal structures were also optimised using the DFTB3+[105] method to gauge the balance between model cost and accuracy. The DFTB calculations were run with the Grimme D3 dispersion correction[130]and three different dampening methods, standard Becke-Johnson, the H5 and Boese[148] models. The reduced computational cost of the DFTB method comes with minimal basis sets[105] that generally require

corrections, such as the H5 method that improves the description of hydrogen bonded systems.[113] The DFTB method can also be improved by fitting the geometries with the Boese method, aiming to capture dispersion effects.[148] These different methods of improving the predictive power of the DFTB method can be incorporated along with the dispersion corrections as described above (in this case, DFTB-D), while keeping the computational overhead at a fraction of that of full DFT. Further details on the DFT and DFTB optimisation methods are provided in the supplementary information (**Appendix A**).

4.2.3 Estimation of co-crystal stability

Assuming that the entropic contribution to the free energy is negligible going from the single component crystals to the co-crystal, which is reasonable for many sets of similarly sized, neutral molecules, the driving force for the co-crystal formation can be approximated using **Equation 4-2**.[65]

$$\Delta E_{co-cryst}(A_nB_m) = E_{tot}(A_nB_m) - [mE_{tot}(A) + nE_{tot}(B)]$$

Equation 4-2 Calculation of lattice enthalpy change of co-crystal structures

Here, $E_{tot}(A_nB_m)$ is the calculated enthalpy of the co-crystal, and $E_{tot}(A)$ and $E_{tot}(B)$ are the enthalpies of the single-component crystal structures of functional molecule A alone and co-former B alone, respectively, with *m* and *n* defining the stoichiometric ratio of A and B in the co-crystal. **Table 4-1** shows the list of co-crystals used in this study, including their CSD reference codes, molecular composition in the co-crystal, and the indication of the presence or absence of H-bonds in the co-crystal structure. Meanwhile, **Table 4-2** has the complete list of the single component crystals, which are included in **Table 4-1** with their CSD code, chemical name, chemical structure, and presence or absence of H-bonds in the crystal structure.

Table 4-1 The calculated co-crystal compositions

CSD reference code			composition A_mB_n		H-bonding in the crystal structure
Co-crystal	Co-former A	Co-former B	m (A)	n (B)	
GUDSUV	OXALAC05	BACKAU	1	1	yes
UMINAF	OXALAC05	EVESIJ04	1	1	yes
UROXAM01	OXALAC05	UREAXX12	1	1	yes
XAPMIK	OXALAC05	PHENAZ11	1	1	yes
XEJWUF	OXALAC05	BAPLOT04	1	2	yes
GIPQEB01	HIQWEJ03	FUMAAC01	1	1	yes
GOKCEQ	HIQWEJ03	FORMAC01	1	2	yes
LOYRIC	HIQWEJ03	BENZDC11	1	2	yes
MEWNUA	HIQWEJ03	ADOGUW	1	2	yes
NUJFEF	HIQWEJ03	HOPHAL11	1	1	yes
PAVXAN	HIQWEJ03	TEPHTH14	1	1	yes
ROQYED	HIQWEJ03	ROQXUS	1	2	yes
RUXMAZ	HIQWEJ03	ETYNBZ01	1	1	no
SITDIJ	HIQWEJ03	ACETAC03	1	2	no
SOVFOY01	HIQWEJ03	TGLYCL01	1	1	yes
UCEXIJ	HIQWEJ03	PAXNIL	1	1	yes
VEXQOE	HIQWEJ03	CYURAC14	1	2	yes
XOWKEB01	HIQWEJ03	XYANAC06	1	2	yes
KIGLUI01	HXACAN13	BAPLOT04	1	1	yes
LUJSOZ	HXACAN13	PHENAZ11	1	2	yes
CUQKAC	HXACAN13	WEMWEQ15	1	1	yes
LUJSIT	HXACAN13	NAPHTA15	2	1	yes
LUJTAM	HXACAN13	OXALAC05	1	1	yes
LUJTAM	HXACAN13	OXALAC11	1	1	yes
DIPJAQ	ACSALA05	BAPLOT04	1	1	yes
HUNJEH	ACSALA05	JAKGEH	1	1	yes
SIBYUA	ACSALA05	HIQWEJ03	2	1	yes
TAZRAO	ACSALA05	CBMZPN21	1	1	yes

Table 4-2 The reference single component crystals

CSD reference code	Name	H-bonding*	Chemical structure	CSD reference code	Name	H-bonding*	Chemical structure
ACETAC03	Acetic acid	yes		HXACAN13	Paracetamol	yes	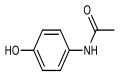
ACSALA05	Aspirin	yes		JAKGEH	Pentoxifylline	no	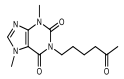
ADOGUW	O-Isopropyl N-phenyl thiocarbamate	no	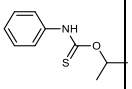	NAPHTA15	Naphthalene	no	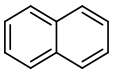
BACKJAU	Pyrazine	no		OXALAC05	Oxalic acid alpha polymorph	yes	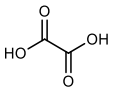
BAPLOT04	Theophylline	yes		OXALAC11	Oxalic acid beta polymorph	yes	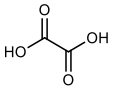
BENZDC11	Isophthalic acid	yes	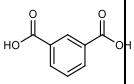	PAXNIL	Cyclo-diaspartic acid	yes	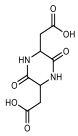
CBMZPN21	Carbamazepine	yes	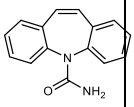	PHENAZ11	β-Phenazine	no	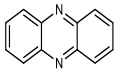
CYURAC14	1,3,5-triazinane-2,4,6-trione	yes	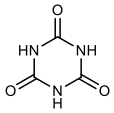	ROQXUS	Succinamic acid	yes	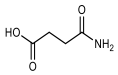
ETYNBZ01	1,4-Diethynylbenzene	no	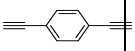	TEPHTH14	Terephthalic acid	yes	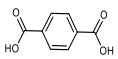
EVESIJ04	Azapyridine	no	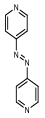	TGLYCL01	Thiodiglycolic acid	yes	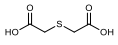
FORMAC01	Formic acid	yes		UREAXX12	Urea	yes	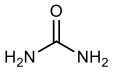
FUMAAC01	Fumaric acid	yes	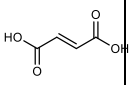	WEMWEQ15	Betaine	no	
HIQWEJ03	4,4'-bipyridine	no	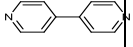	XYANAC06	2-[(2,3-dimethylphenyl) amino] benzoic acid	yes	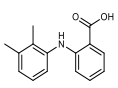
HOPHAL11	2-(Carboxymethyl) benzoic acid	yes	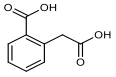				

* Presence of H-bonds in the crystal structure

4.3 Results and discussion

4.3.1 Density functional theory (DFT) results

We start our study with the alpha polymorph of oxalic acid (OXALAC05) co-crystals, including five different common co-formers from small molecules of urea and pyrazine to larger molecules including phenazine, theophylline and azapyridine (**Table 4-1** and **Table 4-2**). From **Table 4-1**, it can be noted that all oxalic acid co-crystals have hydrogen bond interactions.

The predicted lattice enthalpies of the oxalic acid co-crystals are presented in **Figure 4-1**. All four methods, PBE, PBE-TS, PBE-MBD and PBE0-MBD, rank the azapyridine co-crystal (UMINAF) as the most stable co-crystal with the pyrazine co-crystal (GUDSUV) being the 2nd most stable and identify the co-crystal with theophylline (XEJWUF) as the least stable. The stability rank of the remaining two oxalic acid co-crystals, with phenazine (XAPMIK) and urea (UROXAM01), depends on the method implemented. All the DFT computational methods used show negative values for the enthalpy of oxalic acid co-crystal. As shown in **Figure 4-1**, the four different DFT computational methods provide similar values for the enthalpy of co-crystal for each oxalic acid co-crystal. A clear message from **Figure 4-1** is the lack of dependence on the dispersion method used on the $\Delta E_{co-cryst}(A_nB_m)$ estimation for oxalic acid co-crystal. This lack of dependence on the dispersion method is expected due to the presence of hydrogen bond interactions in all the oxalic acid co-crystals (**Table 4-1**), as hydrogen bond interactions are well described by the exchange correlation functionals.[125]

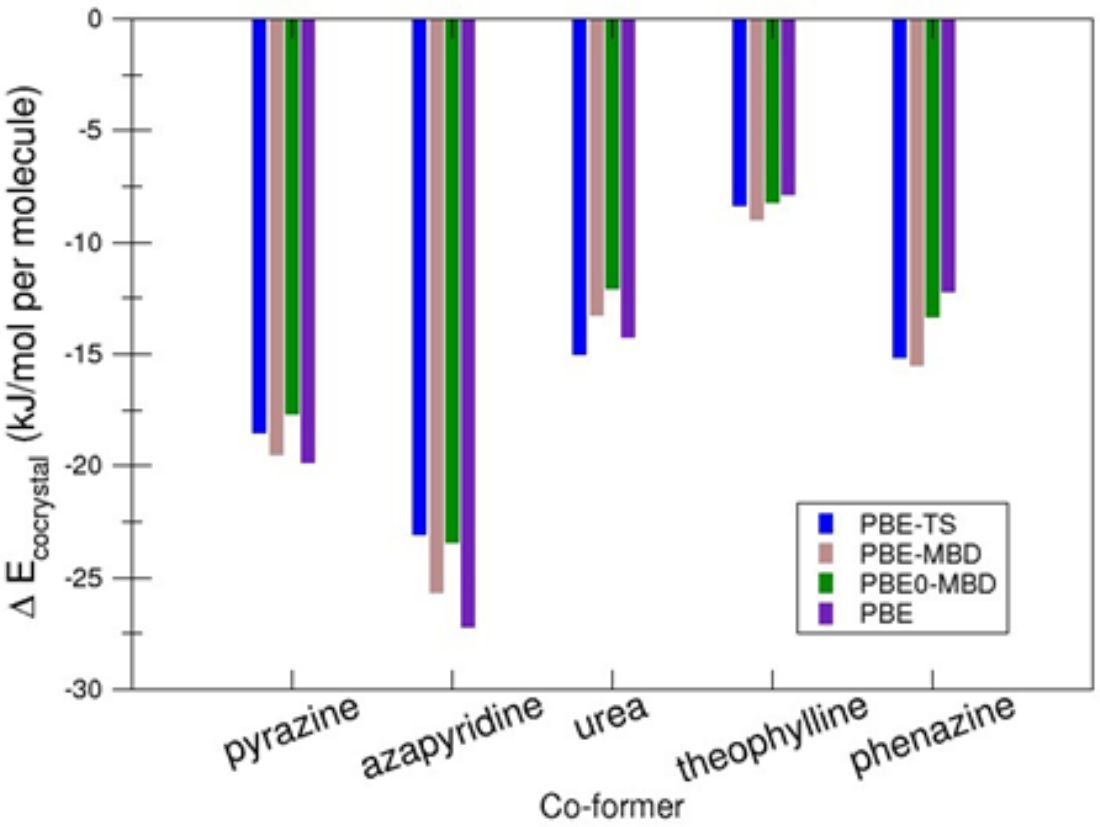

Figure 4-1 Predicted relative stabilities of five oxalic acid-based co-crystals lattice enthalpy, $\Delta E_{co\text{-}crystal}$, calculated using three dispersion-inclusive DFT models and one uncorrected DFT model.

Table 4-3 List of 4,4'-bipyridine co-formers

	Co-former name	Co-former CSD reference code	Co-crystal CSD reference code
1	1,3,5-triazinane-2,4,6-trione	CYURAC14	VEXQOE
2	fumaric acid	FUMAAC01	GIPQEB01
3	thiodiglycolic acid	TGLYCL01	SOVFOY01
4	O-isopropyl N-phenylthiocarbamate	ADOGUW	MEWNUA
5	1,4-diethynylbenzene	ETYNBZ01	RUXMAZ
6	acetic acid	ACETAC03	SITDIJ
7	isophthalic acid	BENZDC11	LOYRIC
8	terephthalic acid	TEPHTH14	PAVXAN
9	2-(carboxymethyl)benzoic acid	HOPHAL11	NUJFEF
10	formic acid	FORMAC01	GOKCEQ
11	cyclo-diaspartic acid	PAXNIL	UCEXIJ
12	succinamic acid	ROQXUS	ROQYED
13	2-[(2,3-dimethylphenyl)amino]benzoic acid	XYANAC06	XOWKEB01

The next subset of co-crystals studied are for 4,4'-bipyridine. The stability of the single component crystal of 4,4'-bipyridine (HIQWEJ03) is primarily driven by dispersive interactions, as the molecule does not have any H bond donor group, and two nitrogen atom H bond acceptor groups (**Table 4-2**). These Hydrogen bond acceptor nitrogen atoms have potential for strong Hydrogen bond interactions in co-crystals with co-formers with Hydrogen bond donor groups. **Figure 4-2** shows the calculated lattice enthalpy of the co-crystals for 4,4'-bipyridine.

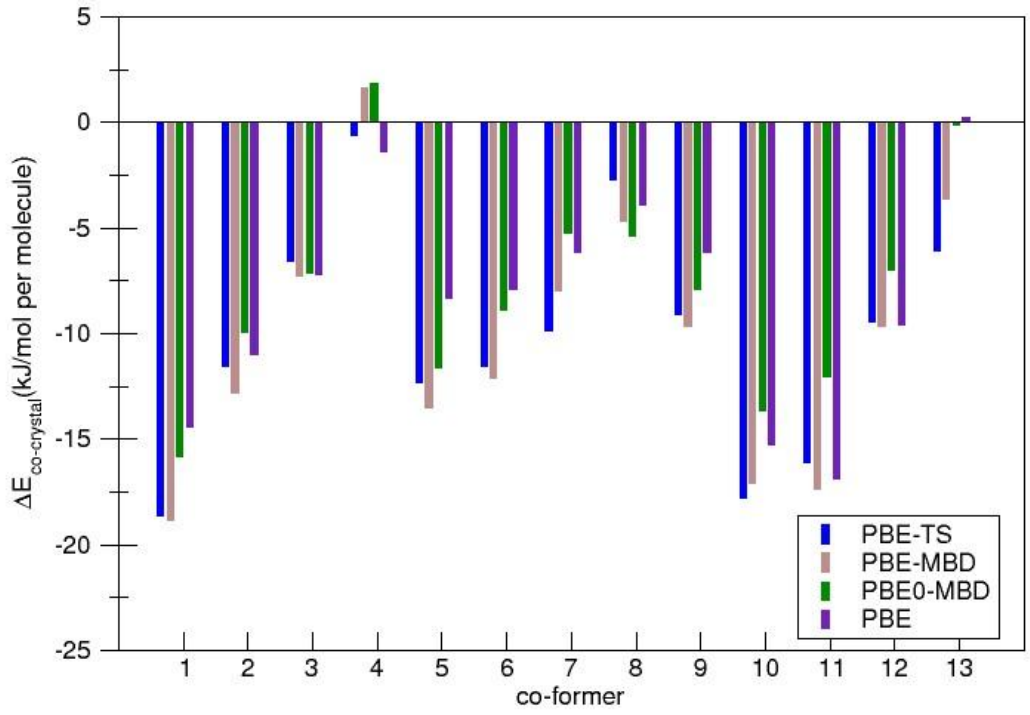

Figure 4-2 Predicted relative stability for thirteen 4,4'-bipyridine-based co-crystals lattice enthalpy, $\Delta E_{co\text{-}crystal}$, calculated using three DFT-D models and uncorrected DFT model. Co-formers 1-13 on the horizontal axis are identified in **Table 4-3**

For all but two of the 13 co-crystals (**Table 4-3**), the four DFT computational methods agree on large negative values for the co-crystals formation energy (**Figure 4-2**). The two co-crystals where the co-crystal enthalpy is dependent upon the computational DFT method are O-Isopropyl N-phenylthiocarbamate (no. 4, MEWNUA) and 2-[(2,3-dimethylphenyl)amino]benzoic acid (no. 13, XOWKEB01). The discrepancy between the small negative values with uncorrected PBE and PBE-TS and the small positive values with PBE-MBD and PBE0-MBD in the case of MEWNUA may be numerical noise but nevertheless this co-crystal is predicted to be weak. For no. 13, the near-zero prediction for uncorrected PBE and PBE0-MBD but modest negative values for PBE-TS and PBE-MBD is difficult to rationalise, though we note that PBE-MBD predicts the largest negative enthalpy for eight of the co-crystals, consistent with more complete treatment of dispersive interactions by MBD.[149] The co-crystal with 1,4-diethnylbenzene (no. 5, RUXMAZ) is the only co-crystal where there are no Hydrogen bond interactions in the co-crystal nor in their single component crystals, as reflected in the most significant and consistent percentage increase in magnitude of negative lattice enthalpy on switching from uncorrected PBE to the three dispersion-inclusive models.

The degree of dependence of results on the choice of model is increased as the complexity of the functional molecule is increased, as demonstrated by the calculated stabilities of co-crystals for aspirin or paracetamol. Both APIs engage in both hydrogen bonding and π–π stacking with van der Waals stabilisation. Previous calculations on aspirin have shown that the crystal packing relies heavily on dispersive interactions.[150] The paracetamol results, in general, show favourable, negative values for the formation of the six available co-crystals (**Table 4-1** and **Figure 4-3**). Only the naphthalene (LUJSIT) and phenazine (LUJSOZ) co-crystals are predicted as unfavourable in some cases by two out of four models. Paracetamol oxalic acid (LUJTAM) is the most stable co-crystal, reflecting the strong Hydrogen bonding character of the co-former, which may also influence its compressibility in paracetamol tabletting.[7]

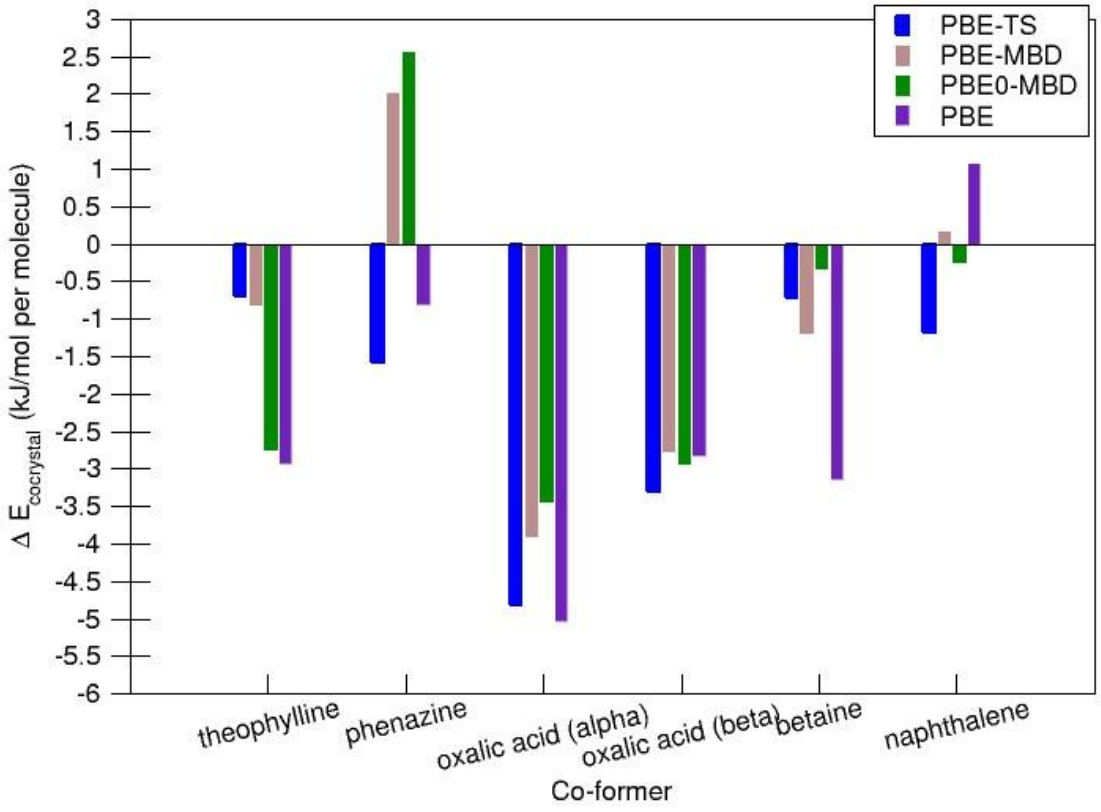

Figure 4-3 Predicted relative stabilities for six paracetamol-based co-crystals lattice enthalpy, $\Delta E_{co\text{-}crystal}$, calculated using three DFT-D models and uncorrected DFT model.

The final co-crystal dataset studied using the full DFT methodology are the aspirin co-crystals. The predicted enthalpy of formation for the aspirin co-crystals using uncorrected and dispersion-inclusive DFT is presented in **Figure 4-4**. Aspirin co-crystals are clearly challenging to predict, with some enthalpies of co-crystals predicted as positive, some negative and some close to zero. Uncorrected PBE performs best and only fails for the co-crystal with theophylline. This result highlights the challenge of predicting the stability using DFT models for these complex co-crystals with mixed hydrogen bonding and van der Waals contacts, with dispersion corrections likely overestimated and leading to unphysical co-crystal structures.

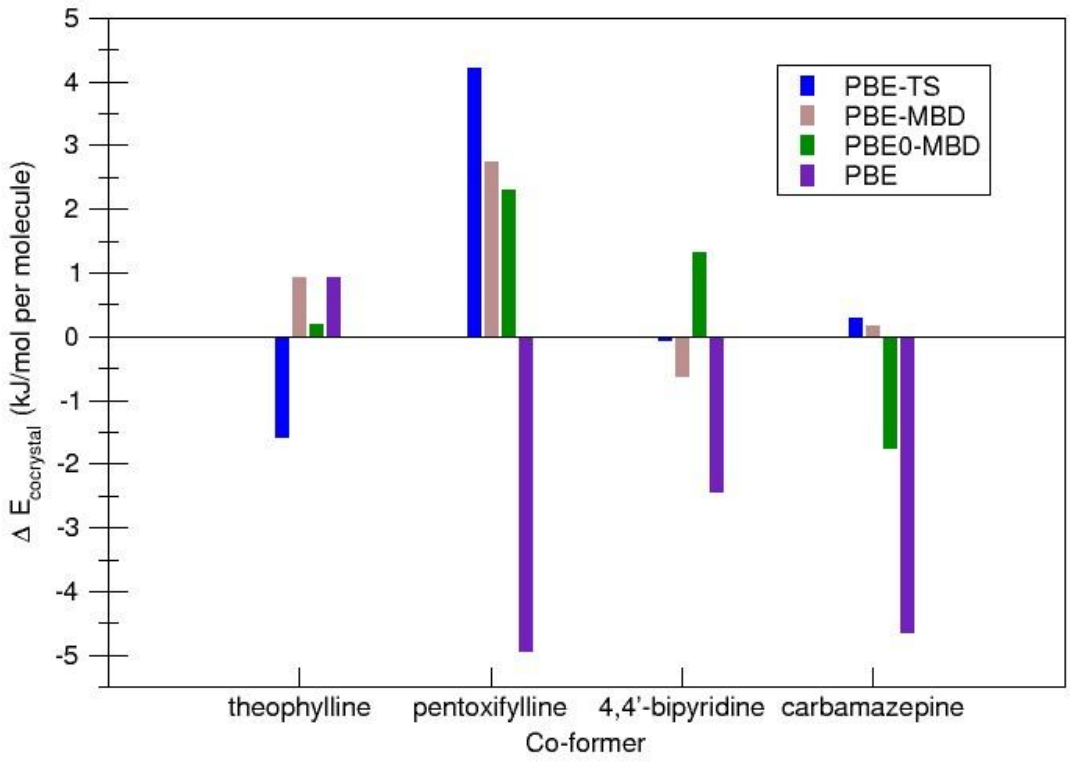

Figure 4-4 Predicted relative stabilities for four aspirin-based co-crystals lattice enthalpy, $\Delta E_{co\text{-}crystal}$, calculated using three DFT-D models and uncorrected DFT model.

Overall, the DFT results show that the enthalpy of co-crystallisation is negative and so thermodynamically favourable for the majority of the co-crystals. The PBE-TS method predicts 93% of co-crystals with negative enthalpy. When PBE-MBD and PBE0-MBD methods are used, negative enthalpy is predicted for 83% of the co-crystals. It is important to highlight that the entropy contribution to the free energy was not calculated in our study, therefore co-crystals structures with positive values of enthalpy of formation may be stabilised through entropic contributions.

4.3.2 Density functional tight binding (DFTB) results

Full DFT calculations represent a medium to low throughput method of predicting co-crystal stability for assemblies of low to moderate complexity in terms of crystal size and molecular weights. Faster high-throughput methods more suitable for large datasets and/or large crystals, may be in principle obtained using DFTB methods.

Here, to directly compare with full DFT, we test the predictive power of DFTB methods for the same set of co-crystals. We compared the effectiveness of three methods of DFTB-D, one with standard Becke-Johnson (BJ) dampening and two using the Boese method and H5 parametrisation.

Compared with DFT, the computationally more expedient but approximate DFTB-D method showed significantly less predictive power. For co-crystals with oxalic acid (**Figure 4-5**), the assemblies formed with pyrazine or urea are predicted to be stable. Note the very large absolute values of the energies in some cases, reflecting numerical instability and poor quantitative power of DFTB-D to predict energies. Of the three DFTB methods tested, H5 parameterisation performed best, predicting stable co-crystals for all but the with co-crystal phenazine, reflecting its ability to model hydrogen bonding more effectively than the alternative schemes.

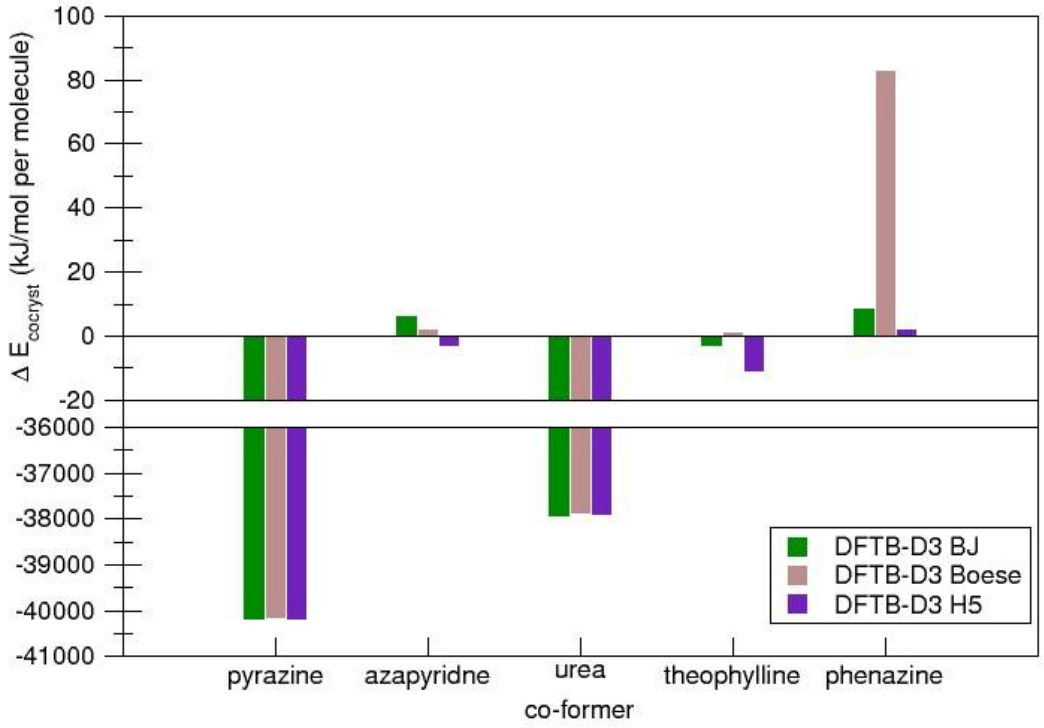

Figure 4-5 Predicted relative stabilities for five oxalic acid-based co-crystals lattice enthalpy, $\Delta E_{co\text{-}crystal}$, calculated using three DFTB+ parameterisations.

One limitation of the DFTB-D method is the possibility of large errors in the calculation of weak dispersive interactions, such as van der Waals packing, as a result of the semi-local origins of the DFTB approximation.[105]

The limitations of the approximations made in the DFTB-D methods are clearly evident for the 4,4'-bipyridine co-crystal dataset (**Figure 4-6**), for which DFTB-D fails. Note that when the DFTB-D3 H5 parameterisation was used for the fumaric acid (no. 2, GIPQEB01) co-crystal and DFTB-D3 BJ for the formic acid co-crystal (and no. 10, GOKCEQ), numerical instabilities prevented the successful completion of the calculation.

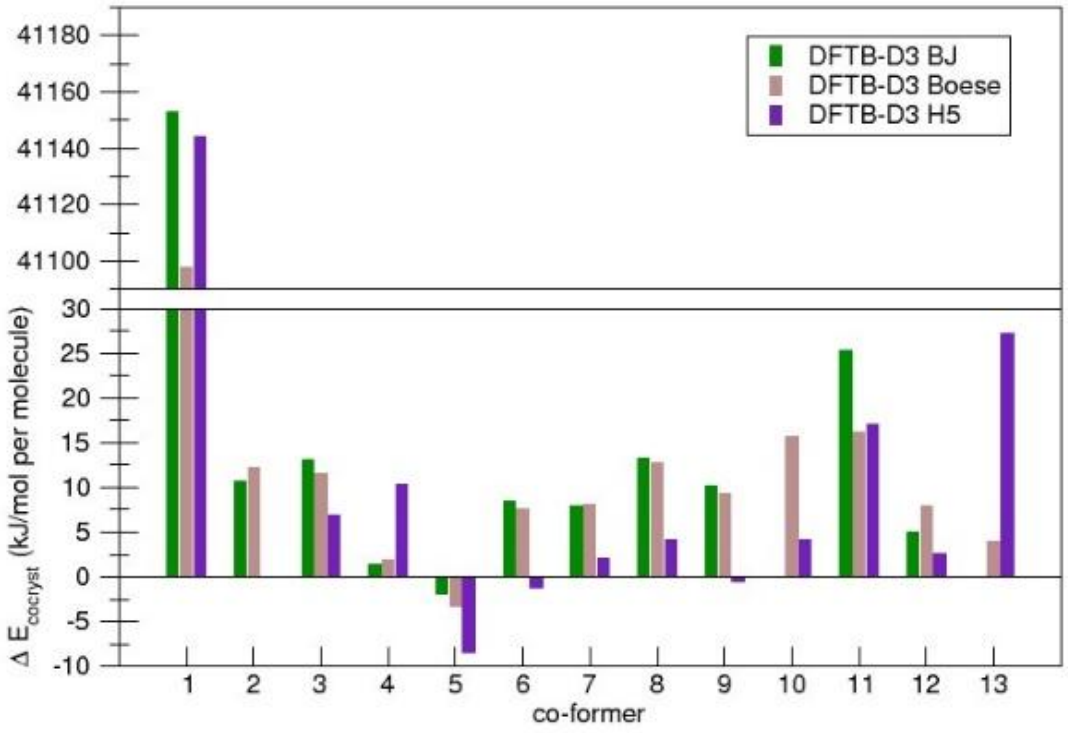

Figure 4-6 Predicted relative stabilities for thirteen 4,4'-bipyridine-based co-crystals lattice enthalpy, $\Delta E_{co\text{-}crystal}$, calculated using three DFTB+ parameterisations.

Not surprisingly then, DFTB-D also fails for the more complex co-crystals with APIs paracetamol or aspirin. For paracetamol co-crystals (**Figure 4-7**), DFTB-D3 BJ performs better than the others but is still unreliable, erroneously predicting unstable structures for two out of the six co-crystal lattices. Aspirin co-crystals, which also challenged DFT to some extent (**Figure 4-4**) cannot be predicted by DFTB (**Figure 4-8**).

Overall, the DFTB-D method does not predict stable lattice energies for these known, synthesised co-crystals, highlighting the poor predictability of these putative high-throughput methods for co-crystal design.

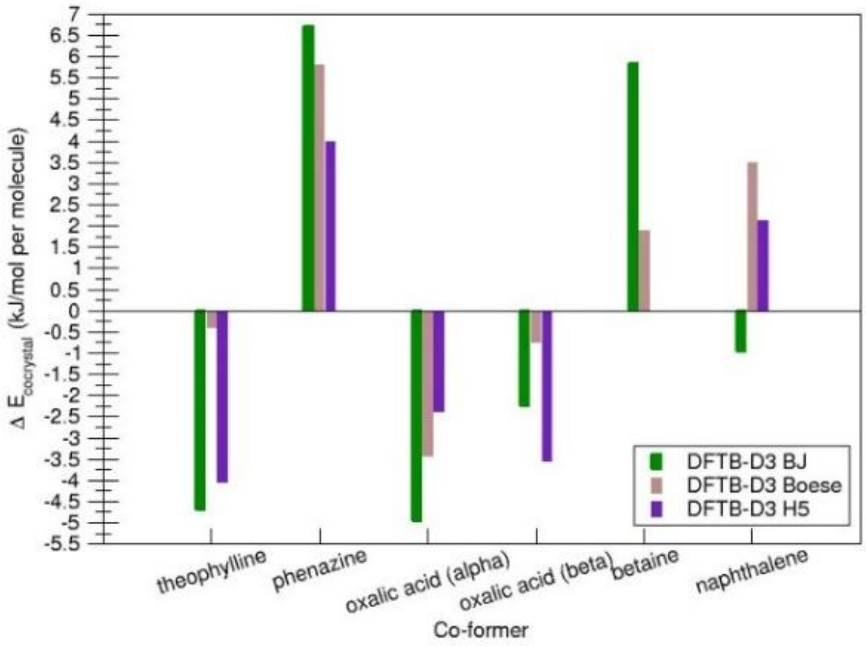

Figure 4-7 Predicted relative stabilities for six paracetamol-based co-crystals lattice enthalpy, $\Delta E_{co\text{-}crystal}$, calculated using three alternative DFTB+ parameterisations.

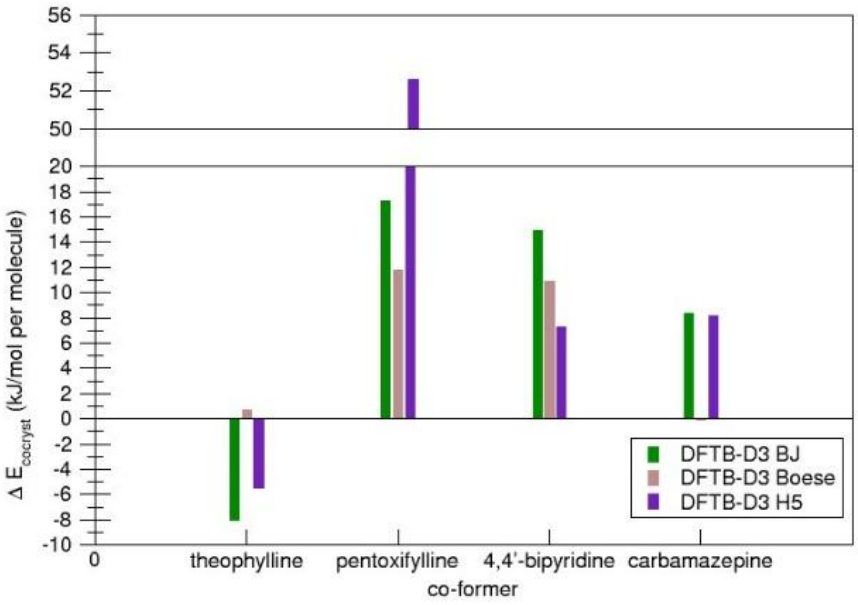

Figure 4-8 Predicted relative stabilities for four aspirin-based co-crystals lattice enthalpy, $\Delta E_{co\text{-}crystal}$, calculated using three DFTB+ parameterisations.

4.4 Conclusions

Our results show that the prediction of co-crystal stability is heavily dependent upon the computational model used. For simple co-crystals such as the oxalic acid and 4,4'-bipyridine datasets, the different DFT models largely agreed. However, for more complex co-crystals, such as the paracetamol and aspirin datasets with more diverse interactions, the enthalpy of formation depends on the DFT model, as seen most dramatically in the case of aspirin-based co-crystals.

Implementation of the computationally more demanding PBE0-MBD calculations did not significantly change the predicted lattice enthalpy of formation of the chosen co-crystals, relative to the less computationally demanding PBE functional. The dispersion corrections TS and MBD performed similarly well overall.

Our dataset confirms previous findings that co-crystallisation is a thermodynamically favourable process, with the PBE-TS method predicting favourable assemblies for 93% of co-crystals. The alternative PBE-MBD and PBE0-MBD methods predict 83%

to be favourable. Structures with predicted positive values of enthalpy of formation may be stabilised through entropic contributions in crystallisation experiments.

By contrast, the computationally lighter DFTB-D method predicts a high population of unstable co-crystals with large positive and values of enthalpy. This failure of prediction is particularly prominent for the more complex systems such as the aspirin co-crystals. The difficulty in predicting these systems could be due to the semi-local origins of this method, resulting in the lack of dispersion forces,[146] which are only marginally compensated by dampening corrections. Hence, using DFTB-D for co-crystal research at a significantly lower computational cost, which would allow for the study of larger crystal structures, requires careful pre-parametrisation and testing. Any such pre-parametrisation will need benchmarking against full DFT to ensure that the DFTB-D model is used only in cases where it can overcome, or be improved to overcome, the semi-local approximation. Perhaps the development of more advanced dispersion/dampening schemes that do not carry prohibitive computational overhead could achieve the required balance between accuracy and computational cost, with integration of AI methods also promising high predictive power for large, complex datasets.[67,151–153]

Chapter 5 Computational analysis of the binding energies of thiophene-based copper complexes.

The work from this chapter has been published in Angewandte Chemie (DOI: https://doi.org/10.1002/anie.202305759)

A. Gibney, R. E. F. de Paiva, V. Singh, R. Fox, D. Thompson, J. Hennessy, C. Slator, C. J. McKenzie, P. Johansson, V. McKee, F. Westerlund, and A. Kellett, Angewandte Chemie, 2023, **135**, e202305759

The computational calculations of the simple thiophene based copper complexes and complex Tri-Click structures was performed by me with the DNA biophysical analysis being conducted by Dr Alex Gibney from the Andrew Kellett group in Dublin City University.

5.1 Introduction

Metallodrugs represent an exciting new development in chemotherapeutic treatment of cancerous cells through damage to the genetic sequence preventing the loss of genetic integrity or overactivation of DNA damage repair mechanisms which ultimately results in cell death.[154] The damage mechanism to the DNA structure is influenced by the choice of metal with commonly used metals being platinum, copper, iron and ruthenium each with distinct modes of action.[155] With the platinum metal preventing the transcription of the DNA sequence through the coordinative bonding to the nucleobase residue blocking the RNA polymerase enzyme.[156] Whereas the copper and iron induces DNA damage by generating reactive oxygen species (ROS) through the biologically available redox potential of the metal ion. Meanwhile, ruthenium structures are photoactive, cleaving the DNA upon irradiation due to the production of ROS when the electrons are moved to the excited state and an intersystem crossing takes place. These generation of ROS must be done proximally to the target cleavage site.[157] The central metal ions used are chiefly responsible for the drug properties by identifying the biological pathway together with the metal of choice, the safest administration route can be identified, thereby minimising interference with other biological processes and damage to non-target structures.[158] Metallodrug-DNA binding modes are often sequence-selective, so the binding mode depends upon the DNA sequence context.[159] In general, the metal complex structure is vital for the application. Copper is an emerging metallodrug due to its biologically accessible redox properties, bioavailability, and broad adaptability to hard and soft ligands.[160]

Click chemistry is a general term for a reliable modular mechanism for producing more complex structures.[161] Among the most commonly used click reaction mechanisms is the Cu(I)-catalysed azide-alkyne cycloaddition (CuAAC) and strain-promoted azide-alkyne cycloaddition (SPAAC) reaction. The CuAAC reaction was developed by both Sharpless and Meldal separately in 2001,[161,162] and exploits the electronic resonance within the azide functionality and allows for a greater regioselectivity, over thermal Huisgen [3+2] cycloaddition (**Figure 5-1a-b**). SPAAC was developed later in 2006 by Bertozzi and aimed to reduce the use of the Cu(I) catalyst by exploiting the bond strain of the alkyne within the cyclooctyne structure

(**Figure 5-1c**).[163] The impact of this seminal work was acknowledged with Morten P. Meldal, K. Barry Sharpless and Carolyn R. Bertozzi being awarded the Nobel prize in Chemistry in 2022 for “the development of click chemistry and biorthogonal chemistry”.[164]

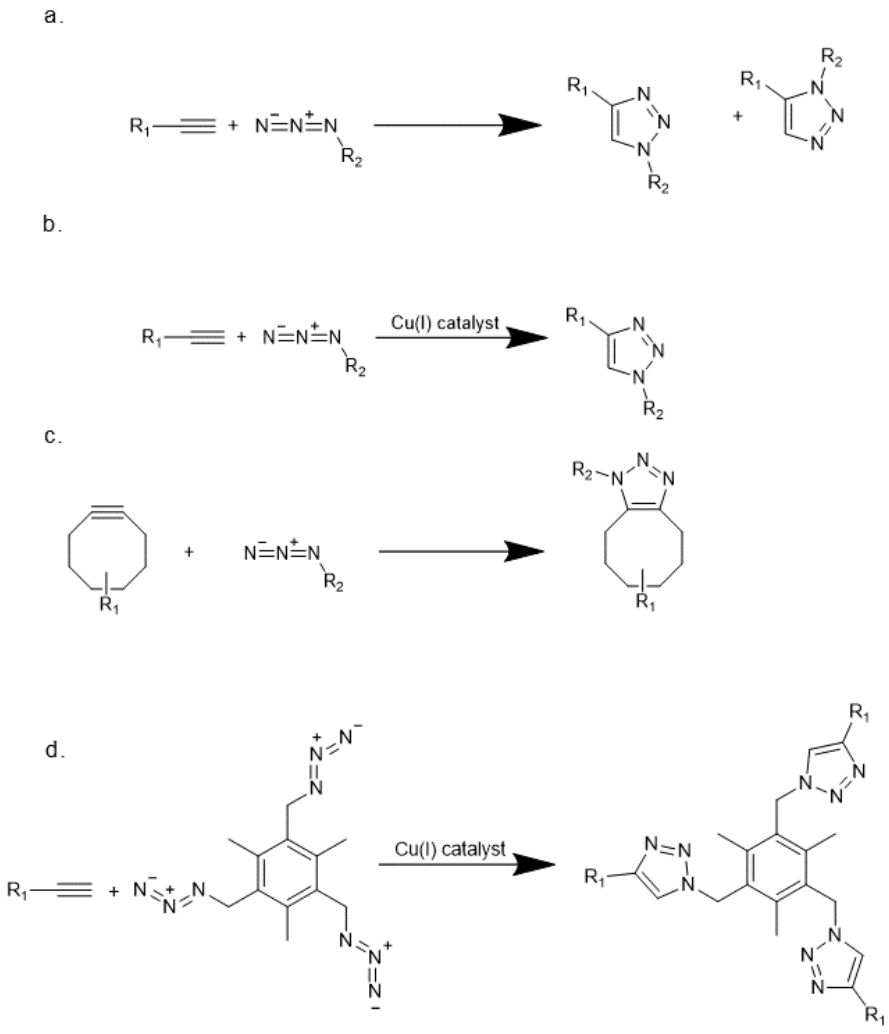

Figure 5-1(a) Thermal Huisgen [3+2] cycloaddition **(b)** General CuAAC reaction scheme **(c)** General SPAAC reaction scheme **(d)** General CuAAC reaction to generate the 1,2,3-triazole structures

In 2021 McStay *et. al.* used the CuAAC reaction to introduce modularity to the development of new artificial metallonuclease (AMN), resulting in a new lead Tri-Click ligand called TC-1 (**Figure 5-1d**) where R_1 was a methylamine group.[165] The

modular approach allowed for identification of key terminal groups that along with the 1,2,3-triazole could coordinate the copper ions in solution and catalyse DNA cleavage through the reduction of Cu(II) to generate ROS. The Tri-Click ligand produced within this chapter exchanges terminal methylamine group within the TC-1 ligand for a thiophene ring which could provide enhanced coordination to both Cu(II) and Cu(I) metal centres through the incorporation of both hard and soft Lewis acid and Lewis bases thereby stabilising the redox pair required for DNA damage mediation.

Dispersive forces are formed through the induction of charges. The formation and strength of these forces depend upon the molecules' polarizability,[166] defined as the ease at which the electron cloud is distorted, when a neighbouring molecule has an opposing partial charge. When this electron cloud is distorted, it is said to be an induced dipole. Generally, the higher the electron density and the more diffuse the electron cloud is, the greater the polarizability of the molecule. The more diffuse the electron cloud resulting in weaker attractive forces to the nucleus.[166] The dispersive forces are typically viewed as weaker interactions, with the bond strength approximately 2 kJ mol^{-1}.[29] These dispersive forces can be influenced by the electronegativity of the atoms that molecule this influences the size of the dipoles partial charges the more significant the difference between temporary dipoles; the stronger the influence of the long range forces. The influence of these dispersive forces is limited by the van der Waals radii of the atoms which is the maximum distance that these long range forces can be felt this could influence the final structure of the TC molecule this structural change will alter the downstream efficacy of the ligand.[159]

Both the binding strength and dispersive forces can be modelled using Density Functional Theory (DFT). Calculating these energies is possible through the implementation of high-level exchange correlation functionals coupled with a high-level basis set. The average ionisation energy for transition metals has previously been calculated with both 6-31G** and triple zeta valence potential (TZVP) basis sets coupled with a range of exchange functionals such as generalised gradient approximation (GGA), hybrid-GGA's, meta-GGA's and hybrid-meta-GGA.[167] One study compared the experimental ionisation energy to the predicted ionisation energy using TZVP and 6-31G** basis sets. Within this work the TZVP basis set

performed better than the 6-31G** basis set giving an potential error ranging from 0.64 to 0.37 eV, whereas the 6-31G** gave a potential error ranging between 1.12 to 0.79 eV.[167]

In this chapter the aim is to develop a polynuclear AMN that, due to their high potency, do not require reduction agents, such as ascorbate or peroxide, and can undergo unattended reduction. This work originated with simple copper structures incorporating a thiophene based organic structure that informed the optimum computational methodology for calculating the binding energy for a more complex thiophene TC scaffold. To assess the suitability of the thiophene TC structure as DNA damaging agent this was synthesized and further biophysical characterization applied.

5.2 Methods

All the experimental generated thiophene ring metallic complexes are reported crystal structures on the Cambridge Crystallographic datacentre (CCDC) this search returned 11 structures. These initial structures used simple organic molecules with a single coordination site for the metallic component to bind to. These simple structures could be broken down into four classes each of which increases in complexity with different counter ion that makes up the metallic component changing within the class of organic component.

The complexes were optimised utilising the ORCA 5.0.4 software with an implicit water solvent imparted using the Conductor-like Polarizable Continuum Model (CPCM). These were run with tight self-consistent field (SCF) criteria and the def2-TZVP basis set with the auxiliary basis set being def2/J. The complexes were modelled using progressively higher order exchange coefficients incorporating Purdew-Burke- Ernzerhof (PBE), Becke 3-parameter Lee-Yang-Parr (B3LYP) and the PBE0 exchange coefficients paired with the Grimme D3 dispersion correction using a Becke-Johnson dampening. This enables the minimisation of the molecule's energetics, E_{AB}, through the optimisation of the molecule's geometry. The optimised geometry was then taken, and these were subsequently separated into their singular organic ligand and their metal ion component, and the energies of the organic and metallic components were subsequently calculated, E_A and E_B respectively.

Following these calculations, the geometries were treated with a geometry counterpoise correction (gCP) to mitigate the effect of minimal basis sets.

This method was then scaled up to incorporate structures with multiple coordination sites using the synthesised TC-Thio ligand. Initially, the structure was treated as binding solely to a single counter ion this was then built up to incorporate a single water ligand from the water sphere surrounding the molecule to each metal unit. This process also entailed a visual analysis method to ensure the structures produced were experimentally feasible. Later, incorporating multiple ligand types to generate more experimentally feasible geometries for complex TC-Thio complex.

The optimised geometries were subsequently used to model the binding within the Dickerson-Drew dodecamer (DDD) using Autodock vina software. The Cu_3TC-Thio complex was treated as a flexible ligand allowing for the rotation of the bonds to allow for the docking of the TC-Thio complex the explicit solvent ligands were removed from the copper complex with the DDD structure was treated as a rigid body preventing the flexing of the DDD structures with the atomic charges assigned and any missing hydrogen bonds added. The entire DDD fragment was incorporated. To enable the Cu_3TC-Thio to dock within the entire DDD fragment the grid boxes were sized to incorporate the full fragment the 10 docking conformations were tested and ranking in accordance with their stability utilising AutoDock Vina's scoring function.[168]

5.3 Results and discussion

5.3.1 Binding energy of simple structures

To calculate the binding energies (B.E.) the energies with the gCP correction were inputted into the formula:

$$B.E. = E_{AB} - 2E_A - E_B$$

Equation 5-1 Equation for the calculation of the binding energy

The CCDC search showed four different classes of organic compounds these differ due to the counter ion being used. These classes are shown in **Table 5-1** increasing in complexity as further down **Table 5-1**.

Table 5-1 Table of different classes of organic components	
class	
1	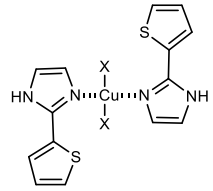
2	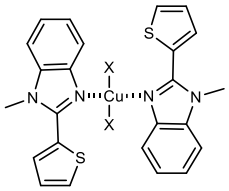
3	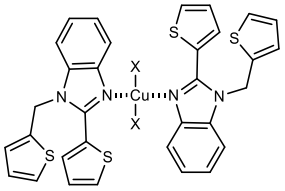
4	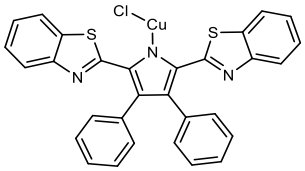

Initially the PBE exchange correlation functional was used to calculate the binding energy with the experimental structures later incorporating the B3LYP and PBE0 exchange functionals. The hybrid B3LYP and PBE0 show consistent binding energies however the PBE exchange functional shows larger differences from these hybrid functionals.

Class 3 contains the broadest range of counter ions with 4 counter ions incorporating nitrate, chloride, azide bridging and iodine bridging counter ions. Both hybrid functionals predicted the nitrate and azide counterions the strongest bound metal structures and the iodine being the weakest bound metal, **Figure 5-3** and **Figure 5-4**. Whereas the PBE predict the nitrate to be the weakest bound metal with the iodine and the azide being the strongest bound metals, **Figure 5-2**. Which is repeated in the class 2 which contains fewer counter ions these being chloride, nitrate and iodine bridging counter ions. Whereas the B3LYP and PBE0 exchange functional predict the complex incorporating chloride counter ions to be the strongest

bound with the iodine bridging structure being the weakest bound structure, **Figure 5-3** and **Figure 5-4**. In comparison when using the PBE exchange functional the iodine bridging complex is the strongest bound complex with the nitrate complex being the weakest bound, **Figure 5-2** This might be a result of the PBE reduced complexity not reflecting the binding energy correctly, as the PBE exchange correlation functional does not include the Hartree-Fock energies. The PBE exchange functional might not fully reflect the chemical complexity within the metal structures and the secondary interactions that take place within these structures with a more accurate view represented within the hybrid functionals giving a more complete view of the interactions between the molecules. However, the B3LYP maybe exhibiting some over binding that could be a result of the empirical parameterisation of the functional which focus on the thermochemistry of the experimental training set with the training set not incorporating transition metal in the parameterisation of this functional.[84]

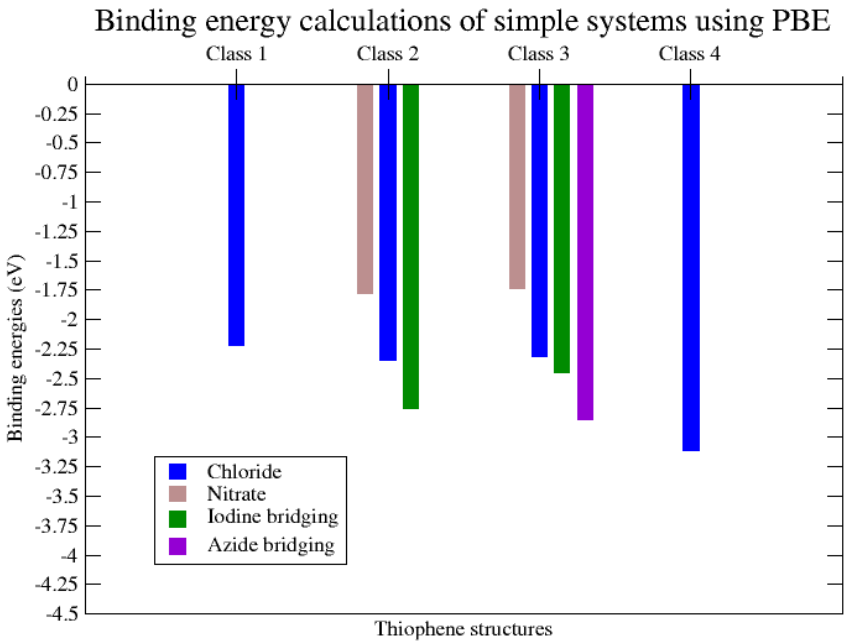

Figure 5-2 Binding energy of experimental copper structures using the PBE exchange functional.

Interactions between the copper and the thiophene ring have been discussed in previous experimental papers[169] due to the moderate distance between the thiophene ring and the metal centre, allowing for secondary interactions. The experimental structures used shows, the distance between the copper and sulphur atom ranges from 3.02 Å through to 4.71 Å, **Table B-5** and **Table B-3**. This distance is within the range for the formation of Cu-S interactions with this being previously cited by S.S. Batsanov to be 3.2 Å.[169] Within the experimental structures 4 of the 8 experimental structures have the thiophene ring within the 3.2 Å radius when optimised (**Table B-1, Table B-3** and **Table B-5**). These secondary interaction will improve the energy of the complex through additional bonding to minimise the energy.

When using the B3LYP exchange-correlation function, the predicted binding energy for some structures is over-estimated. When looking at structure 3 with the nitrate counter ions as when using the PBE and PBE0 exchange functional, the binding energy is predicted to be -1.84 eV and -2.59 eV when compared against the B3LYP, which predicts a binding energy of -4.13 eV which is 2.30 eV larger than PBE and 1.55 eV larger than PBE0, **Table B-1- Table B-6**. The B3LYP exchange functional energy is much greater than those of the comparable structures, indicating that this binding energy is predicted to be unreasonably high; this may be a result of the empirical parameterisation of the B3LYP exchange functional. B3LYP was parameterised on organic molecules;[84] this could be why the binding energy produces differing results from the parameter-free PBE and PBE0 functionals. This difference is not due to the added sophistication due to the addition of Hartree-Fock methods, as both the PBE and PBE0 have more reasonable, and mutually agreeing, energies. The DFT screen could describe the binding energies more completely as there is a greater variation in the binding energies through changing the counter ions involved in the copper binding as the Iodine bridging structure has a much weaker binding energy.

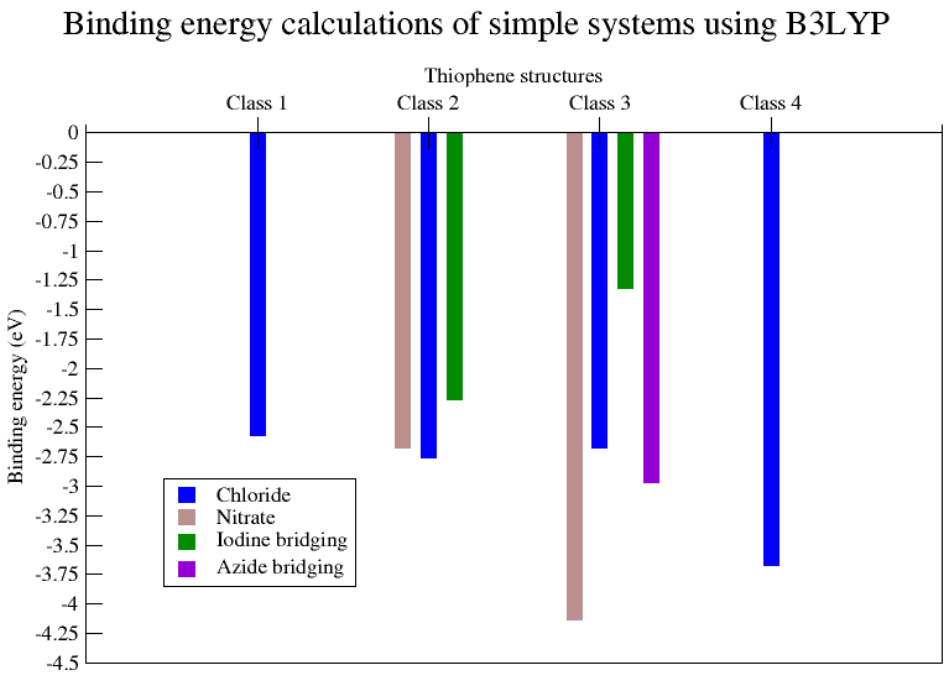

Figure 5-3 Binding energy of experimental copper structures using the B3LYP exchange functional.

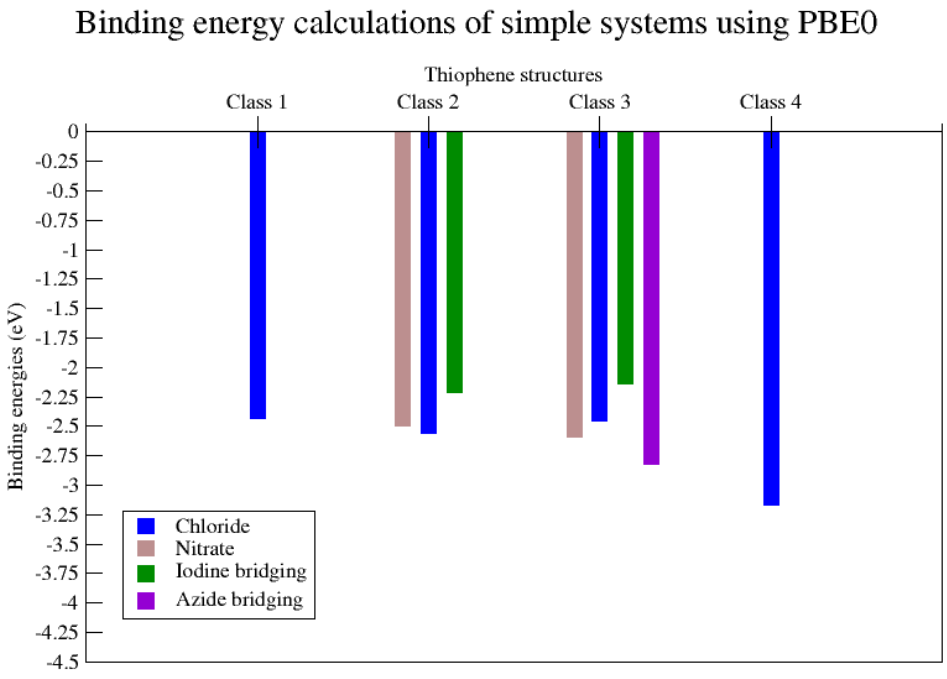

Figure 5-4 Binding energy of experimental copper structures using the PBE0 exchange functional.

5.3.2 Tri-Click thiophene structures

The simple thiophenes classes examined can be used as a structural basis for the more complex TC molecule prepared in this study. This work is built upon the synthesis of a thiophene TC structure through a 'click' reaction between 2-ethynylthiophene and a tris(azidomethyl)mesitylene (triazide) core (**Figure 5-5**).

The use of electrospray ionization mass spectroscopy (ESI-MS) within a 50:50 DMF: water solution containing TC-Thio and three molar equivalents of $Cu(NO_3)_2$ showed the TC-Thio ligand can bind to up to three copper atoms with the presence of the tri-, di- and mono nuclear species identified (**Figure 5-6**). Each fragment was generated through the loss of a single nitrate ion with $[Cu(TC\text{-}Thio)\text{-}(NO_3)]^+$ at 734.07 m/z, $[Cu_2(TC\text{-}Thio)(NO_3)_3]^+$ at 920.98 m/z and $[Cu_3(TC\text{-}Thio)(DMF)(NO_3)]^+$ at 1182.916 m/z with the tri-copper adduct being viewed as the active component.

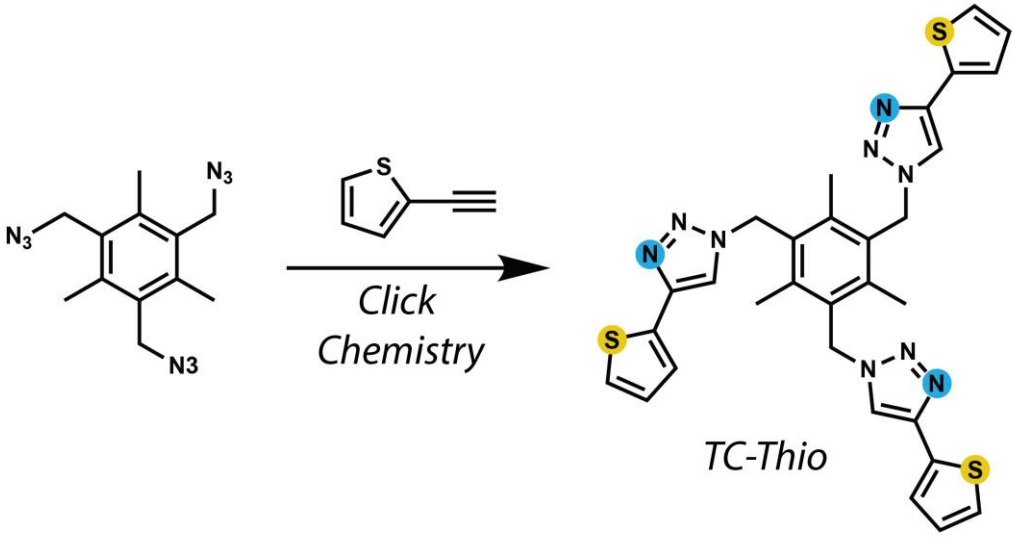

Figure 5-5 Synthesis of the thiophene Tri-Click ligand (TC-Thio)

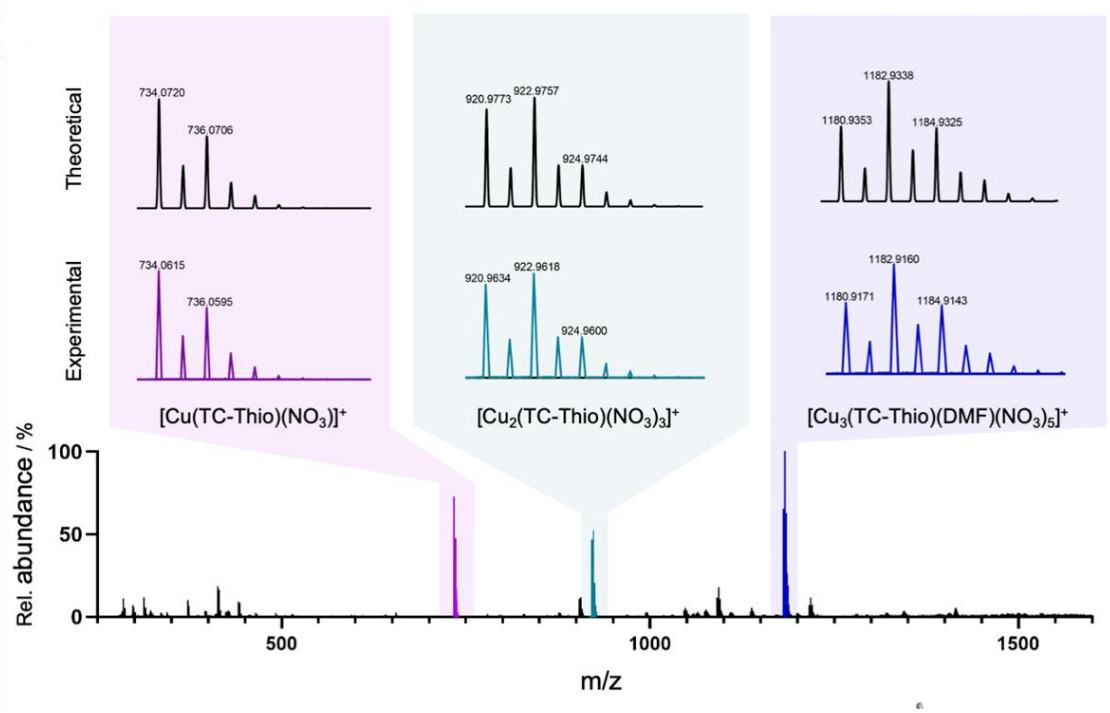

Figure 5-6 Mass spectrum of Cu_3TC-Thio compounds.

Following the production of the trinuclear Cu_3TC-thio complex arising from its exposure to Cu(II) ions, it is possible to reduce Cu(II) to Cu(I) with sodium-*L*-ascorbate to promote oxidative DNA-damaging effects. The strength with which the Cu centre is bound to the Cu_3TC-Thio molecule provides vital knowledge to ensure that the Cu(II) is not lost before DNA binding due to the Cu(II) promoting the binding of the Cu_3TC-thio to the DNA.

The presented work is incorporating the TC-Thio system which was ran with various exchange functionals to obtain a broad view of how these structures are modelled, along with the incorporation of nitrate and water ligands. These various exchange functionals were incorporated to ensure the geometry of the TC-Thio is modelled accurately. Initially, these incorporated one ligand type using nitrate or water ligands with three Cu(II) ions (**Figure B-1**-**B-4**). However, the optimised geometries do not correspond to the identified comparable experimental crystal structures (**Figure 5-7**). Thus, further water molecules were incorporated to replicate experimental conditions as a complete coordination sphere of 5 ligands can bind to the copper structure to achieve experimentally consistent geometries.

Implementing these additional water molecules aided the prediction of experimentally consistent geometries particularly for the Cu(I) structures (**Figure**

5-7). However, due to the limitation of the PBE exchange functionals having a limited description of electronic effects, this is shown through the optimised Cu(I) structure (**Figure B-8, Table B-15**), which has a much-reduced distance between the side-arms with a 7.135 Å distance between the thiophene rings with a 108.49° bond angle so this will incorporate a large amount of bond strain. When compared to the PBE0 geometries (**Figure B-10, Table B-17**), this has 7.327 Å between the thiophene rings and a bond angle of 111.72° between the side-arm and the central ring, so through the implementation of higher-level exchange functionals such as B3LYP and PBE0 (**Figure B-9, Table-B16, Figure B-10, Table B-17**), these achieved a structure that is more consistent with experiment.

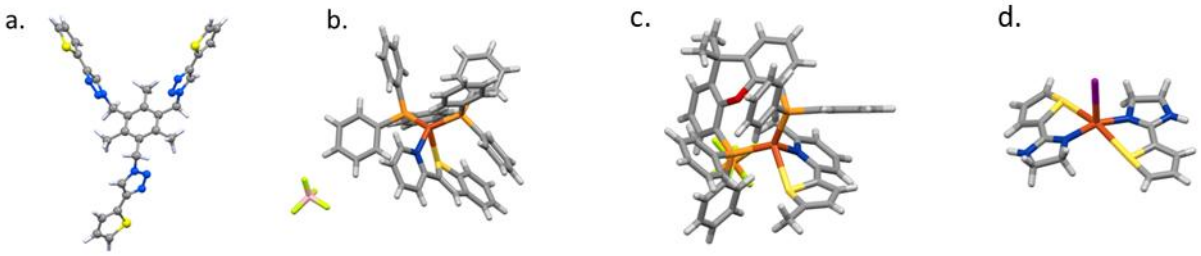

Figure 5-7 Existing experimentally synthesised crystal structures used to refence the input structure of the Cu(I)-TC-Thio from left to right CCDC IDs: QEYTEM, POFQIN and WAPFOM.

When optimising the geometries using the more computationally demanding exchange functional, B3LYP, this model predicted a Cu(II) coordination geometry more akin to square pyramidal than trigonal pyramidal structure. The optimised modelled geometry also shows Cu(I) within the counterion plane, at odds with the known experimental structures.

Subsequently, the PBE0 exchange functional was used test whether the optimised complex geometry achieves better structural similarity to the experimental structures to ensure that the optimised structures can reliably predict the coordination structures. The PBE0 exchange functional is rooted in a parameter free framework. As a result, the optimised geometries with both Cu(II) and Cu(I) showed similarity to the experimental structures (**Figure 5-7**). In particular, the Cu(I) side arms show more experimentally consistent bond angles between the neighbouring side arms.

These angles measured 111.87° and 111.72° between the central benzene ring and the side arm, effectively minimising bond strain. The PBE0 model showed further potential interactions between the Cu(I) ion and the thiophene ring with predicted distances of 2.922 Å, 2.911 Å, and 2.875 Å between the Cu and S atoms. Notably, the experimentally anticipated distorted tetrahedral coordination geometry is maintained through the PBE0 exchange functional. This depiction was absent when employing the B3LYP exchange functional. This is presumably a result of the physical properties not reflecting the geometry of the complex along with the parameterisation set not including transition metals so may not correctly reflect the properties of this parametrisation set.[84]

Each exchange functional shows the expected weakening in binding energy when Cu(II) is reduced to Cu(I). When looking closer into how the difference between the binding energies is affected through the choice of exchange functional, there is a clear distinction between the PBE functional and both hybrid functionals, PBE0 and B3LYP. With a much smaller gap predicted by the PBE functional of 2.8291 eV. In contrast, the B3LYP and PBE0 exchange functionals predict binding energy difference of 3.8268 and 4.2178 eV respectively. This underestimation of the difference between Cu(II) and Cu(I) complex stability for PBE might result from the lower complexity of the PBE not accounting for further electronic effects that could indicate that the Cu(I) is weaker bound within the complex. This is due to the PBE functional predicting a binding energy of -2.1323 eV for the Cu(I), which is 0.9034 eV stronger than the binding energy predicted by PBE0 and 0.6727 eV stronger than the B3LYP predicted binging energy (**Table B-7** and **Figure B-11**).

The PBE0 model predicts weaker binding of Cu(I) to the TC-Thio scaffold than does the B3LYP model. The PBE0 structure has a binding energy of -1.2288 eV per copper unit as opposed to the B3LYP, which has a binding energy of -1.4596 eV per copper unit. This improvement in the binding energy could result from the bridging nitrate ligand within the B3LYP optimised geometry.

5.3.3 Biophysical analysis

Biophysical assays can be used to identify various qualities about the binding of a metallodrug to the DNA structure. These can be analysed using competitive displacement assays, fluorescence melting, circular dichroism spectroscopy (CD), and microscale thermophoresis (MST).[159] The displacement assays identify the affinity and region that the metallodrug binds to the DNA with the use of fluorescent binding agents which only fluoresce when bound to DNA. The intercalating agent ethidium bromide (EtBr) has a well-documented binding affinity, allowing for the calculation of the apparent binding of the metallodrug through reduction in the fluorescence because of the EtBr being displaced. Other fluorescent binding agents can indicate the region with which the metallodrug binds to the DNA through the displacement of the fluorophore. To identify the region which the metallodrug is bound two commonly used binding agents are used these being, Hoechst 34580 and methyl green, which bind within the minor groove and major groove, respectively. When these molecules are displaced, the fluorescence diminishes due to metallodrug binding within this region.[159] Another technique is fluorescent melting which utilises hairpin DNA sequences containing terminal fluorophore and quencher tags that fluoresce when separated due to thermal denaturation. When a metallodrug binds to this hairpin, this alters the temperature with which the DNA structure unzips due to changes on the intrinsic DNA stability.[159] CD spectroscopy measures the helicity of DNA using circular polarised UV light. The technique measures the difference between the absorption intensities between the right and left circularly polarised UV light.[170] B-DNA has two key regions; one positive at ~270 nm and one negative at ~250 nm.[171] These are generated as a result of the asymmetry of the DNA environment.[159] Here the peak at ~250 nm is the signal associated with the helicity of the DNA structure and the peak at ~270 nm is indicative of the base pair stacking interactions.[159] When there is an increase in helicity, this means that the DNA structure has changed, meaning that the DNA structure has wound tighter.[172] A decrease in intensity indicates a loss in helicity so the DNA structure has unwound. Similarly, an increase in the peak at ~270 nm indicates stronger π-π interactions between the base pairs, whereas when these interactions are weaker, the π-π interactions lead to a weaker intensity peak.[159] Microscale thermophoresis (MST) analysis identifies the interactions between a molecule and the DNA structure with this method measuring the time taken for the

DNA structure to be displaced by an infrared laser. When bound, the metallodrug will extend the time a biomolecule takes to migrate from the laser shone on the sample. MST assesses the mobility of the DNA structure along a temperature gradient when bound the metallodrug reduces the mobility of the DNA structure as the mobility is based upon the size, charge and hydration shell of the DNA structure.[173] This means when the metallodrug is bound the detected fluorescence will be reduced allowing for the calculation of the metallodrugs binding affinity to the DNA structure.[174]

The fluorescence quenching shows enhancement to the displacement of ethidium bromide (EtBr) by TC-Thio with increasing concentration of Cu(II) ions. In the presence of three equivalents of Cu(II) ions, Cu_3TC-Thio was identified to have an apparent DNA binding constant of 1.1 x 10^7 M^{-1} (**Figure 5-8b**). This binding constant was additionally calculated using fluorescence melting experiments, which identified that the binding constant, K_b, is 5.8 x 10^7 M^{-1}. This high binding constant shows that the Cu_3TC-Thio tightly binds to DNA with consistency between both K_{app} and the K_b values.

Next, fluorescence melting showed binding within the DNA due to the increase in the thermal melting point (T_m) of the DNA where the unbound DNA has a T_m of 79°C (**Figure 5-8c**), which increased dependent upon the dose of the Cu_3TC-Thio that is indicative of the Cu_3TC-Thio binding to the DNA structure promoting the stability of the DNA structure enabling higher temperatures to be reached before degrading.

The competitive fluorescence displacement method indicates the site where Cu_3TC-Thio potentially occupies within the DNA duplex. This was shown to be the minor groove due to greater displacement of Hoechst 34580 compared to methyl green (**Figure 5-8b**). This shows the minor groove residency since Hoechst 34580 is a known fluorescent minor groove binder whereas methyl green is a known fluorescent major groove binder.

CD data indicates that there are both reductions in the π-π stacking interactions of the nucleic acid bases and the helicity of the Dickerson-Drew Dodecamer (DDD) hairpin. This shows potential DNA condensation effects associated with exposure to Cu_3TC-Thio with reductions at 250 nm and 280 nm (**Figure 5-8e**) demonstrating non-intercalative interactions consistent with minor groove recognition by the

complex. These non-intercalative and minor groove recognition result in the loss of helicity hence the reduced intensity at 250 and 280 nm.

Finally, MST measurements were conducted to enable the quantification of molecular interactions based upon the movement of the molecule within a temperature gradient induced by a laser. For Cu_3TC-Thio exposed to the DDD hairpin sequence, the point at which half of the effective concentration, EC_{50}, was calculated to be ~70 μM (**Figure 5-8f**). Experiments also showed characteristics of DNA condensation earlier identified with both CD and competitive fluorescence melting experiments. This was later confirmed through analysis of the initial MST fluorescence signal with a dose dependant signal decrease.

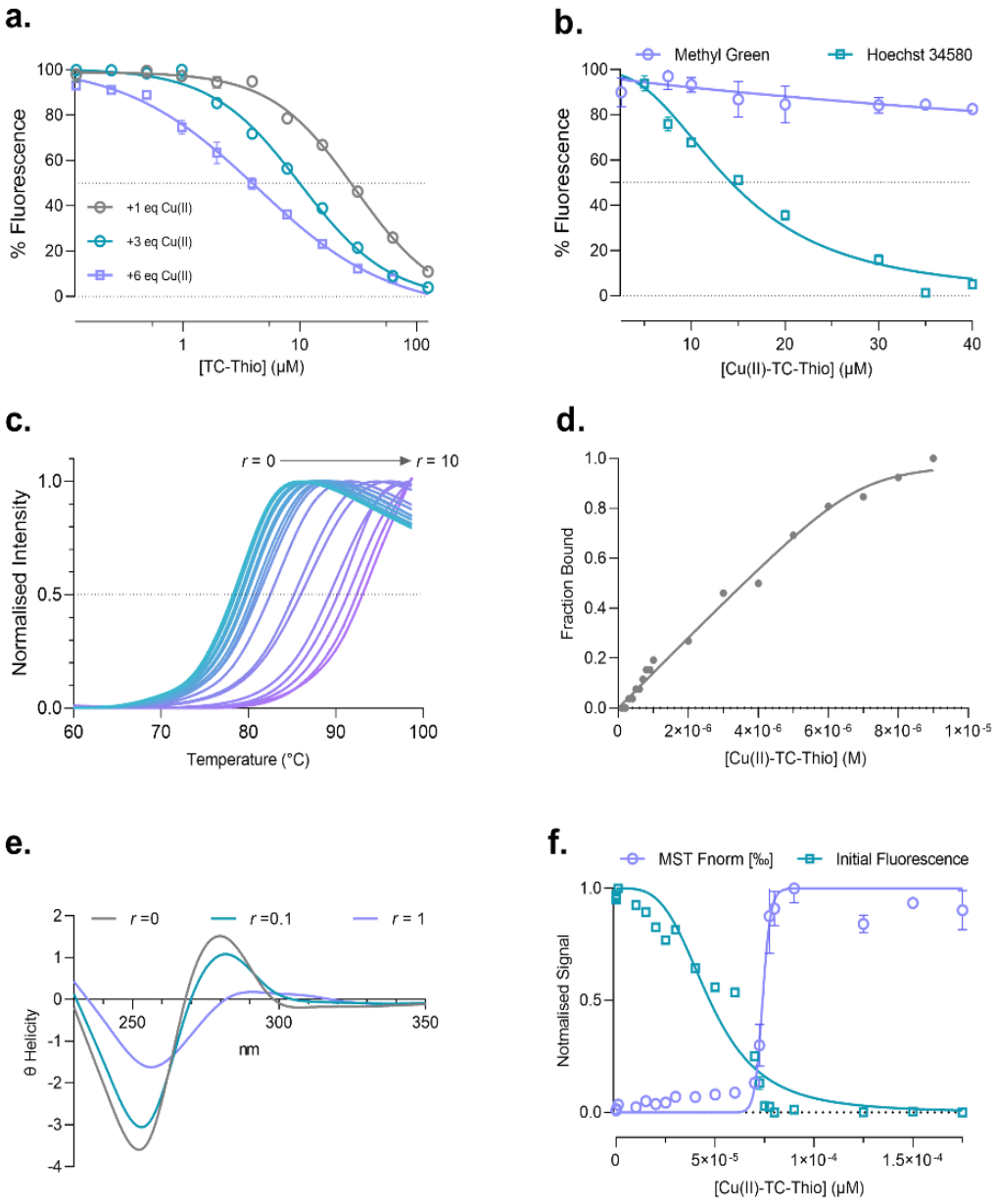

Figure 5-8a. Displacement assay of Ethidium bromide (EtBr) from DNA by TC-Thio in 2 and 3 equivalent of Cu(II) nitrate (the graph of 3 equivalents was used to calculate K_{app}=1.1×10^{7}Mbp). **b.** Competitive displacement of minor groove binder Hoechst 34580 and major groove binder methyl green from DNA. **c.** Fluorescence melting of DNA with increasing Cu_3TC-Thio loading, T_m is taken as the midpoint of the normalised melting curve **d.** Fitting of Bard equation with the fluorescence melting data obtained in c. **e.** CD analysis of DNA in the presence of 0.0, 0.1 and 1.0 equivalents of Cu_3TC-Thio. **f.** Normalised data and initial intensity data obtained from MST experiments conducted with DNA.

5.3.4 Modelling complex-DNA Binding

To confirm the binding mode that has been assumed through the biophysical analysis, we modelled the binding of the molecules to DNA using the AutoDock Vina molecular docking program utilising the synthetic DNA Dickerson-Drew dodecamer, DDD. Using the AutoDock tools the atomic tools, and rotatable bonds were defined within the flexible Cu_3-TC-Thio. The rigid DNA receptor was treated through removal of the solvent molecules, incorporating missing hydrogen atoms and assigning atomic charges. To enable the Cu_3TC-Thio to dock within the entire DNA fragment the grid boxes were sized to incorporate the full fragment. This grid box model enables the prediction of the strongest binding poses. Though scoring ligand-receptor binding affinity which are added through the implementation of Gasteiger–Marsili atomic charges[175] these consider the orbital electronegativity and the hybridisation to generate a electrostatic potential through the summation of all atomic electronic densities within the molecule.[176] These binding predictions are calculated through the summation of the interaction functions over all atomic pairing excluding 1-4 interactions which are atoms separated by 3 covalent bonds which allow the movement of these atoms relative to each other. This enables the calculation of both intermolecular interactions and intramolecular interactions this allows for the binding affinity and rank confirmations to be determined.[168] These are calculated through the implementation of van der Waals like potentials defined through two Gaussian functionals and a repulsive term along with nondirectional hydrogen bonding and hydrophobic terms and a conformational entropy penalty.[177] Ten docking conformations were produced and ranked in accordance with their stability utilising AutoDock Vina's scoring function.

Of these ten docking conformations, all show minor groove recognition with no major groove residency within the most stable configurations. The computed structures (**Figure 5-9)** indicate the Cu1 binds within the minor groove between the initial cytosine and guanine on strand A, binding to the cytosine groups carbonyl group and the oxygen group of the guanine group. The second copper is bound to the phosphate chain, binding to the phosphate group and the subsequent bridging oxygen. The third copper binds within the minor groove, binding to the cyclic oxygen

group within the sugar group and the bridging oxygen group on the phosphate backbone between the fifth and sixth base pairs. Both the first and third copper groups expose the sugar groups through rotation of these groups with the DNA receptor treated as a rigid structure. This Cu_3TC-Thio interaction could initiate condensation through the Cu binding to the phosphate group.

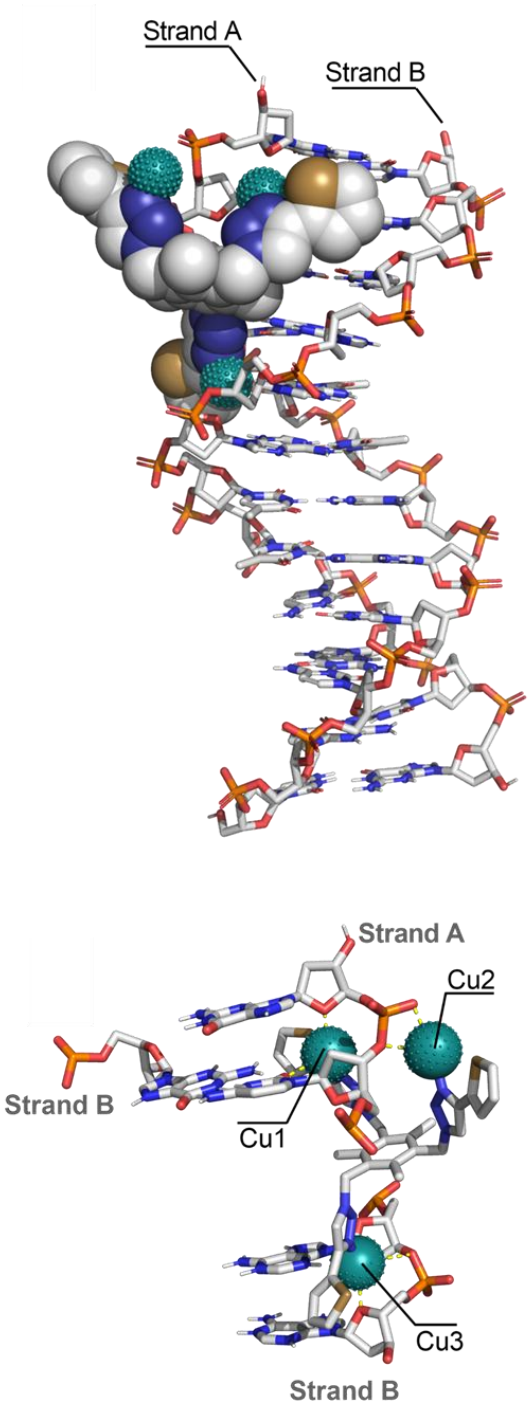

Figure 5-9 Best ranked pose of docking simulations conducted using the Dickerson–Drew dodecamer (PDB:1BNA) as the receptor and Cu_3TC-Thio (in space-filling representation) as the ligand.

5.4 Conclusion

The PBE method is a reliable initial step that allows for the quick generation of starting models for new complexes. Calculations enable a geometry close to the experimentally seen geometries for metal complex structures, with the binding energies being predicted close to the PBE0 energies that include Hartree Fock energies. By contrast, the B3LYP functional produced a broad variation in the binding energies. These energies might be artificially inflated through the over binding that appears to present within the copper systems.

This work confirms weak interactions between the copper and the thiophene ring in the computed structures. For the more complex systems with multiple copper ions, the structures are generally predicted close to experiment when using the Cu(II) for the metal centres. However, the reduced Cu(I) provided a significantly greater challenge with two of the three models predicting unreasonable geometries. It was shown there is systematic weakening of the binding strength of Cu(I) when compared to Cu(II) metal ion coordination strength.

The biophysical analysis validates the computational model that predicted the binding within the minor groove of duplex DNA. This was further validated using various biophysical analytical methods displaying the minor groove binding properties of Cu_3TC-Thio. Overall, it appears that the computational methods employed here provide reliable predictions of artificial metallonuclease binding to DNA.

Chapter 6 Binding energy of an extended series of Tri-Click structures

The density functional theory work on all extended series of Tri-Click structures was performed by me. The synthesis of the Tri-Click pyridine structure was performed by Dr Alex Gibney from the Kellett group in Dublin City University. Molecular dynamics work was performed by Dr Lilly Arrué and Dr Shayon Bhattacharya from University of Limerick

6.1 Introduction

Metallodrugs can be used in a broad range of applications such as anti-cancer, antitumor, antibacterial, antimicrobial, and malarial treatments.[178–181] When applied to a pharmaceutical context these metallodrugs operate through the targeting and damage of the DNA sequence.[182] These drug-DNA interactions are typically initiated by a pre-associative electrostatic attraction between the cationic metallodrug and the anionic DNA phosphate backbone. Following pre-association, the drug-DNA binding can take place through one of three distinct non-covalent modes of: groove binding; intercalation (including semi-intercalation); and insertion.[159,183] Groove binding occurs when the drug sits between the phosphate chains in either the major or minor groove. Insertion and intercalation binding modes differ to groove binding as they involve hydrophobic interactions between planar, heteroaromatic, ligands within the metal complex and the nucleobases present within DNA. The insertion and intercalation binding modes are different as insertion binding mode ejects one base pair which is replaced by the incoming complex, whereas the intercalation binding mode promotes the unwinding of the DNA's helical structure and inserting the ligand between the nucleotide base pairs without displacing the base pairs from the core helical axis.[159]

One prominent example of a commonly used metallodrug is the active form of the glycopeptide, bleomycin. Bleomycin chelates Fe(II) in the presence of oxygen and a one-electron reductant to form the active bleomycin-Fe(II)-OOH that then catalyses DNA cleavage.[184] Activated-bleomycin has shown clear clinical success with applications for the treatment of both testicular cancer and non-Hodgkin's lymphoma when treated with a number of combination therapy chemotherapy protocols. when used in combination with cisplatin and etoposide, the treatment of testicular cancer can be 90% curative showing an improvement from the 25% cure rate of cisplatin and etoposide alone.[184,185] Activated-bleomycin typically binds in a multi-modal fashion with intercalation from the minor groove, and subsequent production of reactive oxygen species that ultimately causes cleavage of the phosphodiester backbone.[184,186] Bleomycin induces both single and double strand breaks - single strand breakages are promoted by H_2O_2 whereas the double strand breakages are promoted by O_2. Here there has been previous work showing

preferential single strand breakages by activated-bleomycin with the ratio of single strand to double strand breaks between 6:1 and 20:1.[184,186]

Activated Bleomycin is an example of an artificial metallonuclease (AMN). AMNs target and cleave the DNA backbone through two distinct mechanisms: hydrolytic and oxidative.[187] Hydrolytic AMNs act via Lewis acid activation of water, promoting nucleophilic attack to the phosphodiester.[188] As hydrolytic AMNs mimic the mechanism of enzymatic AMNs, so too do the cleavage products which can be repaired by ligase enzymes.[188] Oxidative AMNs, however, act via activation of oxygen species which produce radical oxygen species allowing for the generation of reactive oxygen species (ROS) which then damages the DNA structure. Many oxidative lesions can be formed, but hydrogen atom abstraction from the C4' on the ribose ring can trigger radical formation and through a series of reactions ultimately results in cleavage of the backbone. The exact site of oxidation is highly reliant on the proximity of the redox-active metal involved, which is directed by the associated ligand.[157,187,189] Oxidative AMNs can undergo several mechanisms to generate suitable ROS for oxidative damage that resemble Fenton and superoxide dismutase (SOD) activity,[165] but differ in that they react using metal-oxo intermediates rather than diffusible ROS. It has been found that molecules incorporating multiple metal centres have greater oxidative damage efficiency than comparable scaffolds incorporating a single metal centre.[190]

When designing AMNs, the metal centre can be selected based on its biologically accessible redox properties combined with low toxicity and high bioavailability. Commonly used metals found within AMNs include iron, copper, magnesium and zinc.[191,192] These metals are chosen to increase the likelihood of being absorbed by the body due to the presence of these metals within nature while minimising the effects on off-target biological pathways.[158] While the metal centre serves to partake in the redox cycling required for AMN activity, the ligand carrying the metal centre plays a key role in ensuring ROS production occurs in the vicinity of DNA. As such, the literature contains an abundance of highly varied and complex ligand structures used in AMN design. Most recently, AMN design has been simplified with the use of click chemistry as outlined in **section 5.1**.[165,193]

The strength that the metal centre is bound to the Tri-Click scaffold can be explored using density functional theory (DFT) as described in **Chapter 5**. The stability of the complexes will be influenced through alterations to the terminal group which in combination with the 1,2,3-triazole group generated within the click mechanism will bind the metal centre to the Tri-Click AMN scaffold. Previous modelling studies have explored the electronic structures and properties of both tri-copper structures[193] and di-copper structures.[194] The molecular DFT models use basis sets to model the valence electronic structure, typically double-hybrid basis sets, such as PWPB95, ωB97M(2), revDSD-PBEP86-D4.[195] Relativistic corrections[196] can be used for heavier elements starting from ruthenium.[197] The Ahlrichs basis sets second default-triple zeta valence potential (def2-TZVP) basis set has been shown to have very small mean errors and standard deviation at approximately 0.02 eV $atom^{-1}$ up to second-row transition metals, indicating that it is suited for predictive DFT modelling.[198] Exchange-correlation functionals are used together with the basis set to implement and iteratively solve the Kohn-Sham equations. The PBE functional typically gives good accuracy for organic structures,[199] with the higher level hybrid PBE0 functional suitable for metal-organic molecules.[193] One of the most used functionals, B3LYP, has been shown in previous work to underestimate the energies of polynuclear complexes.[194]

In this chapter, the aim is to expand upon the previously reported work on click chemistry based AMNs, including TC-1 and TC-Thio, as DNA damaging agents,[193] and to predict the structures of AMNs with a wider range of alternative terminal groups. These predictive models aim to identify the scaffold that provides the strongest binding between the scaffold and the metal centre. This extended series of Tri-Click structures includes carboxylate, pyridine, and pyrimidine terminal groups, which allows us to identify key structural features that promote the binding of the metal center to the scaffold. To assess the suitability of the extended series of these Tri-Click structures as DNA damaging agents these were synthesized and further biophysical characterization applied with molecular dynamics simulations used to support the experimental binding properties.

6.2 Methods

6.2.1 Binding energy calculations

Six Tri-Click complexes were modelled using the ORCA 5.0.4 software, with the structures optimised in implicit water using the conductor-like polarizable continuum model (CPCM).[200–202] The electronic structure calculations were performed with tight self-consistent field (SCF) convergence criteria of 2.7×10^{-7} eV and the geometry convergence tolerance energy change tolerance being 1.4×10^{-4} eV and root mean squared (RMS) convergence gradient being 5×10^{-3} eV/Å. The molecular orbitals were built from the def2-TZVP basis set, with the def2/J auxiliary basis set used for density fitting. The DFT calculations used the PBE0 exchange coefficient functional[88] with the Grimme D3 dispersion correction and Becke-Johnson dampening.[118] This enables the calculation of the energy of the full complex, E_{AB}. The optimised geometry was then separated into the scaffold and their metallic components. The energies of the ligand and metallic components, E_A and E_B, respectively, were subsequently taken using single-point calculations. Following these calculations, the geometries were treated with a geometry counterpoise correction (gCP) to reduce the effect of basis set superposition error.[89,90] To confirm that the structures generated were experimentally viable, the Cambridge Crystallographic Datacentre (CCDC) mogul search tool was used. This identified if the computed geometry is within the range of previously reported experimental structures.

6.2.2 DNA Binding by Fluorescence Displacement

Competitive ethidium bromide displacement was conducted as previously reported.[203] Using a triplicate serial dilution of test compound prepared on a 96 well plate to a volume of 50 µL. 50 µL of a working solution of EtBr (25.2 µM) and ctDNA (25 µM) was then added to give a final volume of 100 µL, 12.5 µM EtBr, 12.5µM ctDNA. All solutions were prepared in 80mM HEPES, 25 mM NaCl, 5% DMSO. Control wells contained EtBr and ctDNA at equivalent concentration to the test. Blank wells contained EtBr only in the same buffer. The binding apparent binding strength was calculated with **Equation 6-1**.

$$K_{app} = (8.8 \times 10^6 M^{-1}) \left(\frac{12.5}{C_{50}}\right)$$

Equation 6-1 Calculation of the apparent binding constant

Within **Equation 6-1** is calculated as the is the EtBr binding constant is $8.8x10^6$ and the concentration of the EtBr is 12.5 and the C_{50} is the micromolar concentration of copper Tri-Click complex to reduce the EtBr fluorescence by 50% with the K_{app} being the apparent binding constant. Experiments conducted with Hoechst 34580 and Methyl green (MG) were conducted under equivalent conditions but with 5 μM fluorophore. Data was collected on a TECAN® Spark microplate reader. Fluorescence quenching of MG and Hoechst 34580 were conducted in an equivalent manner but with final fluorophore concentrations of 5 μM. Excitation emission wavelengths used were 530/590 nm for EtBr, 350/450 nm for Hoechst 34580 and 630/670 for MG.

6.2.3 DNA Cleavage Experiments

Cleavage reactions were prepared to a final volume of 20 μL in 100 μL Eppendorf tubes and contained 400 ng supercoiled pUC19 DNA, 1 mM Na-*L*-ascorbate (where indicated) and 25 mM NaCl in 80 mM HEPES buffer (pH = 7.4). Cleavage reactions with ROS scavengers were prepared to contain 10 mM of the ROS scavenger by addition of 1 μL of a 200 mM stock solution prior to DNA addition. Reactions probing the cleavage site were prepared by preparing reaction mixtures to contain 16 μM and 8 μM MG and netropsin respectively from stock solutions prepared in 80 mM HEPES buffer (pH = 7.4). Upon addition of pUC19 the samples were incubated for 30 minutes at 37 °C, quenched with 6x loading dye (Thermo Fisher R0611) and loaded on to a 1.3 % agarose gel, prepared using 1x TAE buffer and run at 70 v for 90 min.

6.2.4 Molecular Dynamics

Molecular dynamics (MD) simulations were performed using the GROMACS-2018.4 code.[204,205] The topology and parameters for the DNA model was defined by the CHARMM36m classical mechanics force field.[206] The topology and parameters for Cu_3-TC-Pyridine (Cu_3-TC-Pyr) were obtained from Density Functional Theory (DFT)

calculations using the Gaussian 16 package followed by charge fitting with Antechamber7 using Restrained Electrostatic Potential (RESP) calculations.[207]

The Cu_3-TC-Pyr DNA complex was solvated in a large cuboid of TIP3P water molecules with counterions added to balance any formal charge. 0.15 M NaCl was added to model physiological salt concentration. Energy minimisation was followed by thermalisation at 298 K and equilibration under constant volume (NVT) and then constant pressure (NPT) of 1 bar of pressure these enable the calculations to be ran at physiological conditions to allow for the maintenance of physically realistic DNA structures. Production MD simulations were carried out for 4 μs for each complex, starting with Cu_3-TC-Pyr in the minor groove or Cu_3-TC-Pyr in the major groove, for a total of 8 μs of free dynamics.

6.3 Results and Discussion

6.3.1 Extended Tri-Click structures

A small library of TC ligands was studied to evaluate the binding efficiency of copper ions to the organic scaffold, **Figure 6-1**. These ligands were experimentally produced and were rationally designed AMNs that aim to enhance the metal binding from the previously established polynuclear AMNs, such as the TC-1 and TC-Thio scaffolds, **Figure 6-1a**.[165] The AMNs were designed with various terminal groups that can be easily attached to a central 1,3,5-*tris*(azidomethyl)-2,4,6-trimethylbenzene (tri-azide) group through a click chemistry mechanism. The terminal groups bind copper ions with differing strengths to the organic scaffold. This strength can be calculated using **Equation 6-2**:

$$B.E. = E_{AB} - E_A - E_B$$

Equation 6-2 Equation for the calculation of binding energy

This expression evaluates the stability of the complete optimised complex E_{AB} relative to the isolated metal-free organic scaffold, E_A, and the isolated metal, E_B. The charge and spin multiplicity of each complex is carefully set to account for different metal redox states. To compensate for basis set superposition error, a final

geometry counterpoise correction, gCP, is included. These were modelled incorporating the solvent through the through the incorporation of CPCM water and explicit nitrate and water molecules as within the previous work that is incorporated within this thesis this aided in obtaining experimental consistent geometries.

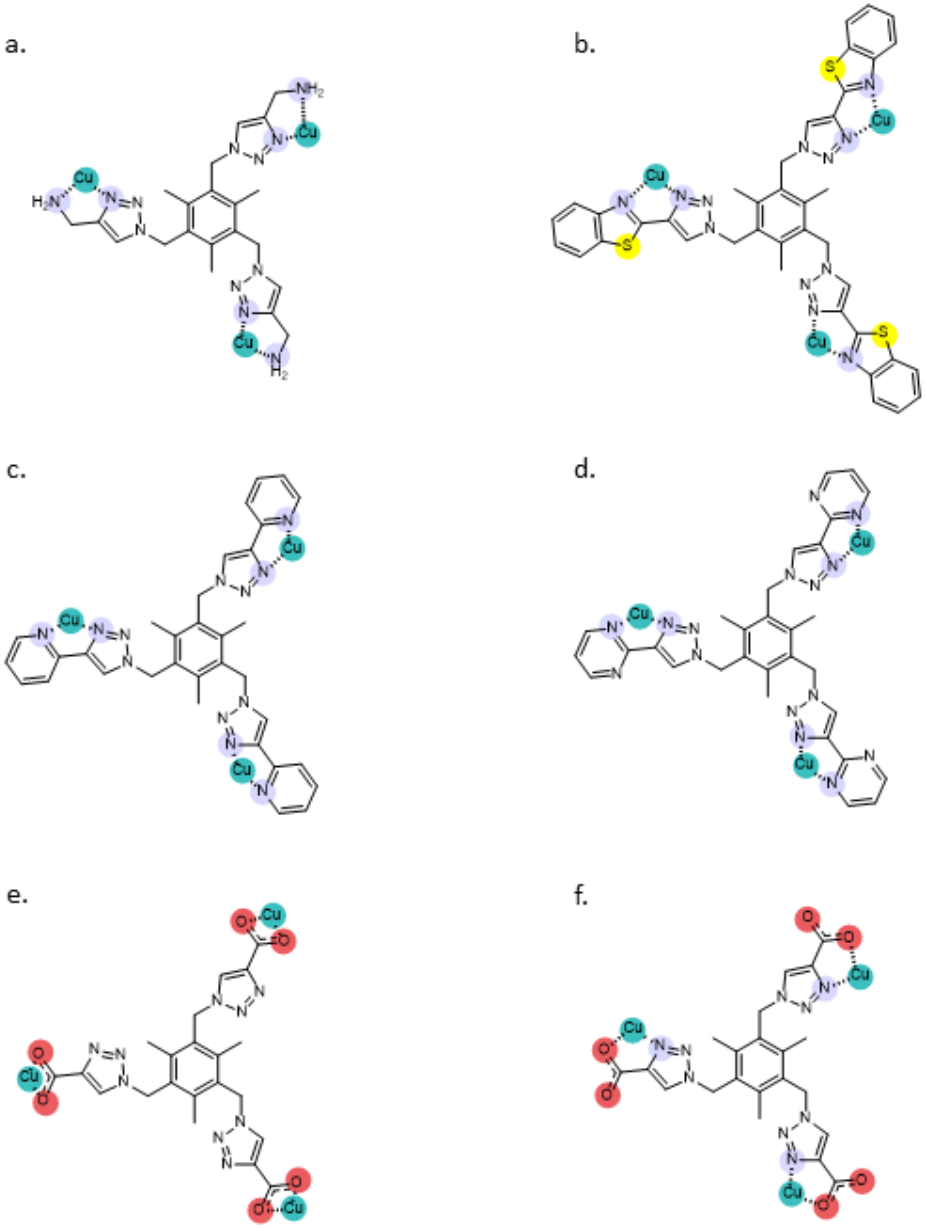

Figure 6-1 Structures of Tri-Click ligands synthesised using CuAAC click chemistry.

6.3.2 Extended series geometries

The computationally generated Cu(II) complexes show close similarity to earlier reported experimental structures. Previously reported structures indicated bond angles ranging between 105.00 and 118.73° for the C-C-N bond angle between the central mesitylene ring and the triazole group, as measured from 720 structures retrieved from a Mogul search on the CCDC. All our computed geometries fall within this range of C-C-N bond angles, indicating formation of physically realistic structures (**Table 6-1**). These structures correspond to the structures depicted within **Figure 6-1** with explicit solvent molecules included as shown in **Figure 6-2**. The Cu---N triazole coordination contacts in the Cu(II) complexes range between 1.96 and 2.00 Å, and were extended by 0.07 ± 0.15 Å in the corresponding weaker-bound Cu(I) complexes.

Table 6-1 C-C-N bond angle

Extended TC structures	bond angles for Cu(II) (°)			bond angles for Cu(I) (°)		
TC-1	110.0	110.7	112.3	111.0	111.0	108.6
TC-Benzothiazole	107.9	111.1	111.3	108.2	109.6	109.3
TC-Pyridine	110.8	112.6	107.5	110.5	106.3	108.3
TC-Pyrimidine	110.7	111.2	111.3	108.7	108.7	109.7
TC-Carboxylate (O-Cu-O binding)	112.2	111.4	114.1	109.5	109.0	111.3
TC-Carboxylate (N-Cu-O binding)	110.9	110.2	110.9	109.9	108.8	110.3

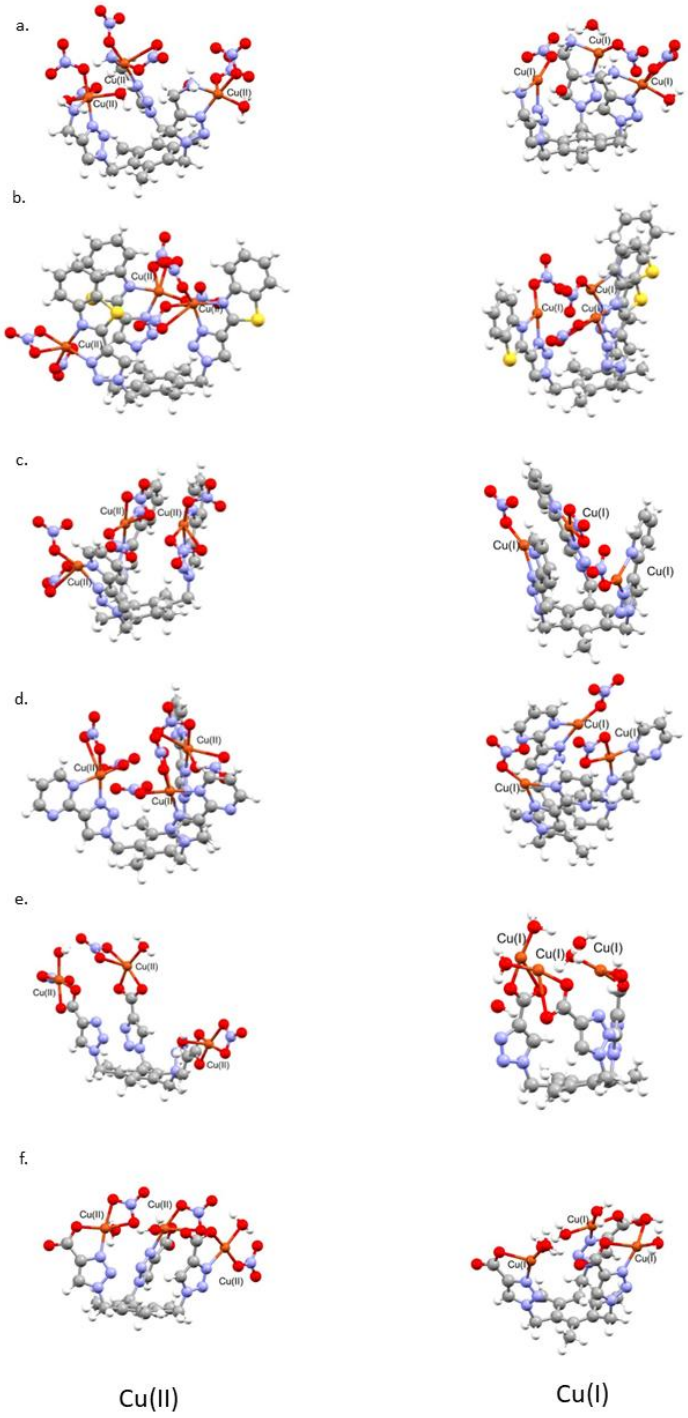

Figure 6-2 (a) Optimised TC-1 structure (**Table C-1, Table C-2**). **(b)** Optimised TC-Benzothiazole structure (**Table C-3, Table C-4**). **(c)** Optimised TC-Pyridine structure (**Table C-5, Table C-6**) **(d)** Optimised TC-Pyrimidine structure (**Table C-7, Table C-8**). **(e)** Optimised TC-Carboxylate structure with O-Cu-O binding (**Table C-9, Table C-10**) **(f)** Optimised TC-Carboxylate structure with N-Cu-O binding (**Table C-11, Table C-12**).

6.3.3 Extended series binding energy

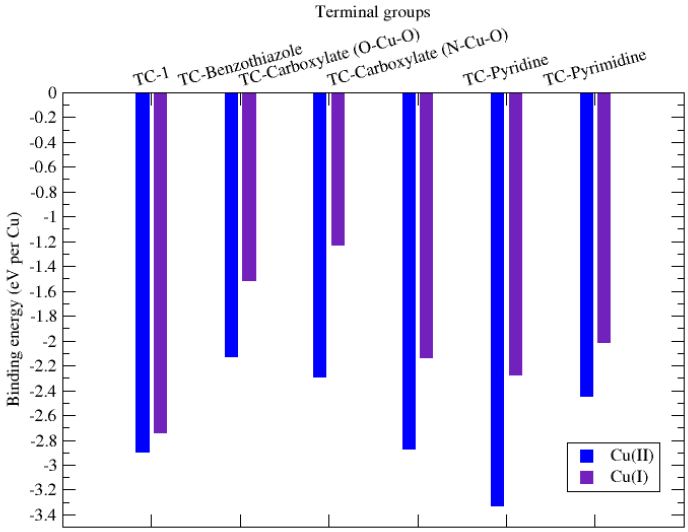

Figure 6-3 Calculated binding energy of the extended series of Tri-Click structures.

Each Tri-Click ligand showed comparable binding within ± 0.76 eV of the parent Tri-Click structure (TC-1) (**Figure 6-1a**). The TC-1 scaffold binds copper to the ligand with -2.89 eV per Cu and the extended series examined here demonstrate an average binding energy of -2.55 ± 0.53 eV per Cu, with the weakest binding energy being the TC-Benzothiazole (**Figure 6-1b**) of -2.12 eV per Cu (**Figure 6-3**). This lower binding energy could be attributed to the electron-withdrawing nature of the ligand resulting in weaker binding to the metal ion. Differences in electron density are illustrated in **Figure 6-4** and show the pyrimidine group has a lower electron density compared to the pyridine group upon binding to copper. This is reflected by the darker shading on the binding amine group of TC-Pyridine (**Figure 6-4a**), while the TC-Pyrimidine group shows lighter shading on the amine (**Figure 6-4b**). The lighter shading indicates that the electron density in TC-Pyrimidine is more evenly distributed across both amine groups. As a result, the binding strength of the pyrimidine is reduced.

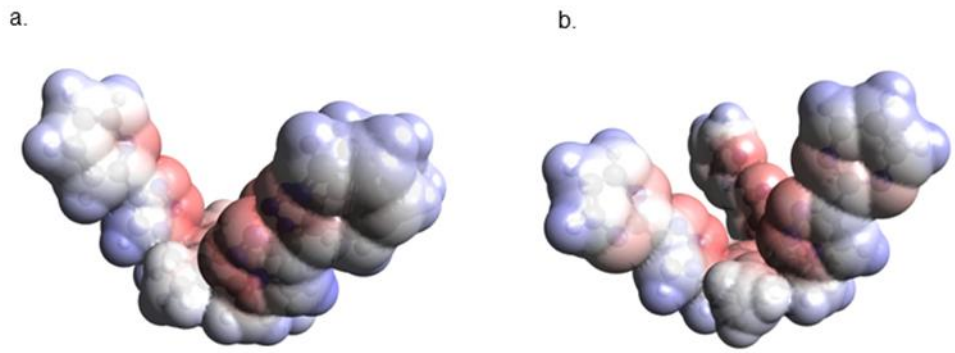

Figure 6-4(a) Electrostatic potential of TC-Pyridine generated using Avogadro (Iso value 0.1)[208,209]. (**b)** Electrostatic potential of TC-Pyrimidine generated using Avogadro (Iso value 0.1).[208,209]

There is a clear energetic preference for the TC-Pyridine scaffold over the TC-Pyrimidine scaffold (**Figure 6-3**), of 1.18 eV per Cu ion. This could be due to the electron density localised on a singular nitrogen group within the TC-Pyridine group instead of the TC-Pyrimidine group, which will distribute the electron density across both amine groups (**Figure 6-4**). This would mean that within the pyridine donor, the charge within this group would be concentrated on this amine group, allowing for a greater charge differential with the metal group, enhancing the binding.

Within the TC-carboxylate scaffold there is two possible binding regions. One is to both oxygens on the carboxylate group (**Figure 6-1e**) and the other is chelated between the N-triazole group and a carboxylate oxygen (**Figure 6-1f**). Of these two possibilities, our data predicts a preference of 0.58 eV per Cu for binding between the triazole and carboxylate. The Cu binding energy is weakened by 0.62 ± 0.38 eV per Cu when the metal is reduced from Cu(II) to Cu(I). We note that the weakest bound Cu(I) metal ion in the TC-Carboxylate scaffold retains a significant binding strength of -1.23 eV per Cu ion, indicating that the metal can be reduced to generate DNA damaging reactive oxygen species without dissociation.

6.3.4 DNA binding of the extended Tri-Click series

Fluorescent displacement assays were performed as they provide a simple and rapid method to assess the binding properties of the Tri-Click complexes. These assays measure the reduction in emission spectrum when the complex is introduced, displacing the fluorophore. This reduction in emission occurs due to the fluorophore, only able to fluoresce when bound, being ejected by the complex. This study involved well established fluorophores, ethidium bromide (EtBr), Hoechst-34580 (Hoechst), and Methyl Green (MG), to evaluate the affinity and regioselectivity of Cu(II) Tri-Click complexes. Here the major groove is occupied by Hoechst-34580 and the minor groove is occupied by MG this is further outlined in **Section 5.3.3**.

Fluorescent displacement assays using Hoechst and MG showed that the Hoechst 34580 was more efficiently displaced than MG. The Cu_3-TC-Pyr complex showed the most efficient displacement of both Hoechst 34580 and MG fluorophores of the extended TC series (**Figure 6-5**). These fluorophore displacement assays show that with the entire class of extended Tri-Click structures preferentially displaced the Hoechst 34580 over the MG this showing selectivity for the minor groove (**Figure 6-5**). Here, the apparent binding constant ranges from 3.6×10^6 to 5.8×10^7 M^{-1} with Cu_3-TC-Pyr having the strongest DNA binding constant. Due to Cu_3-TC-Pyr having an exceptionally high DNA binding strength with groove binding capabilities, the complex was subsequently modelled with both molecular docking and molecular dynamics methods to identify its binding mode to DNA.

Complex	C_{50}	K_{app}	$Q_{Hoechst}$	Q_{MG}
Cu(II)-TC-Acid	13.3 ± 0.1	8.3×10^6	89.19 ± 13.7	183.0 ± 32.5
Cu(II)-TC-Pyrm	7.8 ± 0.1	1.4×10^7	13.2 ± 0.7	23.8 ± 1.8
Cu(II)-TC-Pyr	1.9 ± 0.2	5.8×10^7	12.0 ± 1.2	22.7 ± 1.5
Cu(II)-TC-Benzo	30.2 ± 0.1	3.6×10^6	69.32 ± 6.3	181.6 ± 22.3

Figure 6-5 Fluorescence quenching experiment results. C_{50}, $Q_{Hoechst}$ and Q_{MG} are the concentrations of Cu-TC needed to reduce fluorescence of EtBr, Hoechst and MG respectively

As a result of the fluorescence displacement experiments indicating the standout DNA binding agent of this series is Cu_3-TC-Pyr, molecular docking studies were undertaken on a Cu_3-TC-Pyr model complex with the Dickerson-Drew dodecamer (DDD) using AutoDock Vina.[168] Cu_3-TC-Pyr was prepared by first removing solvent from the DFT structure. Atomic charges and rotatable bonds within Cu_3-TC-Pyr with the copper being a Cu(II) to characterise binding the initial binding to the DDD-DNA structure were defined in Autodock tools (version 1.5.7). The DNA receptor was prepared by removing water molecules, building in missing hydrogen atoms, and assigning atomic charges. Subsequently the grid boxes were sized to incorporate the entire DNA fragment as the rigid body and run in AutoDock Vina.[168] Here, Cu_3-TC-Pyr was found to bind predominantly in the minor groove with eight of the docking output poses showing binding within the minor groove and one pose showing major groove binding. **Figure 6-6a** shows that the binding of the Cu_3-TC-Pyr is highly dependent upon the minor groove dimensions of the target DNA structure**.**

Molecular dynamics simulations were run using the GROMACS-2018.4 code to allow for the flexing of the DNA structure as displacement assays indicate that the Cu_3-TC-Pyr has both minor and major groove these molecular dynamic simulations allow for structural changes within the DNA such as axial rise, pitch, helical diameter in addition to short-lived base flipping and total molecule kinking. Structural changes can be influenced by sequence composition, buffer environment, temperature and binding within the DNA. These structural changes can influence the dimensions of the grooves which could influence the binding strength of the Cu_3-TC-Pyr. Here, the starting positions were taken from the highest ranked major and minor groove generated through the Autodock Vina molecular docking poses. The still frames shown in **Figure 6-6b** and **c** indicate the minor and major groove simulations respectively. Here, the Cu_3-TC-Pyr remains bound within the starting groove of the duplex. Two arms of the complex remaining bound within the groove while the third arm is ejected and binds to the phosphate backbone. Alongside this analysis, **Figure 6-6b** and **c**, shows Cu_3-TC-Pyr causes kinking of the DNA groove to allow for stronger complex-DNA interactions, showing a major limitation of the rigid body molecular docking method which does not allow for flexing of the DNA structure.

When looking at the energetic contribution within the simulation, it is shown that most of the binding comes from Coulombic interactions (**Figure 6-6d** and **e**) this could be a result of the complex being highly cationic in nature and the anionic nature of the DNA structure. Here the total energies are increased when bound within the minor groove due to the van der Waals contribution increasing when bound within the minor groove, supporting the experimental findings that Cu_3-TC-Pyr has minor groove selectivity.

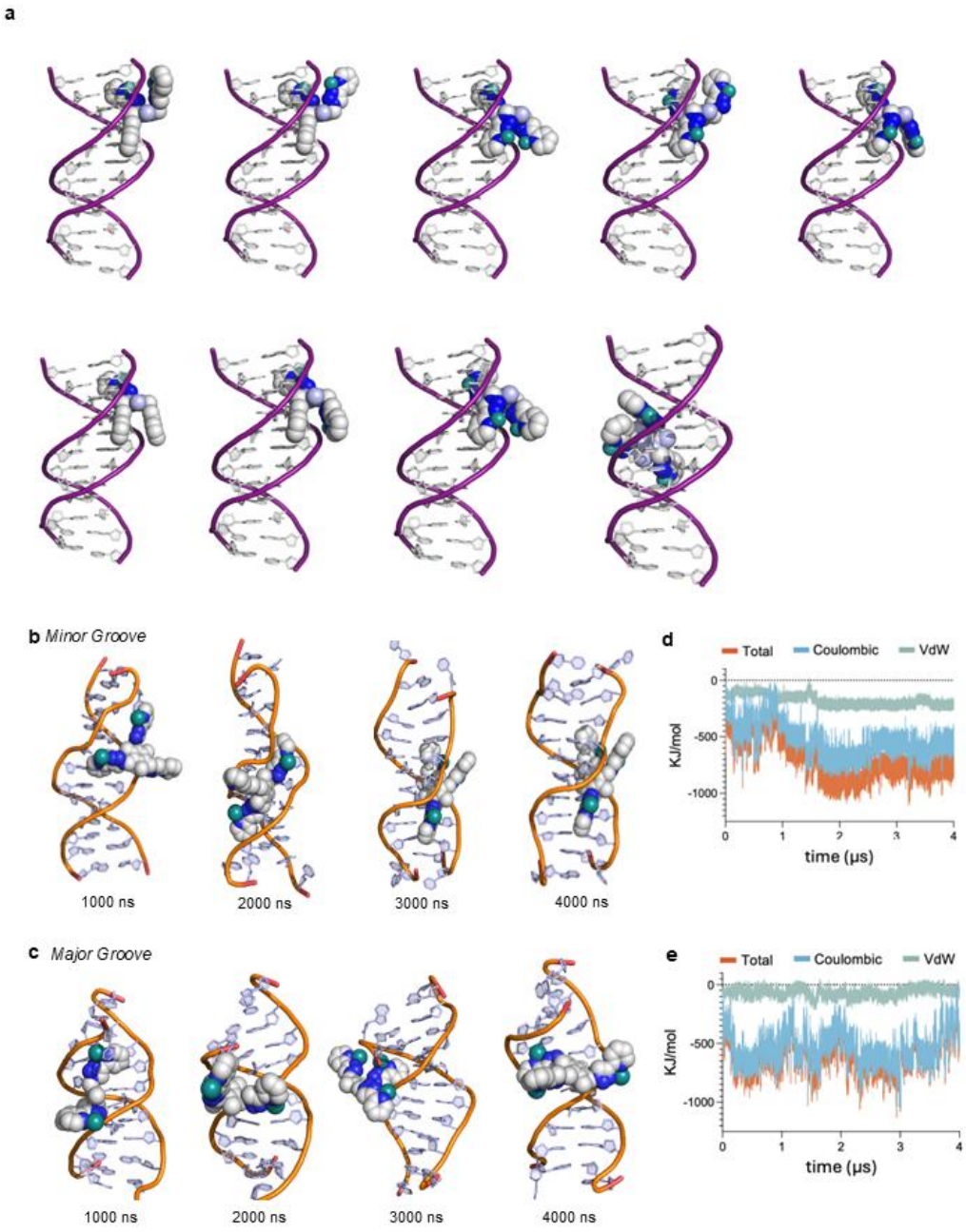

Figure 6-6(a) Nine output poses from docking studies of DNA (PDB: 1BNA) with modelled Cu_3TC-Pyr. **(b)** Still frames from molecular dynamics simulations of Cu_3TC-Pyr bound in the minor groove of duplex DNA (PDB: 1BNA) **(c)** still frames from molecular dynamics simulations of Cu_3TC-Pyr bound in the major groove duplex DNA (PDB: 1BNA) **(d)** Interaction energies over the course of molecular dynamics simulation of Cu_3TC-Pyr bound in the minor groove shown in **(b)**.**(e)** Interaction energies over the course of molecular dynamics simulation of Cu_3-TC-Pyr bound in the major groove shown in **(c)**.

6.3.5 AMN activity of Cu_3-TC-Pyr

Electrophoretic mobility shift assays (EMSAs) offer a simple and convenient method of analysing the activity and damage mechanism of the Cu_3-TC-Pyr. In these experiments, supercoiled pUC19 DNA is damaged and visualised using agarose gels. The initial form I supercoiled pUC19 can move quickly through the gel due to its compact shape and high charge density. When a single strand break (SSB) occurs this produces form II the open circular form of DNA which has reduced gel mobility due to its larger size and flexibility. When two proximal SSBs occur on opposite strands of the duplex this further relaxes the DNA structure producing the form III which is the linearised form which has less resistance than the open circular form allowing for greater migration through the agarose.[159] Each of these forms produce distinct diffusion profiles within the gel due to the different forms migrating through the gel differently. pUC19 plasmid DNA when treated with increasing Cu_3-TC-Pyr concentrations with sodium-*L*-ascorbate (to allow for redox cycling). Using band densitometry**, Figure 6-7,** shows that the Cu_3TC-Pyr gradually coverts the supercoiled pUC19 from Form I to Form II finally converting to Form III. **Figure 6-7** confirms the AMN activity of Cu_3TC-Pyr is consistent with prior click and cut AMNs.[165,193] Along with this it can be seen the formation of linear form III prior to the complete degradation of the supercoiled form I indicating the Cu_3-TC-Pyr is initiating independent double strand breakages.

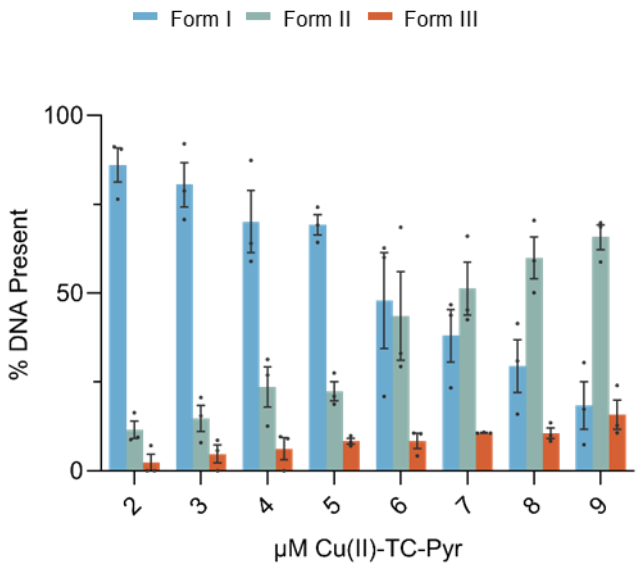

Figure 6-7 Plots of band densitometry values obtained from pUC19 cleavage experiments. Individual values shown as dots.

To identify the cleavage mechanism through cleavage experiments in the presence of DNA binding agents and antioxidants (**Figure 6-8**). Cleavage experiments in the presence of the major groove binding agents, MG showed a significant increase in the cleavage activity of Cu_3-TC-Pyr while cleavage was completely inhibited by netropsin, a known minor groove binding agent, **Figure 6-8a**. Antioxidant experiments, **Figure 6-8b**, next showed that cleavage was maximally inhibited by tiron, a superoxide stabiliser ($O_2^{\bullet-}$) and *N,N*-dimethyl thiourea (DMTU) a peroxide scavenger (H_2O_2). There was minimal inhibition by *L*-methionine and the hypochlorous acid (HOCl) scavenger, sodium azide (NaN_3) which protects against singlet oxygen ($^1O_2$) and *D*-mannitol a hydroxyl radical ($^{\bullet}OH$) scavenger. These cleavage experiments indicate that Cu_3-TC-Pyr mediated DNA damage occurs predominantly within the minor groove involving a Fenton/Haber-Weiss catalytic cycle.

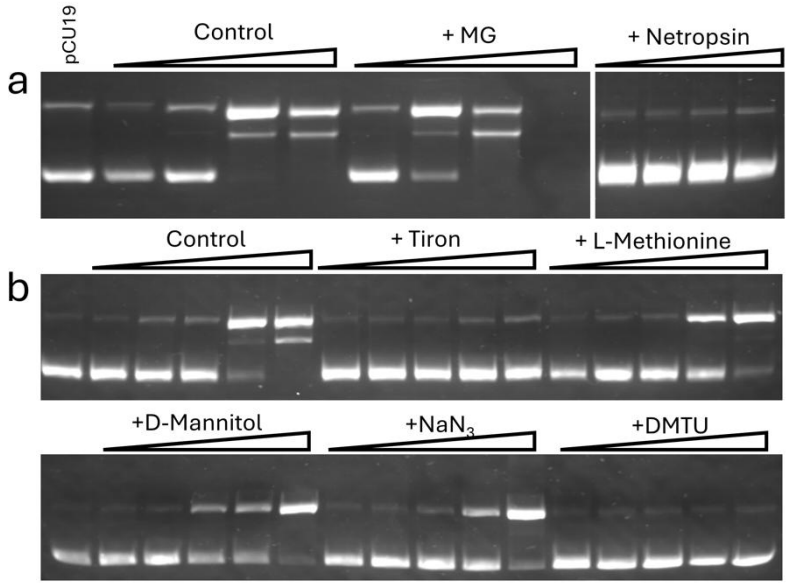

Figure 6-8 (a) Cleavage experiments in the presence of groove blocking agents, methyl green (16 µM) and netropsin (8 µM). Wedges above gels indicate increasing Cu_3TC-Pyr concentrations of 4, 6, 8 and 10 µM. Lane 1 contained pUC19 DNA only. Control ramp contained pUC19 DNA and Cu_3TC-Pyr only with no groove blocking agent. **(b)** DNA cleavage experiment in the presence of antioxidants (10mM). Each wedge indicates increasing Cu_3TC-Pyr concentration at 2, 4, 6, 8, 10 µM. Lane 1 contained pUC19 DNA only. The control gradient contained Cu_3TC-Pyr and pUC19 with no antioxidant. All experiments contained 1 mM Na-L-ascorbate.

6.4 Conclusion

An extended series of Tri-Click scaffolds beyond TC-1 was rationally designed with various terminal donor groups capable of coordinating copper. Cu(II) complexes were invariably more stable than their corresponding Cu(I) analogues. The Tri-Click pyridine ligand (TC-Pyr) when exposed to Cu(II) gave the most stable complexes, and this design rule was further extended to exclude carboxylate terminal groups, thiophene, and additional pyridyl sites in the scaffold. In collaborative testing using fluorescence displacement assays Cu_3-TC-Pyr showed the strongest DNA binding of the extended structures. Cu_3-TC-Pyr demonstrated some minor groove selectivity with some binding within the major groove validated through the use of classical molecular dynamics. The DNA damage mechanism was assessed to be oxidative as a result of using ROS scavenger agents, with a primary single-strand breaking mechanism linked to the production of superoxide. ROS inhibition studies through specific scavengers indicates a Fenton/Haber-Weiss chemistry-type mechanism. Overall, this chapter illustrates the growing ability to reliably predict stable metal complexes, specifically here AMN structures through electronic structure calculations, and pass these predicted stable structures to downstream classical molecular dynamics models to predict target binding, specifically DNA minor groove binding, and experimental tests of stability, binding and drug action.

Chapter 7 Conclusion & Outlook

The work presented within this thesis attempts to fill the knowledge gap on co-crystals with the use of density functional theory (DFT) and density functional tight binding models (DFTB) to predict the enthalpy of the co-crystal structures using a variety of dispersion corrections, showing that the DFT can predict the thermodynamics of co-crystal structures accurately. Along with DFTB models unable to predict the thermodynamics of co-crystals accurately, with large discrepancies between the expected thermodynamics of the experimental co-crystal structures; these have large structural differences between the experimental and the DFTB output geometries. This showed that the dispersion correction and exchange-correlation is essential to identify molecular features that aid co-crystal stability.

The co-crystal work shown within this thesis indicated that dispersion corrected DFT models can reliably predict the formation of co-crystal structures using lattice enthalpies. This work showed that the PBE-TS method showed the most accurate prediction of co-crystal formation with the smallest change from the initial experimental structures and the majority of the co-crystal's structures having a favourable negative lattice enthalpy. However, within this work only binary co-crystal structures were incorporated, these binary co-crystals feature only two different constituent chemical structures, because of limited computational time and resources. The inclusion of higher order co-crystals would be useful to identify how these different structures stability is altered when further chemical structures are incorporated within the crystal structure.[210] This should allow for further hydrogen bonding synthons when incorporating further chemical structures within the more co-crystal structures which together with stronger van der Waals interactions within the crystal structure may improve the lattice enthalpy.

The calculations presented in this thesis indicate that many co-crystal structures are thermodynamically stable. However, at present, the contribution of kinetics in co-crystal structures remains unknown. Some structures predicted to be unstable by the methods used here may be in the future corrected through free-energy calculations incorporating thermal effects as these are optimised at 0 K. The free-energy calculations could be calculated using the phonon calculations available within CASTEP, or other less resource intense programs, such as PHONOPY. These calculations can give the entropic contributions for the co-crystal structure

and the single component crystals to gain a perspective on the Gibbs free energy of the crystal structure to establish if the co-crystal structure forms spontaneously at non-zero temperatures, inferring if the co-crystal structure is thermodynamically stable or kinetically stable.

Within this work the structure of metal complexes was identified; this was done as these structures could not be experimentally crystallised. Along with the models showing that they can be applied to an already synthesised extended series of Tri-Click systems with both Cu(II) and Cu(I) coordination spheres. This enables a gain in the energetic perspective of how strongly the metal binds to the Tri-Click ligand. Here the ESI-MS suggests that the Tri-Click thiophene forms the mono- and di-copper structures along with the tri-copper structure. To enable understanding of how the interaction between the metals centres affects the binding of the copper metal through spin-orbit coupling. These metal-metal interactions along with structural features of the ligand could affect the binding of the metal to the ligand. These binding energy calculations will give an idea of the strength that the metal is bound to the ligand showing the extent with which these influence the binding properties. Further this should allow for future engineering of alternative artificial metallonuclease drugs that will benefit from the enhanced binding developed within this work.

This work has also identified key structural features within the Tri-Click model which aid in the coordination of the Cu(II) metal centre. This knowledge will prevent the loss of the metal centre promoting the DNA damage effects of the artificial metallonuclease (AMN) structures within the body. The generation of experimentally comparable structures using computational models allows for the accurate modelling of the DNA-drug interactions and identifying the region which the AMN binds to. This work should be expanded to include the experimental generation of all the structures modelled. This will allow for confirmation of the modelled geometries and the modelled drug-DNA interaction. This modelling work will allow for the identification of influence of the terminal group on the DNA binding strength and the DNA binding region. This could be further expanded to incorporate further terminal groups that will aid in the backbone binding of the Tri-Click structure, as predicted through the molecular dynamics simulations showing that longer terminal

groups can provide stronger DNA binding to the AMN scaffold through more extensive contacts with the phosphate backbone.

References

1 Z. Hao and A. Iqbal, Some aspects of organic pigments, *Chemical Society Reviews*, 1997, **26**, 203.

2 J. Yang, C. T. Hu, X. Zhu, Q. Zhu, M. D. Ward and B. Kahr, DDT Polymorphism and the Lethality of Crystal Forms, *Angew. Chem. Int. Ed.*, 2017, **56**, 10165–10169.

3 G. Zhanga, D. Lawa, E. A. Schmittb and Y. Qiub, phase transformation considerations during process development and manufacture of solid oral dosage forms – A review, *Advanced Drug Delivery Reviews*, 2004, **56**, 371–390.

4 R. Chang and J. Overby, in *Chemsitry*, 2019, pp. 483–487.

5 S. L. Morissette, S. Soukasene, D. Levinson, M. J. Cima and Ö. Almarsson, Elucidation of crystal form diversity of the HIV protease inhibitor ritonavir by high-throughput crystallization, *PNAS*, 2003, **100**, 2180–2184.

6 P. Vishweshwar, J. A. Mcmahon, J. A. Bis and M. J. Zaworotko, Pharmaceutical Co-Crystals, 2006, **95**, 499–516.

7 S. Karki, T. Friščić, L. Fabián, P. R. Laity, G. M. Day and W. Jones, Improving mechanical properties of crystalline solids by cocrystal formation: new compressible forms of paracetamol, *Advanced Materials*, 2009, **21**, 3817–3957.

8 L. S. Taylor, D. E. Braun and J. W. Steed, Crystals and Crystallization in Drug Delivery Design, *Molecular Pharmaceutics*, 2021, **18**, 751–753.

9 A. V. Yadav, A. S. Shete, A. P. Dabke, P. V. Kulkarni and S. S. Sakhare, Co-crystals: A novel approach to modify physicochemical properties of active pharmaceutical ingredients, *Indian Journal of Pharmaceutical Sciences*, 2009, **71**, 359–370.

10 S. Datta and D. J. W. Grant, Crystal structures of drugs: Advances in determination, prediction and engineering, *Nature Reviews Drug Discovery*, 2004, **3**, 42–57.

11 A. T. Florence and D. Attwood, in *Physicochemical Principles of Pharmacy, 5th edition*, 2011, pp. 8–42.

12 M. Omar, P. Makary and M. Wlodarski, A Review of Polymorphism and the Amorphous State in the Formulation Strategy of Medicines and Marketed Drugs, *UK Journal of Pharmaceutical Biosciences*, 2015, **3**, 60.

13 B. M. Couillaud, P. Espeau, N. Mignet and Y. Corvis, State of the Art of Pharmaceutical Solid Forms: from Crystal Property Issues to Nanocrystals Formulation, *ChemMedChem*, 2019, **14**, 8–23.

14 E. Vrani, Amorphous pharmaceutical solids, *BJBMS*.

15 L. Yu, Amorphous pharmaceutical solids: preparation, characterization and stabilization, *Advanced Drug Delivery Reviews*, 2001, **48**, 27–42.

16 S. R. Vippagunta, H. G. Brittain and D. J. W. Grant, Crystalline solids, *Advanced Drug Delivery Reviews*, 2001, **48**, 3–26.

17 P. Dandekar, Z. B. Kuvadia and M. F. Doherty, Engineering Crystal Morphology, *Annu. Rev. Mater. Res*, 2013, **43**, 359–386.

18 P. L. Toutain and A. Bousquet-Mélou, Bioavailability and its assessment, *Vet Pharm & Therapeutics*, 2004, **27**, 455–466.

19 C. C. Sun, A classification system for tableting behaviors of binary powder mixtures, *Asian Journal of Pharmaceutical Sciences*, 2016, **11**, 486–491.

20 D. Braga, L. Casali and F. Grepioni, The Relevance of Crystal Forms in the Pharmaceutical Field: Sword of Damocles or Innovation Tools?, *Int. J. Mol. Sci*, DOI:10.3390/ijms23169013.

21 P. A. Wood, N. Feeder, M. Furlow, P. T. A. Galek, C. R. Groom and E. Pidcock, Knowledge-based approaches to co-crystal design, *CrystEngComm*, 2014, **16**, 5839–5848.

22 N. D. Blelloch, H. T. Mitchell, C. C. Tymm, D. W. Van Citters and K. A. Mirica, Crystal Engineering of Molecular Solids as Temporary Adhesives, *Chem. Mater*, 2020, **32**, 9882–9896.

23 K. Honer, E. Kalfaoglu, C. Pico, J. Mccann and J. Baltrusaitis, Mechanosynthesis of Magnesium and Calcium Salt − Urea Ionic Cocrystal Fertilizer Materials for Improved Nitrogen Management, *ACS Sustainable Chem. Eng*, 2017, **5**, 8546–8550.

24 S. G. Bratsch, A group electronegativity method with Pauling units, *Journal of Chemical Education*, 1985, **62**, 101–103.

25 W. B. Jensen, Electronegativity from Avogadro to Pauling: II. Late Nineteenth- and Early Twentieth-Century Developments, *J. Chem. Educ.*, 2003, **80**, 279.

26 A. Nangia and G. R. Desiraju, Supramolecular Synthons and Pattern Recognition.

27 A. M. Healy, Z. A. Worku, D. Kumar and A. M. Madi, Pharmaceutical solvates, hydrates and amorphous forms: A special emphasis on cocrystals, *Advanced Drug Delivery Reviews*, 2017, **117**, 25–46.
28 P. Atkins and J. de Paula, in *Physical Chemistry*, 2002, pp. 444–445.
29 P. Atkins and J. de Paula, in *Physical Chemistry*, 2002, p. 700.
30 S. Aitipamula, R. Banerjee, A. K. Bansal, K. Biradha, M. L. Cheney, A. R. Choudhury, G. R. Desiraju, A. G. Dikundwar, R. Dubey, N. Duggirala, P. P. Ghogale, S. Ghosh, P. K. Goswami, N. R. Goud, R. R. K. R. Jetti, P. Karpinski, P. Kaushik, D. Kumar, V. Kumar, B. Moulton, A. Mukherjee, G. Mukherjee, A. S. Myerson, V. Puri, A. Ramanan, T. Rajamannar, C. M. Reddy, N. Rodriguez-Hornedo, R. D. Rogers, T. N. G. Row, P. Sanphui, N. Shan, G. Shete, A. Singh, C. C. Sun, J. A. Swift, R. Thaimattam, T. S. Thakur, R. K. Thaper, S. P. Thomas, S. Tothadi, V. R. Vangala, N. Variankaval, P. Vishweshwar, D. R. Weyna and M. J. Zaworotko, Polymorphs, Salts, and Cocrystals: What's in a Name?, *Crystal Growth & Design*, 2012, **12**, 2147–2152.
31 J. W. Steed, The role of co-crystals in pharmaceutical design, *Trends in Pharmacological Sciences*, 2013, **34**, 185–193.
32 K. Kersten, R. Kaur and A. Matzger, Survey and analysis of crystal polymorphism in organic structures, *IUCrJ*, 2018, **5**, 124–129.
33 A. J. Cruz-Cabeza and J. Bernstein, Conformational polymorphism, *Chem. Rev*, 2014, **114**, 2170–2191.
34 D. K. Bučar, R. W. Lancaster and J. Bernstein, Disappearing Polymorphs Revisited, *Angewandte Chemie - International Edition*, 2015, **54**, 6972–6993.
35 L. Ai Nguyen, H. He and C. Pham-Huy, Chiral Drugs. An Overview, *Int. J Biomed Sci.*, 2006, **2**, 85–100.
36 J. H. Kim and A. R. Scialli, Thalidomide: The tragedy of birth defects and the effective treatment of disease, *Toxicological Sciences*, 2011, **122**, 1–6.
37 C. E. Housecroft and A. G. Sharpe, in *Inorganic Chemistry*, 2001, p. 287.
38 S. D. Parent, P. A. Smith, D. K. Purcell, D. T. Smith, S. J. Bogdanowich-Knipp, A. S. Bhavsar, L. R. Chan, J. M. Croom, H. C. Bauser, A. McCalip, S. R. Byrn and A. Radocea, Ritonavir Form III: A Coincidental Concurrent Discovery, *Crystal Growth & Design*, 2023, **23**, 320–325.

39 M. Mortazavi, J. Hoja, L. Aerts, L. Quéré, J. van de Streek, M. A. Neumann and A. Tkatchenko, Computational polymorph screening reveals late-appearing and poorly-soluble form of rotigotine, *Communications Chemistry*, 2019, **2**, 70.

40 I. A. Olson, A. G. Shtukenberg, B. Kahr and M. D. Ward, Dislocations in molecular crystals, *Rep. Prog. Phys.*, 2018, **81**, 096501.

41 R. Smoluchowski, DISLOCATIONS IN IONIC CRYSTALS (Structure, Charge Effects and Interaction with Impurities), *Le Journal de Physique Colloques*, 1966, **27**, C3-3-C3-11.

42 C. A. Hunter and R. Prohens, Solid form and solubility, *BJBMS*, 2017, **19**, 23–26.

43 D. Cheuk, D. Khamar, P. McArdle and Å. C. Rasmuson, Solid Forms, Crystal Habits, and Solubility of Danthron, *Journal of Chemical & Engineering Data*, 2015, **60**, 2110–2118.

44 D. Sun, W. Gao, H. Hu and S. Zhou, Why 90% of clinical drug development fails and how to improve it?, *Acta Pharmaceutica Sinica B*, 2022, **12**, 3049–3062.

45 P. Prabakaran, B. Umadevi, P. Panneerselvam, P. T. Muthiah, G. Bocelli and L. Righi, Conformational pseudo-polymorphism and hydrogen bonding: benzthiazide anhydrate and monohydrate, an antihypertensive drug, *CrystEngComm*, 2003, **5**, 487–489.

46 R. Censi and P. Di Martino, Polymorph impact on the bioavailability and stability of poorly soluble drugs, *Molecules*, 2015, **20**, 18759–18776.

47 M. D. Eddleston, R. Thakuria, B. J. Aldous and W. Jones, An investigation of the causes of cocrystal dissociation at high humidity, *Journal of Pharmaceutical Sciences*, 2014, **103**, 2859–2864.

48 G. Kuminek, F. Cao, A. Bahia De Oliveira Da Rocha, S. G. Cardoso and N. Rodríguez-Hornedo, Cocrystals to facilitate delivery of poorly soluble compounds beyond-rule-of-5, *Adv Drug Deliv Rev*, 2016, **101**, 143–166.

49 S. Kalepu and V. Nekkanti, Insoluble drug delivery strategies: Review of recent advances and business prospects, *Acta Pharmaceutica Sinica B*, 2015, **5**, 442–453.

50 O. N. Kavanagh, D. M. Croker, G. M. Walker and M. J. Zaworotko, Pharmaceutical cocrystals: from serendipity to design to application, *Drug Discovery Today*, 2019, **24**, 796–804.

51 A. A. Dar and S. Rashid, Organic co-crystal semiconductors: a crystal engineering perspective, *CrystEngComm*, 2021, **23**, 8007–8026.

52 R. Kumar Bandaru, S. R. Rout, G. Kenguva, B. Gorain, N. A. Alhakamy, P. Kesharwani and R. Dandela, Recent Advances in Pharmaceutical Cocrystals: From Bench to Market, *Front. Pharmacol.*, DOI:10.3389/fphar.2021.780582.

53 C. Guo, Q. Zhang, B. Zhu, Z. Zhang, X. Ma, W. Dai, X. Gong, G. Ren and X. Mei, Drug–Drug Cocrystals Provide Significant Improvements of Drug Properties in Treatment with Progesterone, *Crystal Growth & Design*, 2020, **20**, 3053–3063.

54 J.-R. Wang, Q. Yu, W. Dai and X. Mei, Drug–drug co-crystallization presents a new opportunity for the development of stable vitamins, *Chem. Commun.*, 2016, **52**, 3572–3575.

55 M. Guo, X. Sun, J. Chen and T. Cai, Pharmaceutical cocrystals: A review of preparations, physicochemical properties and applications, *Acta Pharmaceutica Sinica B*, 2021, **11**, 2537–2564.

56 H. Young and R. Freedman, in *University Physics*, 2000, pp. 1360–1361.

57 T. E. of E. Britannica, Piezoelectricity.

58 R. A. Wiscons, N. R. Goud, J. T. Damron and A. J. Matzger, Ferroelectric Materials Room-Temperature Ferroelectricity in an Organic Cocrystal, *Angew. Chem. Int. Ed.*, 2018, **57**, 9044–9047.

59 S. L. Price, Predicting crystal structures of organic compounds, *Chemical Society Reviews*, 2014, **43**, 2098–2111.

60 S. Aitipamula, P. S. Chow and R. B. H. Tan, Polymorphism in cocrystals: a review and assessment of its significance, *CrystEngComm*, 2014, 3451–3465.

61 D. A. Bardwell, C. S. Adjiman, Y. A. Arnautova, E. Bartashevich, S. X. M. Boerrigter, D. E. Braun, A. J. Cruz-Cabeza, G. M. Day, R. G. Della Valle, G. R. Desiraju, B. P. Van Eijck, J. C. Facelli, M. B. Ferraro, D. Grillo, M. Habgood, D. W. M. Hofmann, F. Hofmann, K. V. J. Jose, P. G. Karamertzanis, A. V. Kazantsev, J. Kendrick, L. N. Kuleshova, F. J. J. Leusen, A. V. Maleev, A. J. Misquitta, S. Mohamed, R. J. Needs, M. A. Neumann, D. Nikylov, A. M. Orendt, R. Pal, C. C. Pantelides, C. J. Pickard, L. S. Price, S. L. Price, H. A. Scheraga, J. Van De Streek, T. S. Thakur, S. Tiwari, E. Venuti and I. K. Zhitkov, Towards crystal structure prediction of complex organic compounds - A report on the fifth

blind test, *Acta Crystallographica Section B: Structural Science*, 2011, **67**, 535–551.

62 A. M. Reilly, R. I. Cooper, C. S. Adjiman, S. Bhattacharya, A. D. Boese, J. G. Brandenburg, P. J. Bygrave, R. Bylsma, J. E. Campbell, R. Car, D. H. Case, R. Chadha, J. C. Cole, K. Cosburn, H. M. Cuppen, F. Curtis, G. M. Day, R. A. DiStasio, A. Dzyabchenko, B. P. Van Eijck, D. M. Elking, J. A. Van Den Ende, J. C. Facelli, M. B. Ferraro, L. Fusti-Molnar, C. A. Gatsiou, T. S. Gee, R. De Gelder, L. M. Ghiringhelli, H. Goto, S. Grimme, R. Guo, D. W. M. Hofmann, J. Hoja, R. K. Hylton, L. Iuzzolino, W. Jankiewicz, D. T. De Jong, J. Kendrick, N. J. J. De Klerk, H. Y. Ko, L. N. Kuleshova, X. Li, S. Lohani, F. J. J. Leusen, A. M. Lund, J. Lv, Y. Ma, N. Marom, A. E. Masunov, P. McCabe, D. P. McMahon, H. Meekes, M. P. Metz, A. J. Misquitta, S. Mohamed, B. Monserrat, R. J. Needs, M. A. Neumann, J. Nyman, S. Obata, H. Oberhofer, A. R. Oganov, A. M. Orendt, G. I. Pagola, C. C. Pantelides, C. J. Pickard, R. Podeszwa, L. S. Price, S. L. Price, A. Pulido, M. G. Read, K. Reuter, E. Schneider, C. Schober, G. P. Shields, P. Singh, I. J. Sugden, K. Szalewicz, C. R. Taylor, A. Tkatchenko, M. E. Tuckerman, F. Vacarro, M. Vasileiadis, A. Vazquez-Mayagoitia, L. Vogt, Y. Wang, R. E. Watson, G. A. De Wijs, J. Yang, Q. Zhu and C. R. Groom, Report on the sixth blind test of organic crystal structure prediction methods, *Acta Crystallographica Section B: Structural Science, Crystal Engineering and Materials*, 2016, **72**, 439–459.

63 G. M. Day, T. G. Cooper, A. J. Cruz-Cabeza, K. E. Hejczyk, H. L. Ammon, S. X. M. Boerrigter, J. S. Tan, R. G. Della Valle, E. Venuti, J. Jose, S. R. Gadre, G. R. Desiraju, T. S. Thakur, B. P. Van Eijck, J. C. Facelli, V. E. Bazterra, M. B. Ferraro, D. W. M. Hofmann, M. A. Neumann, F. J. J. Leusen, J. Kendrick, S. L. Price, A. J. Misquitta, P. G. Karamertzanis, G. W. A. Welch, H. A. Scheraga, Y. A. Arnautova, M. U. Schmidt, J. Van De Streek, A. K. Wolf and B. Schweizer, Significant progress in predicting the crystal structures of small organic molecules – a report on the fourth blind test, *Acta Crystallogr B Struct Sci*, 2009, **65**, 107–125.

64 D. Valle, V. Eijck and V. D. Streek, Significant progress in predicting the crystal structures of small organic molecules – a report on the fourth blind test, 2009, 107–125.

65 C. R. Taylor and G. M. Day, Evaluating the Energetic Driving Force for Cocrystal Formation, *Crystal Growth & Design*, 2018, **18**, 892–904.

66 L. Iuzzolino, A. M. Reilly, P. McCabe and S. L. Price, Use of Crystal Structure Informatics for Defining the Conformational Space Needed for Predicting Crystal Structures of Pharmaceutical Molecules, *Journal of Chemical Theory and Computation*, 2017, **13**, 5163–5171.

67 J. J. Devogelaer, H. Meekes, P. Tinnemans, E. Vlieg and R. de Gelder, Co-crystal Prediction by Artificial Neural Networks, *Angew. Chem. Int. Ed.*, 2020, **59**, 21711–21718.

68 S. Clark, PhD thesis, University of Edinburgh, 1994.

69 N. M. Harrison, An Introduction to Density Functional Theory, *NATO Science Series Sub Series III: Computer and Systems Sciences*, 2003, **187**, 45–70.

70 A. Willamson, PhD thesis, University of Cambridge, 1996.

71 A. Szabo and N. Ostlund, in *Modern quantum Chemistry: Introduction to advanced electronic structure theory*, 1996, p. 46.

72 F. Jensen, *Introduction to Computational chemistry*, 2007.

73 W. Koch and M. Holthausen, in *A Chemist's Guide to Density Functional Theory*, 2001, pp. 8–13.

74 R. M. Martin, in *Electronic structure Basic Theory and Practical methods*, Cambridge University Press, 2005, vol. 2, p. 63.

75 J. Thijssen, in *Computational physics*, 2012, pp. 43–88.

76 P. Atkins and J. de Paula, in *Physical Chemistry*, 2002, p. 442.

77 P. Hohenberg and W. Kohn, Inhomogeneous electron gas, *Physical Review B*, 1964, **136**, B864–B871.

78 S. Kurth, M. A. L. Marques and E. K. U. Gross, Density-Functional Theory, *Encyclopedia of Condensed Matter Physics*, 2005, 395–402.

79 P. Atkins and J. de Paula, in *Physical Chemistry*, p. 444.

80 Y. Andersson, D. C. Andersson and B. I. Lundqvist, Van der Waals interactions in density-functional theory, *Physical Review Letters*, 1996, **76**, 102–105.

81 J. P. Perdew, K. Burke and M. Ernzerhof, Generalized gradient approximation made simple, *Physical Review Letters*, 1996, **77**, 3865–3868.

82 M. Korth and S. Grimme, 'Mindless' DFT benchmarking, *Journal of Chemical Theory and Computation*, 2009, **5**, 993–1003.

83 P. Hao, J. Sun, B. Xiao, A. Ruzsinszky, G. I. Csonka, J. Tao, S. Glindmeyer and J. P. Perdew, Performance of meta-GGA functionals on general main group thermochemistry, kinetics, and noncovalent interactions, *Journal of Chemical Theory and Computation*, 2013, **9**, 355–363.

84 A. D. Becke, Density-functional thermochemistry. III. The role of exact exchange, *The Journal of Chemical Physics*, 1993, **98**, 5648–5652.

85 N. Handy and A. Cohen, A dynamical correlation functional A dynamical correlation functional, *Journal of Chemical Physics*, 2002, **116**, 5411–5418.

86 J. Baker and P. Pulay, Assessment of the OLYP and O3LYP Density Functionals for First-Row Transition Metals, *Journal of Computational Chemistry*, **24**, 1184–1191.

87 A. D. Becke, Density-functional exchange-energy approximation with correct asymptotic behavior, *Phys. Rev. A*, 1988, **38**, 3098–3100.

88 C. Adamo, Toward reliable density functional methods without adjustable parameters : The PBE0 model, *J. Chem. Phys*, 1999, **110**, 6158.

89 C. D. Sherrill, *Distinguishing Basis Set Superposition Error (BSSE) from Basis Set Incompleteness Error (BSIE)*, 2017.

90 N. Kobko and J. J. Dannenberg, Effect of basis set superposition error (BSSE) upon ab initio calculations of organic transition states, *J. Phys. Chem. A*, 2001, **105**, 1944–1950.

91 C. D. Sherrill, *Counterpoise Correction and Basis Set Superposition Error*, 2010.

92 M. Gutowski, J. H. V. Lenthe, F. B. V. Duijneveldt and I. Introduction, Accuracy of the Boys and Bernardi function, *J. Chem. Phys.*, 1993, **98**, 4728–4737.

93 J. A. Sordo, On the use of the Boys-Bernardi function counterpoise procedure to correct barrier heights for basis set superposition error, *Journal of Molecular Structure (Themchem)*, 2001, **537**, 245–251.

94 E. Bylaska, Quantum Chemistry - Periodic Simulations, *Annual Reports in Computational Chemistry*, 2017, **13**, 185–228.

95 U. von Barth and C. D. Gelatt, Validity of the frozen-core approximation and pseudopotential theory for cohesive energy calculations, *Physical review B*, 1980, **21**, 2222–2228.

96 P. J. Hasnip, Pseudopotentials, https://www-users.york.ac.uk/~mijp1/teaching/grad_FPMM/lecture_notes/lec11_pseudopotentials.pdf.

97 D. Vanderbilt, Soft self-consistent pseudopotentials in a generalized eigenvalue formalism, *Phys. Rev. B*, 1990, **41**, 7892–7895.

98 D. R. Hamann, M. Schlüter and C. Chiang, Norm-Conserving Pseudopotentials, *Phys. Rev. Lett.*, 1979, **43**, 1494.

99 Pseudopotentials, https://www.tcm.phy.cam.ac.uk/castep/documentation/WebHelp/content/modules/castep/thcasteppseudo.htm, (accessed 23 May 2023).

100 R. M. Martin, *Electronic structure : basic theory and practical methods / Richard M. Martin.*, Cambridge University Press, Cambridge, 2004.

101 X. Wu, E. J. Walter, A. M. Rappe, R. Car and A. Selloni, Hybrid density functional calculations of the band gap of GaxIn1−xN, *PHYSICAL REVIEW B*, 2009, **97**, 1–5.

102 P. J. Hasnip, 2019.

103 P. Kratzer and J. Neugebauer, The Basics of Electronic Structure Theory for Periodic Systems, *Frontiers in chemistry*, 2019, **7**, 1–18.

104 P. E. Blöchl, Projector augmented-wave method, *Phys. Rev. B*, 1994, **50**, 17953–17979.

105 B. Hourahine, B. Aradi, V. Blum, F. Bonafé, A. Buccheri, C. Camacho, C. Cevallos, M. Y. Deshaye, T. Dumitric, A. Dominguez, S. Ehlert, M. Elstner, T. Van Der Heide, J. Hermann, S. Irle, J. J. Kranz, C. Köhler, T. Kowalczyk, T. Kubař, I. S. Lee, V. Lutsker, R. J. Maurer, S. K. Min, I. Mitchell, C. Negre, T. A. Niehaus, A. M. N. Niklasson, A. J. Page, A. Pecchia, G. Penazzi, M. P. Persson, J. Řezáč, C. G. Sánchez, M. Sternberg, M. Stöhr, F. Stuckenberg, A. Tkatchenko, V. W. Z. Yu and T. Frauenheim, DFTB+, a software package for efficient approximate density functional theory based atomistic simulations, *J. Chem. Phys.*, 2020, **152**, 124101.

106 M. Elstner and G. Seifert, Density functional tight binding, *Phil. Trans. R. Soc. A.*, 2014, **372**, 20120483.

107 C. M. Goringe, D. R. Bowler and E. Hernández, Tight-binding modelling of materials, *Rep. Prog. Phys.*, 1997, **60**, 1447–1512.

108 G. A. Dolgonos and A. D. Boese, Adjusting dispersion parameters for the density-functional tight-binding description of molecular crystals, *Chemical Physics Letters*, 2019, **718**, 7–11.

109 M. Gaus, A. Goez and M. Elstner, Parametrization and benchmark of DFTB3 for organic molecules, *Journal of Chemical Theory and Computation*, 2013, **9**, 338–354.

110 S. Grimme, S. Ehrlich and L. Goerigk, Effect of the Damping Function in Dispersion Corrected Density Functional Theory, *Journal of computational chemistry*, 2011, **32**, 1456–1465.

111 G. A. Dolgonos, J. Hoja and A. Daniel Boese, Revised values for the X23 benchmark set of molecular crystals, *Physical Chemistry Chemical Physics*, 2019, **21**, 24333–24344.

112 A. M. Reilly and A. Tkatchenko, Understanding the role of vibrations, exact exchange, and many-body van der Waals interactions in the cohesive properties of molecular crystals, *Journal of Chemical Physics*, 2013, **139**, 024705.

113 J. Řezáč, Empirical Self-Consistent Correction for the Description of Hydrogen Bonds in DFTB3, *Journal of Chemical Theory and Computation*, 2017, **13**, 4804–4817.

114 S. Kristyán and P. Pulay, Can (semi)local density functional theory account for the London dispersion forces?, *Chemical Physics Letters*, 1994, **229**, 175–180.

115 J. G. Brandenburg and S. Grimme, Dispersion Corrected Hartree–Fock and Density Functional Theory for Organic Crystal Structure Prediction, *prediction and calculation of crystal structures*, 2013, **345**, 1–26.

116 J. Moellmann and S. Grimme, Importance of London dispersion effects for the packing of molecular crystals: a case study for intramolecular stacking in a bis-thiophene derivative, *Physical Chemistry Chemical Physics*, 2010, **12**, 8500–8504.

117 P. Xu, M. Alkan and M. S. Gordon, Many-Body Dispersion, *Chemical Reviews*, 2020, **120**, 12343–12356.

118 S. Grimme, Density functional theory with London dispersion corrections, *WIREs Comput Mol Sci*, 2011, **1**, 211–228.

119 M. D. King and T. M. Korter, Modified corrections for london forces in solid-state density functional theory calculations of structure and lattice dynamics of molecular crystals, *Journal of Physical Chemistry A*, 2012, **116**, 6927–6934.

120 Y. Liu and W. A. Goddard, A universal damping function for empirical dispersion correction on density functional theory, *Materials Transactions*, 2009, **50**, 1664–1670.

121 S. Grimme, S. Ehrlich and L. Goerigk, Effect of the Damping Function in Dispersion Corrected Density Functional Theory, *Journal of computational chemistry*, 2011, **32**, 1456–1465.

122 S. Grimme, Accurate description of van der Waals complexes by density functional theory including empirical corrections, *Journal of Computational Chemistry*, 2004, **25**, 1463–1473.

123 S. Grimme, Semiempirical GGA-Type Density Functional Constructed with a Long-Range Dispersion Correction, *Journal of computational chemistry*, 2006, **27**, 1787–1799.

124 A. Tkatchenko and M. Scheffler, Accurate molecular van der Waals interactions from ground-state electron density and free-atom reference data, *Physical Review Letters*, 2009, **102**, 073005.

125 L. Kronik and A. Tkatchenko, Understanding molecular crystals with dispersion-inclusive density functional theory: Pairwise corrections and beyond, *Acc. Chem. Res.*, 2014, **47**, 3208–3216.

126 G. X. Zhang, A. Tkatchenko, J. Paier, H. Appel and M. Scheffler, Van der Waals interactions in ionic and semiconductor solids, *Physical Review Letters*, 2011, **107**, 1–5.

127 A. Otero-De-la-Roza, L. M. LeBlanc and E. R. Johnson, What is “many-body” dispersion and should I worry about it?, *Physical Chemistry Chemical Physics*, 2020, **22**, 8266.

128 E. Caldeweyher, S. Ehlert, A. Hansen, H. Neugebauer, S. Spicher, C. Bannwarth and S. Grimme, A generally applicable atomic-charge dependent London dispersion correction, *Journal of Chemical Physics*, DOI:10.1063/1.5090222.

129 E. Caldeweyher, S. Ehlert, A. Hansen, H. Neugebauer, S. Spicher, C. Bannwarth and S. Grimme, A generally applicable atomic-charge dependent London dispersion correction, *Journal of Chemical Physics*, 2019, **150**, 154122.

130 S. Grimme, J. Antony, S. Ehrlich and H. Krieg, A consistent and accurate ab initio parametrization of density functional dispersion correction (DFT-D) for the 94 elements H-Pu, *J. Chem. Phys.*, 2010, **132**, 154104.

131 W. Jankiewicz, R. Podeszwa and H. A. Witek, Dispersion-Corrected DFT Struggles with Predicting Three-Body Interaction Energies, *Journal of Chemical Theory and Computation*, 2018, **14**, 5079–5089.

132 A. Tkatchenko, R. A. Distasio, R. Car and M. Scheffler, Accurate and efficient method for many-body van der Waals interactions, *Physical Review Letters*, 2012, **108**, 236402.

133 E. Grothe, H. Meekes, E. Vlieg, J. H. Horst and R. D. Gelder, Solvates, Salts, and Cocrystals: A Proposal for a Feasible Classification System, *Crystal Growth & Design*, 2016, **16**, 3237–3243.

134 S. L. Childs and M. J. Zaworotko, The reemergence of cocrystals: The crystal clear writing Is on the wall introduction to virtual special issue on pharmaceutical cocrystals, *Crystal Growth & Design*, 2009, **9**, 4208–4211.

135 A. M. Healy, Z. A. Worku, D. Kumar and A. M. Madi, Pharmaceutical solvates, hydrates and amorphous forms: A special emphasis on cocrystals, *Advanced Drug Delivery Reviews*, 2017, **117**, 25–46.

136 Particle Sciences, Biopharmaceutical Classification System and Formulation Development, *Particle Sciences*, 2011, **9**, 1–4.

137 N. Pandey and A. Ghosh, An outlook on permeability escalation through cocrystallization for developing pharmaceuticals with improved biopharmaceutical properties, *Journal of Drug Delivery Science and Technology*, 2022, **76**, 1773–2247.

138 E. R. Johnson and G. A. DiLabio, Structure and binding energies in van der Waals dimers: Comparison between density functional theory and correlated ab initio methods, *Chemical Physics Letters*, 2005, **419**, 333–339.

139 A. G. Shtukenberg, C. T. Hu, Q. Zhu, M. U. Schmidt, W. Xu, M. Tan and B. Kahr, The Third Ambient Aspirin Polymorph, *Crystal Growth & Design*, 2017, **17**, 3562–3566.

140 J. Hermann and A. Tkatchenko, Density Functional Model for van der Waals Interactions: Unifying Many-Body Atomic Approaches with Nonlocal Functionals, *Physical Review Letters*, 2020, **124**, 146401.

141 S. Grimme, A. Hansen, J. G. Brandenburg and C. Bannwarth, Dispersion-Corrected Mean-Field Electronic Structure Methods, *Chemical Reviews*, 2016, **116**, 5105–5154.

142 A. Ambrosetti, A. M. Reilly, R. A. Distasio and A. Tkatchenko, Long-range correlation energy calculated from coupled atomic response functions, *Journal of Chemical Physics*, 2014, **140**, 1818A508.

143 J. G. Brandenburg and S. Grimme, Accurate modeling of organic molecular crystals by dispersion-corrected density functional tight binding (DFTB), *Journal of Physical Chemistry Letters*, 2014, **5**, 1785–1789.

144 F. H. Allen, The Cambridge Structural Database: A quarter of a million crystal structures and rising, *Acta Crystallographica Section B: Structural Science*, 2002, **B58**, 380–388.

145 J. P. Perdew, M. Ernzerhof and K. Burke, Rationale for mixing exact exchange with density functional approximations Rationale for mixing exact exchange with density functional approximations, *J. Chem. Phys.*, 1996, **105**, 9982–9985.

146 S. J. Clark, M. D. Segall, C. J. Pickard, P. J. Hasnip, M. I. J. Probert, K. Refson and M. C. Payne, First principles methods using CASTEP, *Zeitschrift fur Kristallographie*, 2005, **220**, 567–570.

147 W. A. Al-Saidi, V. K. Voora and K. D. Jordan, An assessment of the vdW-TS method for extended systems, *Journal of Chemical Theory and Computation*, 2012, **8**, 1503–1513.

148 G. A. Dolgonos and A. D. Boese, Adjusting dispersion parameters for the density-functional tight-binding description of molecular crystals, *Chemical Physics Letters*, 2019, **718**, 7–11.

149 A. M. Reilly and A. Tkatchenko, Van der Waals dispersion interactions in molecular materials: Beyond pairwise additivity, *Chem. Sci.*, 2015, **6**, 3289.

150 G. S. Nichol and W. Clegg, Classical and weak hydrogen bonding interactions between 4,4′-bipyridine and organic acids: From co-crystal to organic complex, *Crystal Growth & Design*, 2009, **9**, 1844–1850.

151 R. Birolo, F. Bravetti, E. Alladio, E. Priola, G. Bianchini, R. Novelli, A. Aramini, R. Gobetto and M. R. Chierotti, Speeding Up the Cocrystallization Process: Machine Learning-Combined Methods for the Prediction of Multicomponent Systems, *Crystal Growth & Design*, 2023, **23**, 7898–7911.

152 C. V. Essen and D. Luedeker, In silico co-crystal design: Assessment of the latest advances, *Drug Discovery Today*, 2023, **28**, 103763.

153 P. Kim, I.-S. Lee, J.-Y. Kim, M. E. Mswahili, Y.-S. Jeong, W.-J. Yoon, H.-S. Yun, M.-J. Lee and G. J. Choi, A study to discover novel pharmaceutical cocrystals of pelubiprofen with a machine learning approach compared, *CrystEngComm*, 2022, **24**, 3938–3952.

154 E. S. Henle and S. Linn, Formation, Prevention, and Repair of DNA Damage by Iron/Hydrogen Peroxide, *Journal of Biological Chemistry*, 1997, **272**, 19095–19098.

155 A. Kellett, Z. Molphy, V. McKee and C. Slator, in *Metal- based Anticancer Agents*, 2019, pp. 91–115.

156 A. Casini and A. Pöthig, Metals in Cancer Research: Beyond Platinum Metallodrugs, *ACS Cent. Sci.*, 2024, **10**, 242–250.

157 M. Pitié and G. Pratviel, Activation of DNA Carbon−Hydrogen Bonds by Metal Complexes, *Chem. Rev.*, 2010, **110**, 1018–1059.

158 A. L. Lainé and C. Passirani, Novel metal-based anticancer drugs: A new challenge in drug delivery, *Current Opinion in Pharmacology*, 2012, **12**, 420–426.

159 A. Kellett, Z. Molphy, C. Slator, V. McKee and N. P. Farrell, Molecular methods for assessment of non-covalent metallodrug-DNA interactions, *Chem. Soc. Rev.*, 2019, **48**, 971.

160 A. Kellett, Z. Molphy, V. McKee and C. Slator, in *Metal-based anticancer agents*, 2019, pp. 91–120.

161 H. C. Kolb, M. G. Finn and K. B. Sharpless, Click Chemistry: Diverse Chemical Function from a Few Good Reactions, *Angew. Chem. Int. Ed.*, 2001, **40**, 2004–2021.

162 C. W. Tornøe, C. Christensen and M. Meldal, Peptidotriazoles on Solid Phase: [1,2,3]-Triazoles by Regiospecific Copper(I)-Catalyzed 1,3-Dipolar Cycloadditions of Terminal Alkynes to Azides, *J. Org. Chem.*, 2002, **67**, 3057–3064.

163 L. O. Brockway and L. Pauling, The Electron-Diffraction Investigation of the Structure of Molecules of Methyl Azide and Carbon Suboxide, *Proc. N. A. S.*, 1933, **19**, 860–867.

164 The Nobel Prize in Chemistry 2022, https://www.nobelprize.org/prizes/chemistry/2022/summary/.

165 N. McStay, C. Slator, V. Singh, A. Gibney, F. Westerlund and A. Kellett, Click and Cut: a click chemistry approach to developing oxidative DNA damaging agents, *Nucleic Acids Research*, 2021, **49**, 10289–10308.

166 R. Chang and J. Overby, in *Chemistry*, 2019, pp. 464–465.

167 K. E. Riley and K. M. Merz, Assessment of Density Functional Theory Methods for the Computation of Heats of Formation and Ionization Potentials of Systems Containing Third Row Transition Metals, *J. Phys. Chem. A*, 2007, **111**, 6044–6053.

168 O. Trott and A. J. Olson, AutoDock Vina: Improving the speed and accuracy of docking with a new scoring function, efficient optimization, and multithreading, *J. Comput. Chem.*, 2009, 455–461.

169 S. S. Batsanov, Van der Waals Radii of Elements, 2001, **37**, 871–885.

170 P. Atkins and J. de Paula, in *Physical chemistry*, Seventh edition., 2002, p. 696.

171 J. Vanloon, T. Harroun and H. Yan, Circular dichroism spectroscopy of DNA duplexes at near-biological concentrations, *Bioorganic & Medicinal Chemistry Letters*, 2021, **43**, 128053.

172 J. Kypr, I. Kejnovska, D. Renciuk and M. Vorlickova, Circular dichroism and conformational polymorphism of DNA, *Nucleic Acids Research*, 2009, **37**, 1713–1725.

173 B. McGorman, S. Poole, M. V. López and A. Kellett, Analysis of non-canonical three- and four-way DNA junctions, *Methods*, 2023, **219**, 30–38.

174 M. Jerabek-Willemsen, T. André, R. Wanner, H. M. Roth, S. Duhr, P. Baaske and D. Breitsprecher, MicroScale Thermophoresis: Interaction analysis and beyond, *Journal of Molecular Structure*, 2014, **1077**, 101–113.

175 S. Forli, R. Huey, M. E. Pique, M. F. Sanner, D. S. Goodsell and A. J. Olson, Computational protein–ligand docking and virtual drug screening with the AutoDock suite, *Nat Protoc*, 2016, **11**, 905–919.

176 J. Gasteiger and M. Marsili, Iterative partial equalization of orbital electronegativity—a rapid access to atomic charges, *Tetrahedron*, 1980, **36**, 3219–3228.

177 J. Eberhardt, D. Santos-Martins, A. F. Tillack and S. Forli, AutoDock Vina 1.2.0: New Docking Methods, Expanded Force Field, and Python Bindings, *J. Chem. Inf. Model.*, 2021, **61**, 3891–3898.

178 E. Abás, D. Aguirre-Ramírez, M. Laguna and L. Grasa, Selective Anticancer and Antimicrobial Metallodrugs Based on Gold(III) Dithiocarbamate Complexes, *Biomedicines*, 2021, **9**, 1775.

179 W. Liu and R. Gust, Metal N-heterocyclic carbene complexes as potential antitumor metallodrugs, *Chem. Soc. Rev.*, 2013, **42**, 755–773.

180 J. E. Waters, L. Stevens-Cullinane, L. Siebenmann and J. Hess, Recent advances in the development of metal complexes as antibacterial agents with metal-specific modes of action, *Current Opinion in Microbiology*, 2023, **75**, 102347.

181 P. F. Salas, C. Herrmann and C. Orvig, Metalloantimalarials, *Chem. Rev.*, 2013, **113**, 3450–3492.

182 N. Gugala and R. J. Turner, in *Biomedical Applications of Metals*, eds. M. Rai, A. P. Ingle and S. Medici, Springer International Publishing, Cham, 2018, pp. 129–150.

183 A. Oleksy, A. G. Blanco, R. Boer, I. Usón, J. Aymamí, A. Rodger, M. Hannon and M. Coll, Molecular Recognition of a Three-Way DNA Junction by a Metallosupramolecular Helicate, *Angewandte Chemie*, 2006, **118**, 1249–1253.

184 J. Chen and J. Stubbe, Bleomycins: towards better therapeutics, *Nat Rev Cancer*, 2005, **5**, 102–112.

185 L. H. Einhorn, Curing metastatic testicular cancer, *Proc. Natl. Acad. Sci. U.S.A.*, 2002, **99**, 4592–4595.

186 S. M. Hecht, Bleomycin: New Perspectives on the Mechanism of Action, *J. Nat. Prod.*, 2000, **63**, 158–168.

187 E. J. Anthony, E. M. Bolitho, H. E. Bridgewater, O. W. L. Carter, J. M. Donnelly, C. Imberti, E. C. Lant, F. Lermyte, R. J. Needham, M. Palau, P. J. Sadler, H. Shi, F.-X. Wang, W.-Y. Zhang and Z. Zhang, Metallodrugs are unique: Opportunities and challenges of discovery and development, *Chem. Sci.*, 2020, **11**, 12888.

188 F. Mancin, P. Scrimin and P. Tecilla, Progress in artificial metallonucleases, *Chem. Commun.*, 2012, **48**, 5545–5559.

189 C. Slator, N. Barron, O. Howe and A. Kellett, [Cu(o-phthalate)(phenanthroline)] Exhibits Unique Superoxide-Mediated NCI-60 Chemotherapeutic Action through Genomic DNA Damage and Mitochondrial Dysfunction, *ACS Chem. Biol.*, 2016, **11**, 159–171.

190 A. Prisecaru, M. Devereux, N. Barron, M. McCann, J. Colleran, A. Casey, V. McKee and A. Kellett, Potent oxidative DNA cleavage by the di-copper cytotoxin: [Cu2(μ-terephthalate)(1,10-phen)4]2+, *Chem. Commun.*, 2012, **48**, 6906–6908.

191 A. Kellett and A. Gibney, Gene Editing with Artificial DNA Scissors, *Chemistry A European J*, 2024, e202401621.

192 Y. Aiba, J. Sumaoka and M. Komiyama, Artificial DNA cutters for DNA manipulation and genome engineering, *Chem. Soc. Rev.*, 2011, **40**, 5657.

193 A. Gibney, R. E. F. De Paiva, V. Singh, R. Fox, D. Thompson, J. Hennessy, C. Slator, C. J. McKenzie, P. Johansson, V. McKee, F. Westerlund and A. Kellett, A Click Chemistry-Based Artificial Metallo-Nuclease, *Angew. Chem. Int. Ed.*, 2023, e202305759.

194 C. Slator, Z. Molphy, V. Mckee, C. Long, T. Brown and A. Kellett, Di-copper metallodrugs promote NCI-60 chemotherapy via singlet oxygen and superoxide production with tandem TA /TA and AT/AT oligonucleotide discrimination, *Nucleic Acids Research*, 2018, 1–18.

195 M. Bursch, J. Mewes, A. Hansen and S. Grimme, Best-Practice DFT Protocols for Basic Molecular Computational Chemistry, *Angew. Chem. Int. Ed.*, 2022, 202205735.

196 N. C. Pyper, Relativity and the periodic table, *Phil. Trans. R. Soc. A.*, 2020, **378**, 20190305.

197 C. E. Housecroft and A. G. Sharpe, in *Inorganic chemistry*, Pearson, Fifth Edition., 2018, p. 393.

198 F. Weigend and R. Ahlrichs, Balanced basis sets of split valence, triple zeta valence and quadruple zeta valence quality for H to Rn: Design and assessment of accuracy, *Phys. Chem. Chem. Phys.*, 2005, **7**, 3297.

199 N. McStay, A. M. Reilly, N. Gathergood and A. Kellett, Efficient DNA Condensation by a C3-Symmetric Codeine Scaffold, *ChemPlusChem*, 2019, **84**, 38–42.

200 F. Neese, The ORCA program system, *WIREs Comput Mol Sci*, 2012, **2**, 73–78.

201 F. Neese, Software update: the ORCA program system, version 4.0, *WIREs Comput Mol Sci*, 2018, **8**, e:1327.

202 F. Neese, Software update: The ORCA program system — Version 5.0, *WIREs Comput Mol Sci*, 2022, **12**, e1606.

203 M. McCann, J. McGinley, K. Ni, M. O'Connor, K. Kavanagh, V. McKee, J. Colleran, M. Devereux, N. Gathergood, N. Barron, A. Prisecaru and A. Kellett, A new phenanthroline–oxazine ligand: synthesis, coordination chemistry and atypical DNA binding interaction, *Chem. Commun.*, 2013, **49**, 2341.

204 M. J. Abraham, T. Murtola, R. Schulz, S. Páll, J. C. Smith, B. Hess and E. Lindahl, GROMACS: High performance molecular simulations through multi-level parallelism from laptops to supercomputers, *SoftwareX*, 2015, **1–2**, 19–25.

205 D. Van Der Spoel, E. Lindahl, B. Hess, G. Groenhof, A. E. Mark and H. J. C. Berendsen, GROMACS: Fast, flexible, and free, *J Comput Chem*, 2005, **26**, 1701–1718.

206 J. Huang, S. Rauscher, G. Nawrocki, T. Ran, M. Feig, B. L. De Groot, H. Grubmüller and A. D. MacKerell, CHARMM36m: an improved force field for folded and intrinsically disordered proteins, *Nat Methods*, 2017, **14**, 71–73.

207 J. Wang, W. Wang, P. A. Kollman and D. A. Case, Automatic atom type and bond type perception in molecular mechanical calculations, *Journal of Molecular Graphics and Modelling*, 2006, **25**, 247–260.

208 M. D. Hanwell, D. E. Curtis, D. C. Lonie, T. Vandermeersch, E. Zurek and G. R. Hutchison, Avogadro: an advanced semantic chemical editor, visualization, and analysis platform, *J Cheminform*, 2012, **4**, 17.

209

210 S. Nayak and A. K. Nangia, Single-step synthesis of multicomponent cocrystals and salts: the role of laboratory seeding, *CrystEngComm*, 2024, **26**, 5699–5715.

211 I. Grinberg, N. J. Ramer and A. M. Rappe, Transferable relativistic Dirac-Slater pseudopotentials, *Physical Review B - Condensed Matter and Materials Physics*, 2000, **62**, 2311–2314.

212 M. Kubillus, T. Kubař, M. Gaus, J. Řezáč and M. Elstner, Parameterization of the DFTB3 method for Br, Ca, Cl, F, I, K, and Na in organic and biological systems, *Journal of Chemical Theory and Computation*, 2015, **11**, 332–342.

213 X. Lu, M. Gaus, M. Elstner and Q. Cui, Parametrization of DFTB3/3OB for magnesium and zinc for chemical and biological applications, *Journal of Physical Chemistry B*, 2015, **119**, 1062–1082.

214 M. Gaus, X. Lu, M. Elstner and Q. Cui, Parameterization of DFTB3/3OB for sulfur and phosphorus for chemical and biological applications, *Journal of Chemical Theory and Computation*, 2014, **10**, 1518–1537.

215 V. M. Miriyala and J. Řezáč, Description of Non-covalent interactions in SCC-DFTB methods, *Journal of Computational Chemistry*, 2017, 688–697.

Appendix A

1. Conquest search

Using the ConQuest software provided by the Cambridge Crystallographic Data Centre, CCDC, we searched for systems that included the oxalic acid, 4,4'-bipyridine, aspirin and paracetamol structures. We used crystal structure database version 5.41. The selected structures met the following criteria including:

- Structures must not contain water or other common solvents
- All atomic coordinates must be resolved
- The structures must have low disorder
- All hydrogen atom positions must be determined
- Structures could only contain C, H, N, O, S or Cl
- The database must also contain the single component form of each constituent molecule of the co-crystal being experimentally reported
- Only binary structures with two different types of molecules

This was then further narrowed by limiting the unit cell size to 140 atoms to make PBE0 calculations feasible. This procedure generated the dataset with four aspirin, six paracetamol, five oxalic acid and thirteen 4,4'-bipyridine co-crystals.

2. DFT Optimisation procedure

The calculations were performed using the CASTEP code. The PBE exchange functional was employed with the TS or MBD dispersion correction. A plane wave cut-off of 900 eV was used, and a k-point spacing of 0.06 Å. These values were established through convergence tests. The starting experimental structures were minimised using the PBE-TS and PBE-MBD methods. The geometry optimisation was done using the default optimisation method for CASTEP of LBFGS, which utilised the on-the-fly pseudopotentials generated by CASTEP.

The PBE0 calculations were carried out as single-point calculations using the optimised geometry from the PBE-MBD calculation using the Rappe-Bennett norm-conserving GGA pseudopotential.[211]

3. Density functional tight binding optimisation

The Density functional tight binding calculations utilised the DFTB3+ method, which used Slater-Koster pseudopotentials[109,212–214] and the QuasiNewton method of optimisation with conjugate gradients.

The Boese[108] and H5[113,215] calculations were parameterised using the parameters in Table S1 :

Table A-1: Parameterisation of the DFTB3+ dampening parameters

parameter	Boese	H5
S_{r6}		1.25
S_6	1.0	1.0
S_8	0.5883	0.49
α_6		26.61
a_1	1.3719	
a_2	3.7017	

RMSD analysis

Table A-2a- $RMSD_{20}$ values (Å) for oxalic acid based co-crystal structures							
CSD code (co-crystal)	Co-former	PBE	PBE-TS	PBE-MBD	DFTB-D3	DFTB-D3 Boese	DFTB-D3(H5)
GUDSUV	pyrazine	0.526	0.061	0.078	0.262	0.234	0.287
UMINAF	Azapyridine	0.813	0.09	0.096	0.416	0.684	0.735
UROXAM01	urea	0.449	0.074	0.077	0.381	0.178	0.48
XEJWUF	theophylline	0.587	0.102	0.128	0.394	0.365	0.425
XAPMIK	phenazine	0.617	0.088	0.063	0.367	0.254	0.764

Table A-2b- $RMSD_{20}$ values (Å) of oxalic acid based co-crystal structures co-formers single component crystal							
CSD code (single component)	Co-former	PBE	PBE-TS	PBE-MBD	DFTB-D3	DFTB-D3 Boese	DFTB-D3(H5)
BACJUN	pyrazine	0.519	0.177	0.124	0.515	0.694	0.673
EVESIJ04	Azapyridine	0.601	0.088	0.185	0.341	1.17	0.476
UREAXX12	urea	0.197	0.025	0.014	0.168	0.036	0.043
BAPLOT04	theophylline	1.204	0.061	0.193	0.274	0.507	0.369
PHENAZ11	Phenazine	0.811	0.17	0.227	0.629	0.293	0.663
OXALAC05	Oxalic acid	0.343	0.17	0.147	0.356	0.245	0.87

Table A-3a- $RMSD_{20}$ values (Å) for 4,4'-bipyridine based co-crystal structures							
CSD code (co-crystal)	Co-former	PBE	PBE-TS	PBE-MBD	DFTB-D3	DFTB-D3 Boese	DFTB-D3(H5)
VEXQOE	1,3,5-triazinane-2,4,6-trione	0.526	0.355	0.24	0.503	0.937	0.659
GIPQEB01	fumaric acid	0.869	0.084	(12 out of 20 matches) 1.102	0.406	0.374	N/A
SOVFOY01	thiodiglycolic acid	1.148	0.155	0.173	0.355	0.336	0.431
MEWNUA	O-isopropyl N-phenylthiocarbamate	0.91	0.07	0.714	0.723	0.422	0.359
RUXMAZ	1,4-diethynylbenzene	0.715	0.129	0.338	0.56	0.596	0.676
SITDIJ	acetic acid	0.427	0.133	0.115	(16 out of 20 matches) 0.578	(8 out of 20 matches) 0.837	0.789
LOYRIC	isophthalic acid	0.671	0.21	0.125	0.545	0.335	(7 out of 20 matches) 0.527
PAVXAN	terephthalic acid	0.605	0.159	0.251	0.708	0.514	0.487
NUJFEF	2-(carboxymethyl) benzoic acid	0.633	0.191	0.675	1.165	(19 out of 20 matches) 0.868	(12 out of 20 matches) 0.919
XOWKEB01	2-[(2,3-dimethylphenyl) amino]benzoic acid	0.842	0.336	0.491	0.505	0.472	0.466
UCEXIJ	cyclo-diaspartic acid	0.603	0.158	0.347	0.522	0.225	0.414
ROQYED	succinamic acid	0.855	0.108	(16 out of 20 matches) 0.743	0.366	(18 out of 20 matches) 0.778	0.413
GOKCEQ	Formic acid	(4 out of 20 matches) 1.347	0.149	0.243	N/A	(15 out of 20 matches) 0.359	(15 out of 20 matches) 0.775

Table A-3b- $RMSD_{20}$ values (Å) for 4,4'-bipyridine based co-crystal structures co-formers single component crystal							
CSD code (single component)	Co-former	PBE	PBE-TS	PBE-MBD	DFTB-D3	DFTB-D3 Boese	DFTB-D3 (H5)
CYURAC14	1,3,5-triazinane-2,4,6-trione	0.324	0.08	0.091	0.418	0.416	0.436
FUMAAC01	fumaric acid	0.425	0.247	0.205	0.455	0.363	0.559
TGLYCL01	thiodiglycolic acid	(11 out of 20 matches) 0.547	0.082	0.086	0.477	0.388	0.736
ADOGUW	O-isopropyl N-phenylthiocarbamate	0.784	0.135	0.231	0.73	0.944	0.687
ETYNBZ01	1,4-diethynylbenzene	0.846	0.104	0.162	0.395	0.18	0.288
ACETAC03	acetic acid	(14 out of 20 matches) 0.609	0.065	0.1	0.395	0.209	0.325
BENZDC11	isophthalic acid	0.638	0.04	0.131	0.345	0.298	0.403
TEPHTH14	terephthalic acid	0.622	0.102	0.21	0.486	0.161	0.349
HOPHAL11	2-(carboxymethyl) benzoic acid	0.867	0.118	0.262	0.55	0.485	0.558
XYANAC06	2-[(2,3-dimethylphenyl) amino]benzoic acid	0.978	0.15	0.383	0.897	1.173	0.909
PAXNIL	cyclo-diaspartic acid	(14 out of 20 matches) 1.221	0.184	0.174	0.452	0.243	0.487
ROQXUS	succinamic acid	0.197	0.15	0.109	(6 out of 20 matches) 1.174	0.651	(3 out of 20 matches) 0.352
FORMAC01	Formic acid	0.893	0.069	0.347	0.276	0.736	0.35
HIQWEJ03	4,4'-bipyridine	0.522	0.171	(16 out of 20 matches) 0.687	0.442	0.33	0.33

Table A-4a- $RMSD_{20}$ values (Å) for paracetamol based co-crystal structures							
CSD code (co-crystal)	Co-former	PBE	PBE-TS	PBE-MBD	DFTB-D3	DFTB-D3 Boese	DFTB-D3(H5)
KIGLUI01	Theophylline	0.639	0.1	0.131	0.36	0.327	0.345
LUJSOZ	β-phenazine	0.66	0.144	0.344	0.479	0.366	0.34
LUJTAM	Oxalic acid	0.478	0.1	0.1	0.37	0.273	0.377
CUQKAC	Betaine	0.54	0.075	0.085	0.556	0.411	0.562
LUJSIT	Naphthalene	0.623	0.115	0.125	0.657	0.36	0.523

Table A-4b- $RMSD_{20}$ values (Å) for paracetamol based co-crystal structures co-formers single component crystal							
CSD code (single component)	Co-former	PBE	PBE-TS	PBE-MBD	DFTB-D3	DFTB-D3 Boese	DFTB-D3(H5)
BAPLOT04	Theophylline	1.204	0.061	0.193	0.274	0.507	0.369
PHENAZ11	β-phenazine	0.811	0.17	0.227	0.629	0.293	0.663
OXALAC05	Oxalic acid	0.343	0.17	0.147	0.356	0.245	0.87
WEMWEQ15	Betaine	0.639	0.10	0.186	0.37	0.209	0.302
NAPHTA15	Naphthalene	0.673	0.06	0.066	0.313	0.832	1.162
HXACAN13	Paracetamol	0.731	0.16	0.116	0.786	0.675	1.169

Table A-5a - $RMSD_{20}$ values (Å) for aspirin based co-crystal structures							
CSD code (co-crystal)	Co-former	PBE	PBE-TS	PBE-MBD	DFTB-D3	DFTB-D3 Boese	DFTB-D3(H5)
DIPJAQ	theophylline	0.793	0.123	0.207	0.415	0.193	0.396
HUNJEH	pentoxifylline	0.556	0.244	0.324	0.577	0.399	0.701
SIBYUA	4,4'-bipyridine	0.561	0.375	0.261	1.054	0.627	0.9
TAZRAO	carbamazepine	0.652	0.111	0.138	0.673	0.549	0.579

Table A-5b- $RMSD_{20}$ values (Å) for aspirin based co-crystal structures co-formers single component crystal							
CSD code (single component)	Co-former	PBE	PBE-TS	PBE-MBD	DFTB-D3	DFTB-D3 Boese	DFTB-D3(H5)
BAPLOT04	theophylline	1.204	0.061	0.193	0.274	0.507	0.369
JAKGEH	pentoxifylline	0.656	0.388	0.217	0.555	0.307	0.509
HIQWEJ03	4,4'-bipyridine	0.522	0.171	(16 out of 20 matches) 0.687	0.442	0.33	0.33
CBMZPN21	carbamazepine	(10 out of 20 matches) 1.392	0.093	0.118	0.54	0.376	0.533
ACSALA05	Aspirin	0.736	0.11	0.065	0.433	0.29	0.693

Supplementary references

1. Grinberg, N. J. Ramer and A. M. Rappe, Transferable relativistic Dirac-Slater pseudopotentials, *Physical Review B - Condensed Matter and Materials Physics*, 2000, **62**, 2311–2314.
2 M. Kubillus, T. Kubař, M. Gaus, J. Řezáč and M. Elstner, Parameterization of the DFTB3 method for Br, Ca, Cl, F, I, K, and Na in organic and biological systems, *Journal of Chemical Theory and Computation*, 2015, **11**, 332–342.
3 X. Lu, M. Gaus, M. Elstner and Q. Cui, Parametrization of DFTB3/3OB for magnesium and zinc for chemical and biological applications, *Journal of Physical Chemistry B*, 2015, **119**, 1062–1082.
4 M. Gaus, X. Lu, M. Elstner and Q. Cui, Parameterization of DFTB3/3OB for sulfur and phosphorus for chemical and biological applications, *Journal of Chemical Theory and Computation*, 2014, **10**, 1518–1537.
5 M. Gaus, A. Goez and M. Elstner, Parametrization and benchmark of DFTB3 for organic molecules, *Journal of Chemical Theory and Computation*, 2013, **9**, 338–354.
6 G. A. Dolgonos and A. D. Boese, Adjusting dispersion parameters for the density-functional tight-binding description of molecular crystals, *Chemical Physics Letters*, 2019, **718**, 7–11.

7 V. M. Miriyala and J. Řezáč, Description of Non-covalent interactions in SCC-DFTB methods, *Journal of Computational Chemistry*, 2017, 688–697.
8 J. Řezáč, Empirical Self-Consistent Correction for the Description of Hydrogen Bonds in DFTB3, *Journal of Chemical Theory and Computation*, 2017, **13**, 4804–4817.

Appendix B

Table B-1 C*opper sulphur and copper nitrogen distance in structure 1*									
		experimental		PBE		B3LYP		PBE0	
Counter ions	CSD code	Cu-N (Å)	Cu-S(Å)	Cu-N (Å)	Cu-S (Å)	Cu-N (Å)	Cu-S (Å)	Cu-N (Å)	Cu-S (Å)
Chloride	KUYXUZ	1.949	3.042	1.975	3.101	1.983	3.168	1.978	3.131

Table B-2 *Structure 1 binding energies for the three exchange functionals used*				
		PBE	B3LYP	PBE0
Counter ions	CSD code	Binding energy (eV)	Binding energy (eV)	Binding energy (eV)
Chloride	KUYXUZ	-2.2178	-2.5695	-2.4299

Table B-3 *Copper sulphur and copper nitrogen distance in structure 2*									
		experimental		PBE		B3LYP		PBE0	
Counter ions	CSD code	Cu-N (Å)	Cu-S (Å)	Cu-N (Å)	Cu-S (Å)	Cu-N (Å)	Cu-S (Å)	Cu-N (Å)	Cu-S (Å)
Nitrate	XOVTOT	1.973	3.470	1.993	3.497	1.992	3.523	1.988	3.554
Iodine bridging	XOWHUO	1.981	3.226	1.927	2.962	1.993	3.097	1.981	2.966
Chloride	XOWJAW	1.958	4.711	1.974	4.8	1.977	4.718	1.973	4.695

Table B-4 *Structure 2 binding energies for the three exchange functionals used*				
		PBE	B3LYP	PBE0
Counter ions	CSD code	Binding energy (eV)	Binding energy (eV)	Binding energy (eV)
Nitrate	XOVTOT	-1.7756	-2.6721	-2.4915
Iodine bridging	XOWHUO	-2.7527	-2.2633	-2.2164
Chloride	XOWJAW	-2.3401	-2.7606	-2.5623

Table B-5 *Copper sulphur and copper nitrogen distance in structure 3*									
		experimental		PBE		B3LYP		PBE0	
Counter ion	CSD code	Cu-N (Å)	Cu-S (Å)	Cu-N (Å)	Cu-S (Å)	Cu-N (Å)	Cu-S (Å)	Cu-N (Å)	Cu-S (Å)
Nitrate	DOLPID	1.97	4.653	1.98	4.769	1.981	4.686	1.976	4.671
Chloride	KEBMIQ	1.993	3.305	1.993	1.949	1.992	3.293	1.989	3.246
Azide bridging	KEBMOW	1.979	3.22	1.974	3.077	1.982	3.216	1.974	3.176
Iodine bridging	HOHJAP	1.967	3.02	1.971	2.805	1.993	1.998	1.984	2.932

Table B-6 *Structure 3 binding energies for the three exchange functionals used*				
		PBE	B3LYP	PBE0
Counter ion	CSD code	Binding energy (eV)	Binding energy (eV)	Binding energy (eV)
Nitrate	DOLPID	-1.8359	-4.1344	-2.5872
Chloride	KEBMIQ	-2.3145	-2.6781	-2.4581
Azide bridging	KEBMOW	-2.8439	-2.9728	-2.8187
Iodine bridging	HOHJAP	-2.4458	-1.3172	-2.1346

Table B-7 *Structure 4 binding energies for the three exchange functionals used*				
		PBE	B3LYP	PBE0
Counter ions	CSD code	Binding energy (eV)	Binding energy (eV)	Binding energy (eV)
Chloride	BALCIC	-8.5676	-6.0494	-5.3772

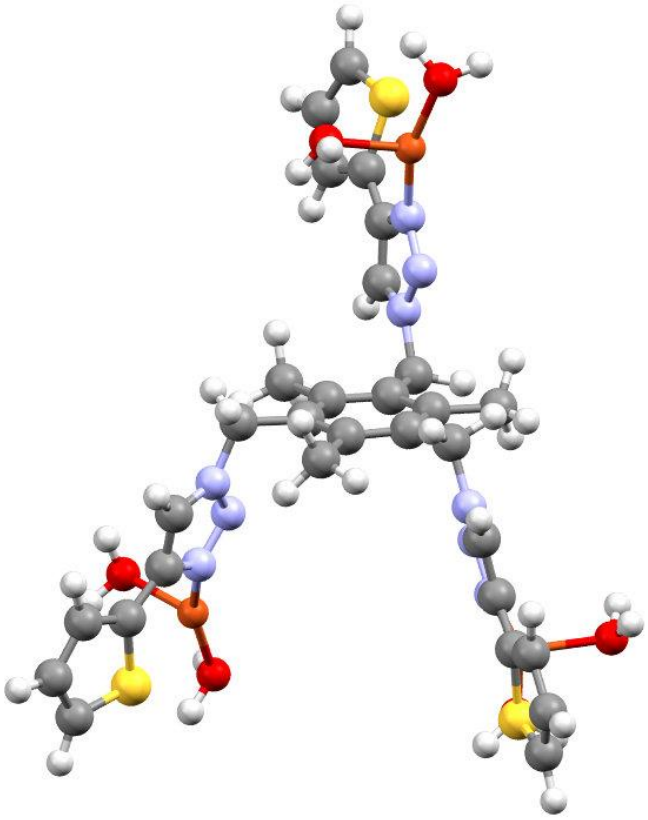

Figure B-1 *Image of Cu(II) TC-Thio with exclusively water ligands using PBE-D3(BJ)*

Table B-8-*XYZ atomic coordinates for Cu(II)- TC-Thio with exclusively water ligands using PBE-D3(BJ) with a charge of 6 and multiplicity of 4*

C	*8.84455482316027*	*7.18001316986460*	*1.78552027595866*
C	*9.99651681508709*	*7.84442476745242*	*2.25380318122224*
C	*9.90946133157709*	*8.83794192487366*	*3.24607030993517*
C	*8.63683964058460*	*9.17155458673460*	*3.75802802744730*
C	*8.99150118195186*	*6.08417302780952*	*0.76140107855296*
H	*8.09083131584628*	*5.47433112028913*	*0.65188823398213*
H	*9.23462852618258*	*6.49908884720176*	*-0.23038566856622*
H	*9.80182241845922*	*5.39425384183796*	*1.03102425459669*
C	*11.13837090767922*	*9.54298478714230*	*3.75676661785524*
H	*12.04817111815036*	*8.95069433474385*	*3.62071175104147*
H	*11.06518603905930*	*9.75911211827699*	*4.83032633312480*
H	*11.28476029575036*	*10.50526173398823*	*3.23963438206307*
C	*11.33335028942203*	*7.49262703957593*	*1.64466676126650*
H	*11.23911323016912*	*7.21743297339146*	*0.58889892556364*

H	*12.04337836953153*	*8.32544560423653*	*1.70560139113043*
N	*11.96986286018449*	*6.33483042024084*	*2.30583702123108*
N	*11.98502949718589*	*6.25758853021134*	*3.64621912694686*
N	*12.61023543589409*	*5.14033918477958*	*3.94208982424972*
C	*12.57066323577325*	*5.28001007267663*	*1.72745250067821*
H	*12.65215036608249*	*5.16127978189115*	*0.65244183082294*
C	*13.00267866555936*	*4.48242845643803*	*2.78930994248265*
C	*13.70412066136404*	*3.24248875656475*	*2.78638302863623*
C	*14.32831978803509*	*2.61394000142530*	*1.70282848677012*
H	*14.32119267417830*	*3.02961128687924*	*0.69617957761387*
C	*14.97182500227325*	*1.42482532083488*	*2.07028065386676*
H	*15.51457180600399*	*0.77962314516595*	*1.38164870197982*
C	*14.83306521951510*	*1.13559532500932*	*3.42471463980378*
H	*15.21879765430110*	*0.27791429528233*	*3.97119237514880*
S	*13.90319981942932*	*2.31003181696238*	*4.24872889795939*
C	*8.52948109942467*	*10.22327302142952*	*4.83436896019076*
H	*7.53754394192550*	*10.24495731128240*	*5.29609296062590*
N	*8.78083508109624*	*11.57644712794359*	*4.30474872430852*
N	*8.14288247747548*	*11.97951584031533*	*3.19263171022758*
N	*8.51916027946125*	*13.22091269536768*	*2.98773111335105*
C	*9.56319087515410*	*12.53914757446960*	*4.82291547711203*
H	*10.15810780207327*	*12.40129381994502*	*5.71918384007791*
C	*11.08932972233704*	*15.35727320631198*	*4.75558385239766*
H	*11.63493607366294*	*14.69918732601588*	*5.43017568405807*
C	*11.41820341602900*	*16.69755683504895*	*4.50684071180231*
H	*12.24085475402896*	*17.22814800119333*	*4.98331781130421*
C	*10.56498252329214*	*17.29853280068485*	*3.58645100080037*
H	*10.58227680260415*	*18.32358475902425*	*3.22327768259324*
S	*9.34914482105041*	*16.23143623828568*	*3.03500828174070*
C	*7.57955009987537*	*7.55970273950019*	*2.28195624195874*
C	*7.46423501255980*	*8.54138010937575*	*3.28641645262963*
C	*6.13255617265254*	*8.91600376918749*	*3.88636720931936*

H	5.29446789635637	8.34790340880989	3.47436693214517
H	6.13257220031169	8.72741293669402	4.97040338014125
H	5.91461023146783	9.98430284296097	3.73852803167956
C	6.34253238716555	6.92920801247470	1.69147078131566
H	6.47477198989956	6.67808145377488	0.63417894631535
H	5.47647962768287	7.59825507436647	1.75462714856639
N	5.96193487544457	5.67018131534488	2.36667206017577
N	6.18172909698589	5.52157137995816	3.68332242541426
N	5.73518576997375	4.32635375918326	3.99692375147352
C	5.38014530751827	4.58814249724018	1.82074748781212
H	5.13043111654417	4.51826102178964	0.76750740179667
C	5.21938575953001	3.69161298925745	2.87911801179138
C	4.65378074038022	2.38493572359625	2.90045597692619
C	3.90117751947909	1.76370029191081	1.89555498887439
H	3.68196031292954	2.24292205102179	0.94242830792712
C	3.45123566445778	0.49231763834830	2.27141338110863
H	2.85269108142728	-0.16162264767080	1.63965740809392
C	3.86572360915166	0.13302002476345	3.55165950881620
H	3.67077154903441	-0.79493059595599	4.08479490628455
S	4.81740669488210	1.34366207769063	4.29333519550720
H	9.26186189852015	10.07483318587993	5.63692792073320
C	9.40623436032869	13.63024174553183	3.96781275590909
C	9.98705303117532	14.93062822216422	4.00933472453826
Cu	13.21746221448130	4.85880554497837	5.73133762617277
Cu	5.55475662632668	3.84045737530576	5.83234848278663
Cu	8.10910182309508	14.08837815272549	1.33851194093348
O	13.19712634006502	4.27449792402642	7.60764559395491
H	13.62680761722520	4.91167343450545	8.21266493381393
H	13.66464641371276	3.42603209031296	7.74409471172566
O	14.99949975332024	5.90641935456956	5.84962407095396
H	15.73749000737192	5.27768860635017	5.98028562283777
H	15.19611627834463	6.35358796239073	5.00249720119988

O	9.60843248861872	13.59566459624123	-0.01925338729727
H	10.30127638046445	13.05805724745260	0.41236264209612
H	9.24816591752120	13.02262849614559	-0.72515185515976
O	7.12633653247364	15.06005358700833	-0.06793773505096
H	6.39172476147484	15.59953271507439	0.28672353521835
H	7.70486791183653	15.68959834354893	-0.54304489319214
O	3.69666247871571	4.47062039021531	6.52108185715336
H	3.74733935536409	5.41231737653846	6.78086303458688
H	3.04339457281570	4.44529291019561	5.79387806626808
O	6.02280753501993	3.16794798108191	7.61797451416599
H	6.64906742044431	2.41741979319185	7.59273861352428
H	5.24030490756242	2.84366226183957	8.10682381209785

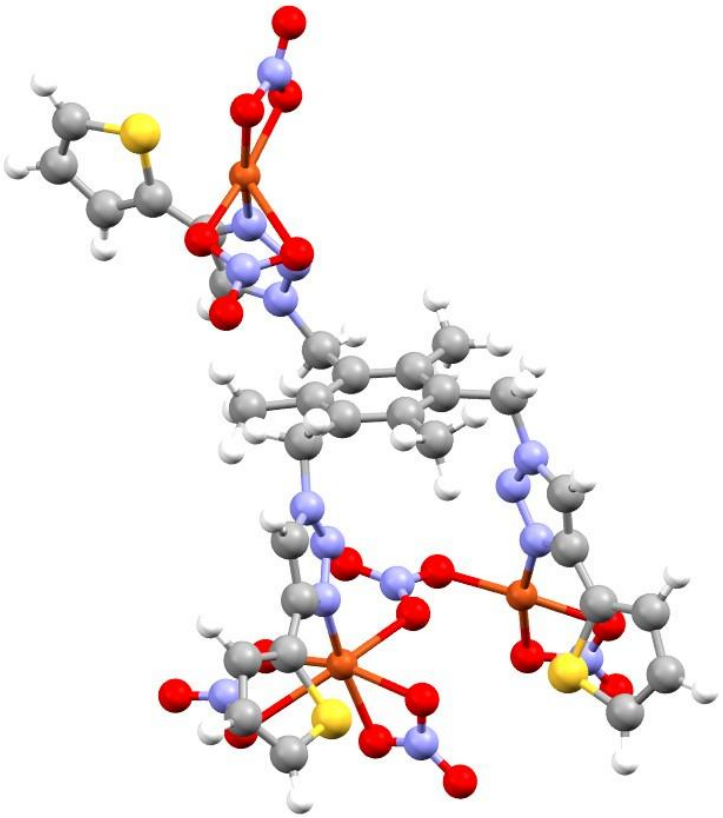

Figure B-2 *Image of Cu(II) TC- Thio with exclusively nitrate ligands using PBE-D3(BJ)*

Table B-9-*XYZ atomic coordinates for Cu(II)- TC-Thio with exclusively nitrate ligands using PBE-D3(BJ) with a neutral charge and multiplicity of 4*

C	*8.22849914077916*	*7.56881524866250*	*1.90241408617415*
C	*9.36948718181196*	*8.25957826554406*	*2.35274858054057*
C	*9.26683325003855*	*9.25986717119646*	*3.33756859023323*
C	*7.99005719224373*	*9.63252018958642*	*3.79921663367443*
C	*8.37359354603627*	*6.43673496400409*	*0.91842566567001*
H	*7.51076198101455*	*6.35169904234923*	*0.24770490145446*
H	*9.26093291007013*	*6.54575933875968*	*0.28514176021304*
H	*8.47375718011493*	*5.47441437078732*	*1.44662192640689*
C	*10.50580341078265*	*9.92666156550143*	*3.87974890300216*
H	*11.33098206554548*	*9.21130496991461*	*3.98691795321688*
H	*10.33700848988503*	*10.36379416586243*	*4.87004601279880*
H	*10.85341368574787*	*10.73786206838010*	*3.21913324468474*
C	*10.71912839523213*	*7.93468904942874*	*1.76849178022400*
H	*10.67708242377487*	*7.85296351823931*	*0.67509147822434*
H	*11.45783450730327*	*8.70888966838520*	*1.99964965161734*
N	*11.26412438084992*	*6.65358436225367*	*2.26099564515229*
N	*10.80337027088206*	*6.09590074624681*	*3.37798049874307*
N	*11.51805674753152*	*5.00147675581292*	*3.56660111144555*
C	*12.27147845748921*	*5.93299836243325*	*1.71592268944721*
H	*12.76127402011688*	*6.21763669804911*	*0.79181500907218*
C	*12.44894840810143*	*4.85029350856495*	*2.56714122106530*
C	*13.42034295134038*	*3.78137917877995*	*2.46232596715627*
C	*14.68295045185466*	*3.87716396063772*	*1.90137818470671*
H	*15.08168158248421*	*4.81165334478549*	*1.50748699494698*
C	*15.39281815131896*	*2.65006330597706*	*1.92234010110520*
H	*16.40398688060072*	*2.52295598236160*	*1.53806669962541*
C	*14.66552848756934*	*1.63000867093653*	*2.49385202472051*
H	*14.95345838386197*	*0.59325483820341*	*2.64853165243807*
S	*13.11268464173240*	*2.15958952459421*	*3.00102996434645*
C	*7.86861193100575*	*10.78963200456617*	*4.76285344259603*
H	*6.83845180320540*	*10.94788386777495*	*5.09530678249659*
N	*8.32971126929557*	*12.04711494586870*	*4.14142524058247*
N	*8.18736081087637*	*12.22814101161483*	*2.83113707810392*

N	*8.71856192399014*	*13.40570188280342*	*2.56533793720306*
C	*8.93841561405477*	*13.10073931350560*	*4.73620088952190*
H	*9.14705734222865*	*13.13279620751499*	*5.79939563433280*
C	*10.50640033505436*	*15.88360552870471*	*4.79721612710176*
H	*10.58750401026450*	*15.41991425644398*	*5.77982951888456*
C	*11.05571843752474*	*17.14777911945709*	*4.46369238005756*
H	*11.60415410384640*	*17.77751000160858*	*5.16288390586467*
C	*10.82383960805713*	*17.50108971607708*	*3.15359185896135*
H	*11.12138014863710*	*18.40340341168247*	*2.62582893860700*
S	*9.92121143065729*	*16.29505008045848*	*2.32395476480342*
C	*6.96429820694165*	*7.90572379750109*	*2.43572761894023*
C	*6.82955218606173*	*8.95835877083002*	*3.36547759901870*
C	*5.49093288188055*	*9.37163899899750*	*3.92735762745524*
H	*4.65379742004900*	*8.80400282151306*	*3.51482644810994*
H	*5.46297245663511*	*9.23370330738101*	*5.01862517730432*
H	*5.29284697258113*	*10.43477334492608*	*3.72530165509493*
C	*5.77415128842888*	*7.06100353413407*	*2.04690226689432*
H	*5.79200404918343*	*6.76975007948590*	*0.99211870469541*
H	*4.81664503539361*	*7.55705593639769*	*2.22818364893663*
N	*5.77259630933205*	*5.79871539231813*	*2.81328721379985*
N	*5.90767823828252*	*5.83757765936898*	*4.13679026234229*
N	*5.93783604073570*	*4.58117948575773*	*4.53603919698731*
C	*5.72082202941188*	*4.52887447804969*	*2.34464066278306*
H	*5.64589293422059*	*4.29474035700288*	*1.28896513815472*
C	*5.83500005472537*	*3.72261188931111*	*3.46928920437692*
C	*5.89639046018900*	*2.28405487483585*	*3.58617142827300*
C	*5.28545891153567*	*1.32994894056025*	*2.79233254650591*
H	*4.63258477002510*	*1.58572481619665*	*1.95838606860371*
C	*5.58376054045171*	*0.00483156484881*	*3.20178634505922*
H	*5.19597819223632*	*-0.88678727379027*	*2.71080586890831*
C	*6.41792878801181*	*-0.03930753186820*	*4.29713677575127*
H	*6.80911383014797*	*-0.90798072436517*	*4.82029364681343*
S	*6.86001945105531*	*1.53514414955788*	*4.82080439019852*
H	*8.48606558223606*	*10.64949939408823*	*5.66011045348086*

C	9.20086428699110	13.99668240479846	3.70615809104739
C	9.85621568768588	15.28213613537292	3.73335302034011
Cu	11.21405635267381	4.02616241309781	5.25849417916377
Cu	6.10782167522018	4.21426631523285	6.44425023747046
Cu	9.03841774702687	13.80777239383343	0.67060397108757
O	10.86878943532141	2.55783044933823	6.67505830393437
O	12.18016295051596	5.32904803324838	6.39452303912891
O	10.76280519285901	12.82627448871987	0.59673803148216
O	9.00353954795155	14.50768032105497	-1.24795524550681
O	7.34159351040908	5.68605011938747	6.88914090952743
O	5.92820797079146	3.52061062556316	8.33134708012565
N	4.88678716775553	2.80837562621634	8.03712465853564
O	4.31190205080932	2.11730899133971	8.85010423928420
O	4.52753679093609	2.90255977896320	6.80528843948795
N	8.54988911296725	5.63689438474127	6.38481235671099
O	9.28064764441737	6.60854443700363	6.57197208863932
O	8.88386857344273	4.60993653041000	5.75099773402933
N	10.33854070110943	1.78097777613215	5.79581575198184
N	13.41775097831980	4.92441147975275	6.59462157891907
O	10.29601522559238	2.27928853882709	4.60898195176305
O	9.91329529909308	0.67267003487710	6.06223661480476
O	14.14760874072000	5.65267175691234	7.27363591933570
O	13.77369416915842	3.84407396216967	6.09043349712076
N	7.88038545533151	15.11345884404695	-1.04986191930417
O	7.41363355736793	14.96512603720951	0.14425791299220
O	7.31726035862823	15.76130619773111	-1.90614448525181
N	10.49776704927239	11.61416000215208	0.15536176373425
O	11.43555590863829	10.82118438946168	0.06152478215464
O	9.31501228441872	11.35027528503888	-0.13929788245399

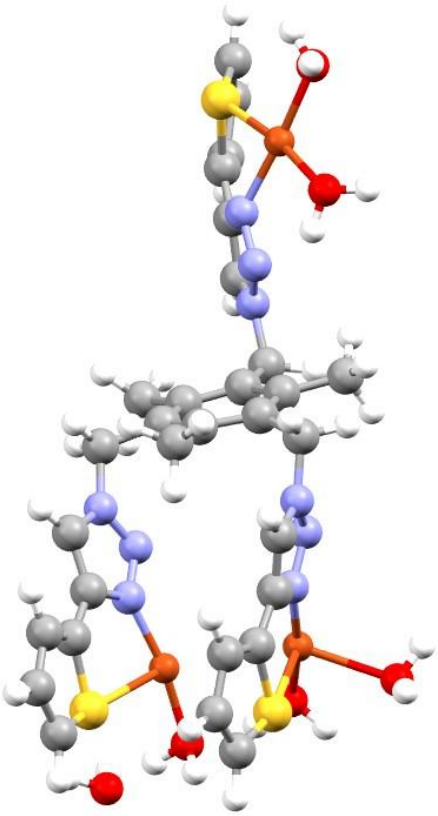

Figure B-3 *Image of Cu(I) TC- Thio with exclusively water ligands using PBE-D3(BJ)*

Table B-10-*XYZ atomic coordinates for Cu(I)- TC-Thio with exclusively water ligands using PBE-D3(BJ) with a charge of 3 and multiplicity of 3*

C	9.17010110795333	7.62585180095830	1.80123977912325
C	10.31130202120660	8.12548273423474	2.45254429064973
C	10.22147559156448	9.22876460797060	3.32396275939827
C	8.95942841963703	9.81518068351108	3.54981432933948
C	9.29984622964790	6.53356461158889	0.77145129104457
H	9.28038686015345	5.52684868506692	1.21522756658837
H	8.48714054697765	6.57878398536535	0.03667148103436
H	10.24332351375261	6.62547758724403	0.21911993875061
C	11.47180732632932	9.76617505004940	3.97684839319482
H	11.90488746872374	9.02786297457126	4.66970882055583
H	11.29925026489347	10.68421024992729	4.54457102432733
H	12.24045698485938	9.99735736019422	3.22547011606260
C	11.62405559102084	7.39515596418772	2.27976382576589
H	11.96270733277641	7.36999194629214	1.23534056122973

H	*12.42510676180162*	*7.84200736810327*	*2.87660559847488*
N	*11.49842342428672*	*5.98363508824829*	*2.69771412644715*
N	*10.91861538458600*	*5.67693712238751*	*3.86089378040192*
N	*10.88577965248130*	*4.35223995582569*	*3.91442600263507*
C	*11.85016299771437*	*4.87925856836086*	*1.99812426004014*
H	*12.32593763386576*	*4.92964823048799*	*1.02560505256535*
C	*11.44817341658090*	*3.80819417293435*	*2.78301817344160*
C	*11.52737058737397*	*2.38911157620959*	*2.53398835296651*
C	*11.77123257236741*	*1.74903305736674*	*1.33176676897889*
H	*11.93827858983309*	*2.28623852074774*	*0.39860051976903*
C	*11.75515477025112*	*0.33475793317904*	*1.44694435638410*
H	*11.91839363330578*	*-0.34579040758428*	*0.61215677810891*
C	*11.50194498401414*	*-0.09088028480074*	*2.73040374506498*
H	*11.42388477806451*	*-1.10583829233892*	*3.11096294502858*
S	*11.28573501878082*	*1.23497663379454*	*3.81010434840296*
C	*8.83956094165560*	*10.99471518697893*	*4.48667123243410*
H	*7.81532316595870*	*11.10846521126987*	*4.85970378722098*
N	*9.20971789927513*	*12.26871007926643*	*3.84247001742584*
N	*8.85876165082815*	*12.48983891145973*	*2.56226826087893*
N	*9.29868727369925*	*13.72298612662089*	*2.26574677635321*
C	*9.86566725233176*	*13.30243967589524*	*4.39432166934983*
H	*10.21457441906811*	*13.28862181958882*	*5.42075357543396*
C	*10.69835339171478*	*16.56229230373501*	*4.34870696574847*
H	*10.91855715257777*	*16.27572237039066*	*5.37543810328114*
C	*10.63071576006616*	*17.86571836499125*	*3.88530703466248*
H	*10.85018119104761*	*18.73825226831133*	*4.50161126733529*
C	*10.28003838435396*	*17.99619033737406*	*2.51773978233416*
H	*10.20570112430456*	*18.90204270476863*	*1.92447907722546*
S	*10.11599858434976*	*16.44982344899252*	*1.75678007872318*
C	*7.90421480304826*	*8.14247672940118*	*2.14341363709308*
C	*7.78957428559565*	*9.27353589521515*	*2.97286768532995*
C	*6.44349144211718*	*9.90443423579947*	*3.23887796321725*
H	*5.72217004507067*	*9.68099817581578*	*2.44571653353708*
H	*6.01152521137859*	*9.55897009487593*	*4.19190209724333*

H	6.52166574960624	10.99772860918977	3.28619858950639
C	6.68563047814970	7.32680380421147	1.76539101867638
H	6.62623065641865	7.08116014342868	0.69892809102157
H	5.74711742874074	7.80807798795104	2.05366953030131
N	6.75731674467108	6.03774990925828	2.48565990764650
N	6.91274040247576	6.04756283707305	3.81319226010453
N	7.11813573873539	4.78931538079934	4.16876546900962
C	6.85005248818174	4.78676469109464	1.97521814814674
H	6.75319687887290	4.57871002788272	0.91612427447245
C	7.09138331501140	3.96517574339951	3.06856656179268
C	7.31913973664283	2.54322761211436	3.14487358876048
C	7.64801448389525	1.66858445954967	2.12501148087150
H	7.78475860473985	1.98878818667785	1.09244875013674
C	7.80696146939804	0.33172314373863	2.57398291475015
H	8.08042790519828	-0.49912665788130	1.92504065519549
C	7.59683378429849	0.19545266437257	3.92632841387436
H	7.66078407845501	-0.69859826148223	4.54076974873333
S	7.20106707961126	1.70267972149803	4.66380378089294
H	9.49036139589624	10.89049643618049	5.36161014799950
C	9.92963244823490	14.28602902364967	3.38946964193650
C	10.35579174340224	15.61123067310807	3.34327522238240
Cu	10.27074283260376	3.39075881494837	5.40793255022093
Cu	7.37847783249349	4.33212859308703	5.97493820329107
Cu	8.28483008559692	14.90528550826038	1.10549244456445
O	9.98385083181024	2.38126717724563	7.04425794605363
H	10.87379615834522	2.22273257218851	7.55309726202365
H	9.60838473126729	1.49976688140963	6.85134202487169
O	12.18209740722888	1.98955102294343	8.30836741010501
H	12.91480666071015	1.89116971068020	7.67124486013388
H	12.41492088383239	2.77718153641973	8.83554212375822
O	7.33374171222898	16.11065846875938	-0.21228837825015
H	7.87997852014269	16.86468939942582	-0.50731035583294
H	7.08253481471250	15.63797817852894	-1.03008742137915
O	6.84320207726433	13.33866473490021	0.73004508571363

H	*7.18391893519457*	*12.65842476162742*	*1.35719487891012*
H	*5.96459717128355*	*13.58678229659158*	*1.07629008468991*
O	*5.22840078104597*	*4.05141483426156*	*6.96607206466259*
H	*4.72553665443780*	*4.87267578903941*	*6.81276804918109*
H	*4.77629127210893*	*3.38589472626184*	*6.41495613385054*
O	*7.97955203863949*	*4.04178336472526*	*7.81619737577863*
H	*8.70683691929622*	*3.36338246620536*	*7.78842091187077*
H	*7.23208162586591*	*3.63733160183426*	*8.29901401896487*

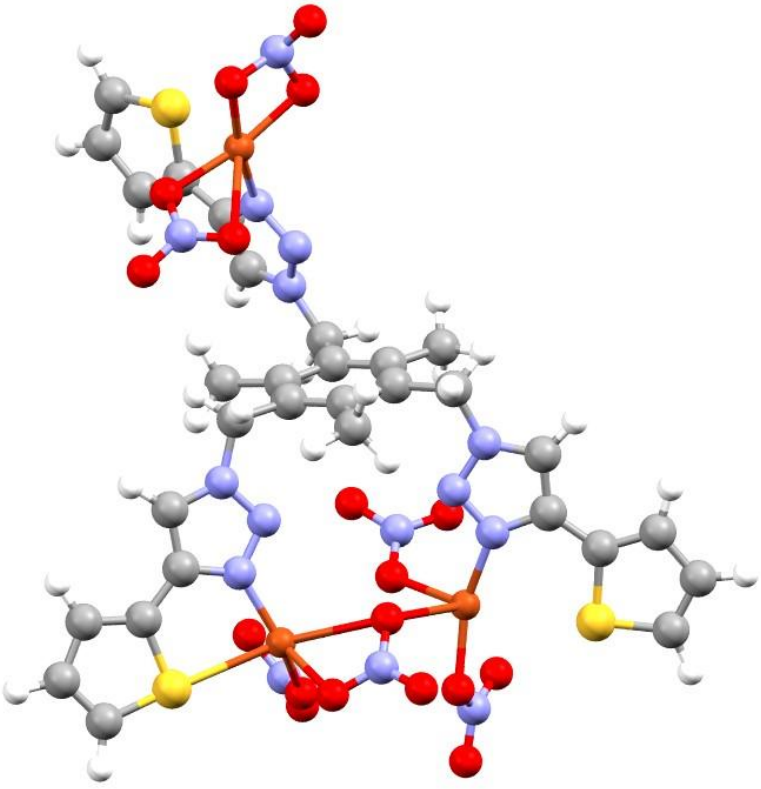

Figure B-4 *Image of Cu(I) TC-Thio with exclusively nitrate ligands using PBE-D3(BJ)*

Table B-11-*XYZ atomic coordinates for Cu(I)- TC-Thio with exclusively nitrate ligands using PBE-D3(BJ) with a charge of -3 and multiplicity of 3*

C	8.55785576048353	7.29162568002953	1.54400004939262
C	9.66532673943527	8.03919096110645	1.98208630935664
C	9.52983318470168	8.99682006649542	3.00682597165549
C	8.25659234421830	9.24540834286147	3.55055324982081
C	8.70375577964513	6.19669690039660	0.51574706077044
H	8.24346695546692	5.26560692321554	0.87593730541711
H	8.21067655041413	6.46330105869328	-0.43228840742047
H	9.74814407140442	5.96280710636057	0.29111207797843
C	10.74011631153864	9.74506222564299	3.50511390795283
H	11.63858825259713	9.11620747651570	3.49681293126133
H	10.61034223285002	10.09822421422775	4.53439909381076
H	10.95001772549884	10.62897203521191	2.88021300330178
C	11.02370513967626	7.81947762083372	1.36504919429979
H	10.94309013835880	7.50111068632666	0.31822314522314
H	11.62502258061227	8.73555297455231	1.37515914599104
N	11.80562284241244	6.79459942304119	2.08532250042717
N	11.19050347800375	5.86446146550456	2.82794227425355
N	12.14330765424023	5.06816285889501	3.28937883131284
C	13.14676819287465	6.60936196564649	2.05371322809513
H	13.81267565175982	7.26265110366914	1.50171243737160
C	13.37401687995851	5.48582706841726	2.83736399128151
C	14.59211656714972	4.79931213943712	3.18673346614844
C	15.89784179478177	5.12225220039903	2.86258515309169
H	16.16092293344202	5.99764351861943	2.26930162993671
C	16.84099726574324	4.19955675475088	3.38600940322614
H	17.91783240881987	4.28363783502657	3.24218606200287
C	16.25052075666358	3.18227885718960	4.09991110406633
H	16.71952457699522	2.34474774093086	4.60969124381905
S	14.52981186320169	3.34518960514132	4.14246482727646
C	8.09432426336041	10.33046921599398	4.58891681237781
H	7.07381044982820	10.37358622477034	4.98168125415399
N	8.40961694424029	11.65499162386485	4.02240507327301
N	8.06440178024886	11.93647406755272	2.76502250112157

N	*8.51053064436647*	*13.15353745864334*	*2.52230983669838*
C	*9.06630250156462*	*12.68437025827279*	*4.60772946146474*
H	*9.42881054324986*	*12.64284399147293*	*5.62847021369919*
C	*10.59329865525270*	*15.49633498918460*	*4.62839124531769*
H	*10.91255215615674*	*14.92930010393347*	*5.50240850902043*
C	*11.00989258985581*	*16.82212389806361*	*4.34239079627874*
H	*11.68244943148124*	*17.39920172781111*	*4.97575122534728*
C	*10.47559212056359*	*17.30572898317100*	*3.16986905565019*
H	*10.61759135169413*	*18.27798490085677*	*2.70537526415008*
S	*9.45161941503241*	*16.14752078472536*	*2.41292746537022*
C	*7.29456758311816*	*7.53805380223021*	*2.12156410713628*
C	*7.13139328038602*	*8.50924161977600*	*3.12733266636808*
C	*5.79278729038761*	*8.74837907878299*	*3.78306635949391*
H	*5.00542694809587*	*8.09253337158857*	*3.40116996803671*
H	*5.85406986799942*	*8.57314729740672*	*4.86754139178444*
H	*5.45731233843150*	*9.78650164308348*	*3.63758255091244*
C	*6.11772137003290*	*6.71101270772219*	*1.66749916836629*
H	*6.28039529323946*	*6.30252173804587*	*0.66323956186949*
H	*5.18743843027532*	*7.28892041245899*	*1.63396075056474*
N	*5.87553955201091*	*5.57068824385385*	*2.57343622627469*
N	*6.87204137297312*	*5.08481256292072*	*3.31774518023160*
N	*6.37691951487138*	*4.04819938312511*	*3.97614133576716*
C	*4.73433107264439*	*4.86001152679592*	*2.73241225984538*
H	*3.81683196226799*	*5.10464633096045*	*2.20948592504161*
C	*5.05566013371902*	*3.86326765243796*	*3.64664682698271*
C	*4.23701647304361*	*2.80525086053620*	*4.18879627756985*
C	*2.90219554982971*	*2.54960877494245*	*3.92370329219307*
H	*2.30450236726571*	*3.16352901971978*	*3.25030143231821*
C	*2.40721538285656*	*1.41477546539994*	*4.61645355972476*
H	*1.38230957502988*	*1.05332047499090*	*4.53860202452038*
C	*3.36622736340477*	*0.81729017489963*	*5.40155431449021*
H	*3.27439114017699*	*-0.05918436119086*	*6.03803695069670*
S	*4.88371720449675*	*1.63540588449674*	*5.30326983390476*
H	*8.76999673195458*	*10.19313669981590*	*5.44336319033277*

C	9.13623442134263	13.66865377474060	3.62913264402333
C	9.74203122465121	14.97937621467045	3.66753545157008
Cu	11.78544561449303	3.59134561551845	4.44325428050456
Cu	7.48858547527461	3.18333152782689	5.26230230874223
Cu	8.54283507522159	13.80276670183869	0.63853670405329
O	11.23525637524092	1.62214650571916	3.82481113184061
O	11.62186064909401	3.09460795671510	6.38025352780317
O	10.51386463450015	13.28580129168148	0.43474826921763
O	8.29599781657806	14.59261425209822	-1.13070318988071
O	8.68741989101795	4.89136623125153	6.11348603829245
O	8.29490285862175	1.75536087550704	6.32845806810117
N	8.01078639784746	1.74846286587929	7.60200188522400
O	8.59221128918422	0.91351214268567	8.32242873276495
O	7.17520687252646	2.56467896663437	8.04711945309015
N	8.13822879023102	6.02315806790990	6.36010938909120
O	6.90928830319167	6.08048115701978	6.62236945730200
O	8.84965499631853	7.06149614857936	6.33874494247160
N	9.98333535115322	1.69278260984305	3.52868766568551
N	11.76010429168934	4.03136890047070	7.27559836436977
O	9.40950691951190	2.81838343842198	3.62363810194136
O	9.37367166490797	0.66995446984704	3.16259910335606
O	11.50456427860509	3.74181345670370	8.46253198449922
O	12.13885865468226	5.16954880669235	6.92764629730399
N	7.01668431873648	15.04569406327301	-0.81297895143082
O	6.69975582681232	14.47340338508662	0.41562287285181
O	6.13624008438108	15.05073501581998	-1.72024568034718
N	10.60528417818914	12.02476669616268	0.11412005203136
O	11.73632588482036	11.51369409500251	0.06137011755759
O	9.55427058281121	11.38985936413745	-0.12501308150482

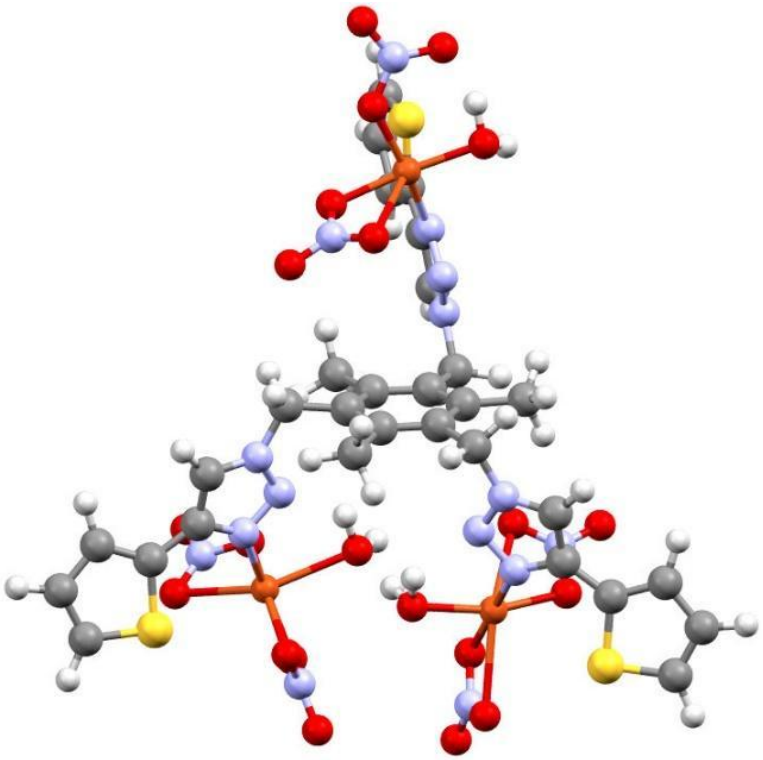

Figure B-5 *Cu(II) TC-Thio structure optimised with PBE-D3(BJ)*

Table B-12-*XYZ atomic coordinates for Cu(II)- TC-Thio with both nitrate and water ligands using PBE-D3(BJ) with a neutral charge and multiplicity of 4*

C	8.83348670856095	7.01525005194863	1.43356043238303
C	9.82123346942877	7.80482907747068	2.05468585584117
C	9.49002077027498	8.68247546430130	3.10474950482761
C	8.13621371976016	8.84355466449969	3.46180555591581
C	9.20656330772409	5.95601387163665	0.42556455294324
H	8.75461038047137	4.99041978383126	0.69530826656461
H	8.85364922808893	6.21146111063764	-0.58551058871595
H	10.28642048750507	5.79062370230331	0.36711736450388
C	10.56758754188101	9.45157253359283	3.82567212151520
H	11.51455776564497	8.90098181829821	3.85877040282115
H	10.29142789629753	9.66323302534061	4.86556789733767
H	10.76117433799516	10.42073981704062	3.33653696086559
C	11.24971996920525	7.73671395079927	1.57676054509199
H	11.30868945272127	7.55059872651850	0.49882535137761
H	11.77779727927878	8.67855631131986	1.76906130746480
N	12.03092416018365	6.66102319385792	2.22398469007135

N	*11.70245834136446*	*6.21736847808577*	*3.43222497955349*
N	*12.61065086949854*	*5.31873349064160*	*3.76788418906942*
C	*13.14982392688053*	*6.05692205323677*	*1.76122372849316*
H	*13.56680437737569*	*6.27282648289208*	*0.78411652001520*
C	*13.53594992607204*	*5.17640838089861*	*2.76707816832890*
C	*14.66627857736462*	*4.27623776521992*	*2.80300122910206*
C	*15.84467491644697*	*4.39134593140586*	*2.08423410466912*
H	*16.04715133384253*	*5.22470459374355*	*1.41188042034626*
C	*16.75032573876225*	*3.33076983844627*	*2.33780609141159*
H	*17.73321783855216*	*3.24423462405577*	*1.87675389500107*
C	*16.25490730034706*	*2.41730258617055*	*3.24179037245359*
H	*16.72455304629887*	*1.51431270026200*	*3.62340330913078*
S	*14.68091602127807*	*2.84214420995249*	*3.78118913216002*
C	*7.77901913961742*	*9.78406661710953*	*4.58710495345008*
H	*6.72320072845872*	*9.71572231900958*	*4.86728601885606*
N	*8.06303198546271*	*11.18546481829895*	*4.22617335933541*
N	*7.87747969504069*	*11.59066699382084*	*2.97229499034409*
N	*8.26377090536837*	*12.85003474436001*	*2.93361856774298*
C	*8.55602144884735*	*12.17313690468168*	*5.01008181562734*
H	*8.77718755389711*	*12.02978809855082*	*6.06155564945542*
C	*9.84021114701147*	*15.02218136325950*	*5.60041559908057*
H	*10.02858153854589*	*14.36868955661450*	*6.45176024840052*
C	*10.22465118742217*	*16.38587378974570*	*5.54223531254511*
H	*10.73761722126533*	*16.90934264933685*	*6.34790251124113*
C	*9.88245911768561*	*16.98519005464127*	*4.35125253194633*
H	*10.04829033322763*	*18.00985196612493*	*4.02924449650093*
S	*9.07908297603792*	*15.88834841162211*	*3.29887897892251*
C	*7.48559152927051*	*7.20791500959465*	*1.79234941659169*
C	*7.12091576978433*	*8.14785753241760*	*2.77814123517671*
C	*5.67064822221850*	*8.37822705968706*	*3.12123289601803*
H	*4.99979331678685*	*8.08262764730615*	*2.30748105682190*
H	*5.37423466738261*	*7.80737601631255*	*4.01664723088572*
H	*5.47104583640623*	*9.43786167121596*	*3.32465798532477*
C	*6.41439412206789*	*6.35173496882105*	*1.15829731055299*

H	6.80253840566901	5.74354331678331	0.33534649498337
H	5.57888779787659	6.94361963009653	0.76479563038344
N	5.83368935499490	5.43509508034132	2.16056545087906
N	6.61470343073275	4.94390215085744	3.11482603959419
N	5.84145203730032	4.22153803505628	3.90614968489652
C	4.55142087924763	5.02529810498498	2.30571564018435
H	3.76314376979497	5.31498741811061	1.62013274146314
C	4.54833224019054	4.23089206287624	3.44852603903707
C	3.45123488882186	3.52914325253298	4.07357842976838
C	2.10112760566391	3.81869910683251	3.97112150250611
H	1.72065624262716	4.66598729188733	3.40123250848841
C	1.28793732621345	2.91418245179740	4.69948222471012
H	0.20185042034594	2.97621698437302	4.75214167664580
C	2.02274297195983	1.94368003085536	5.34440974293862
H	1.66975825186565	1.12837208892069	5.97068180013354
S	3.70689299892318	2.12589717428067	5.06295885137522
H	8.36802328739767	9.57770108849370	5.48993261152898
C	8.69533649964685	13.26996272576238	4.16666739639952
C	9.20460554846961	14.59171022824540	4.44815680790558
Cu	12.41518686043862	4.60533668756293	5.61706660988292
Cu	6.71984165806440	3.91480713404937	5.67140127188645
Cu	8.49237032560411	13.63383750878942	1.11908326383601
O	11.68798333265753	2.71374418042086	5.26528790938222
O	13.08874303006404	6.23110386486456	6.51902134090631
O	10.28811655311574	12.74061807889169	0.98517538690667
O	9.05836261285105	14.66224277766035	-0.51622293609829
O	5.15540820481588	4.72813059553476	6.66480972507806
O	7.62975993464834	3.51681795920973	7.39857819666040
N	7.57868183439659	2.21407486101519	7.55014395843454
O	8.10562420298139	1.72387146159800	8.55057573725436
O	6.99329588595154	1.55175229228010	6.66647256652891
N	5.40559566969254	6.01357370480555	6.74313263843818
O	4.55155358867144	6.73808794751862	7.26190587040022
O	6.49255697216984	6.42832614627181	6.28521748112254

N	*11.61763239771171*	*2.46471454118536*	*6.52975231963451*
N	*14.33945984464966*	*6.05795064799844*	*6.89390461381024*
O	*12.02399246950488*	*3.43260685281607*	*7.27569624885539*
O	*11.20437069239209*	*1.41165468571701*	*6.97203837997620*
O	*14.89288168051504*	*6.99522085071984*	*7.47461331197499*
O	*14.88071906594517*	*4.96634334133383*	*6.64069439986350*
N	*8.51819082407594*	*15.74690278234582*	*-0.99821725571689*
O	*7.39979277716936*	*16.14567187815995*	*-0.57327338332920*
O	*9.13604513186576*	*16.35031681886624*	*-1.87393485393714*
N	*10.08761591751051*	*11.61637068534126*	*0.33762140001871*
O	*11.04573722057367*	*10.85377377183982*	*0.19447368343707*
O	*8.93722406989423*	*11.39077970648261*	*-0.09165507615932*
H	*6.72740209497798*	*15.08383051333596*	*0.43835238931412*
H	*6.24621506105760*	*14.54000705851702*	*1.86641153990678*
O	*6.58979811118292*	*14.25070259553480*	*0.99900536198205*
O	*10.18420785873681*	*5.55790526349519*	*5.63486091231380*
H	*9.90366946112147*	*6.11682540658266*	*6.38284490409755*
H	*10.36652746996277*	*6.16548430707081*	*4.87796460564234*
O	*8.51782742928649*	*3.66806858859156*	*4.71254672795831*
H	*8.34142398939959*	*4.02906688525322*	*3.81518125362433*
H	*9.14028467768816*	*4.34506496431009*	*5.12158669692719*

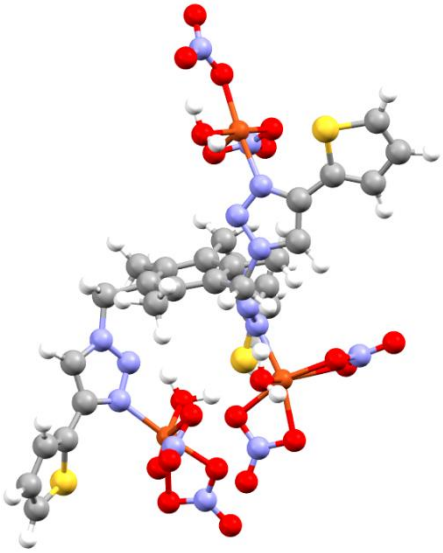

Figure B-6 *Cu(II) TC-Thio structure optimised with B3LYP-D3(BJ)*

Table B-13-*XYZ atomic coordinates for Cu(II)- TC-Thio with both nitrate and water ligands using B3LYP-D3(BJ) with a neutral charge and multiplicity of 4*

C	8.75699155501537	7.20926745463780	1.52771988344629
C	9.72743434393238	7.98113187115152	2.18042401328057
C	9.37232524992469	8.84561257639500	3.22331774955421
C	8.01700914223135	9.01187551216135	3.54194270876484
C	9.14971600866200	6.16516191226347	0.51059092636348
H	8.70933961526323	5.19956955868814	0.76417521366826
H	8.80480592360917	6.43052529484325	-0.49157775882383
H	10.22250158217670	6.01330597663990	0.45904414685882
C	10.43345769486361	9.59629083905786	3.98782284458322
H	11.36485689151073	9.03874202046886	4.03847524943183
H	10.12905134053185	9.78770942709043	5.01425002481895
H	10.64946293921951	10.56296310758690	3.52478448855937
C	11.16709227279887	7.90872359152578	1.74000084965204
H	11.24984262501391	7.77499507918856	0.66544754978944
H	11.70540680218845	8.81872356137371	1.98962636401302
N	11.90337824150679	6.78198527591541	2.34779799105155
N	11.62389837185175	6.36993142068594	3.56848107723595
N	12.46742890177312	5.40397345817000	3.84448104022895
C	12.92901109455591	6.08761504402802	1.81491890777134

H	*13.29221437597043*	*6.26026686305080*	*0.81749605870156*
C	*13.30165481047138*	*5.18238412029388*	*2.78903492157956*
C	*14.35063676174891*	*4.18532956947680*	*2.74305138489091*
C	*15.56890818391314*	*4.31387661798757*	*2.12262471413822*
H	*15.88212908904506*	*5.22375766361763*	*1.62998209121059*
C	*16.36476001519926*	*3.14412589608119*	*2.21976199738395*
H	*17.35821194377141*	*3.05409111687584*	*1.80437367386022*
C	*15.74027456516025*	*2.14059801700241*	*2.90631014161709*
H	*16.10995728536143*	*1.15347404196651*	*3.13440448522200*
S	*14.17597981545433*	*2.60573351662220*	*3.43713264064453*
C	*7.63428509180128*	*9.97976632942415*	*4.63459116879361*
H	*6.57333416525819*	*9.95767114268860*	*4.85589461032034*
N	*7.98770597690216*	*11.36157874108701*	*4.26263855145165*
N	*7.83235675813478*	*11.76559797341775*	*3.01651034591160*
N	*8.30031132326197*	*12.98720421237135*	*2.96095192196725*
C	*8.53875129618378*	*12.32147174486492*	*5.03384047680720*
H	*8.74059632941855*	*12.18219917394185*	*6.08076667111372*
C	*10.23256657728082*	*14.98107785515521*	*5.46404697972669*
H	*10.59469881220921*	*14.24641349380615*	*6.16963367435892*
C	*10.62577839778541*	*16.34371826213490*	*5.46054196012781*
H	*11.31726677268769*	*16.77341634118903*	*6.17105935321709*
C	*10.04127775374622*	*17.05859274445746*	*4.45306312694935*
H	*10.16122388789112*	*18.10300066348133*	*4.21327568492327*
S	*8.99239775496341*	*16.08240163961279*	*3.50609053581703*
C	*7.40823203157858*	*7.39183344510088*	*1.85913246523592*
C	*7.02356139631630*	*8.31173912190646*	*2.84566692098797*
C	*5.56775572479103*	*8.51109749721716*	*3.18998501889165*
H	*4.90299600762880*	*8.13295065068870*	*2.41980414532895*
H	*5.31210184339492*	*7.99840513845659*	*4.12166044326685*
H	*5.33175903785796*	*9.56685746548418*	*3.31765018170160*
C	*6.35894391776910*	*6.53057227693719*	*1.20040115873047*
H	*6.74883695905148*	*5.98166127914628*	*0.35018944101725*

H	5.50150128230778	7.10155092927202	0.85503710898449
N	5.83986206722673	5.54134841111379	2.16717968516276
N	6.63992360433665	5.07698114663177	3.10222420783284
N	5.93693611543412	4.25096248925171	3.83858747412467
C	4.60460610556325	5.00899692057320	2.26885307062988
H	3.80747302820321	5.25054760526185	1.58848669014859
C	4.66228007459043	4.16334652876040	3.36117311529179
C	3.62544001773745	3.32568585780038	3.92303195214252
C	2.28419559156943	3.60779162056538	3.99726590164779
H	1.86249401546024	4.54456326166860	3.66052563009318
C	1.53233453602280	2.55576396190256	4.58037452334670
H	0.46347016905124	2.59174112416792	4.73514492096744
C	2.30981187855122	1.48834143337467	4.93505726915344
H	2.00471024556729	0.56265208140596	5.39661559163448
S	3.96372929627128	1.74951814905262	4.55811840998570
H	8.16451110201170	9.77425121906785	5.56194195076304
C	8.75201130477708	13.38893761079025	4.18422092566446
C	9.35021327595812	14.67619609027344	4.45687550838195
Cu	12.35645808116735	4.68595051885119	5.70191871407451
Cu	6.85557842239120	3.91846528241989	5.59539808940808
Cu	8.60269831580078	13.67068764445562	1.10567938789161
O	11.51907512161552	2.85236225279817	5.38140229492759
O	13.23494166715314	6.22322140229181	6.56315475271214
O	10.52650017670750	13.17308626553524	1.26420655767037
O	9.10327372977578	14.38812038536021	-0.69759335339465
O	5.16190774087921	4.11447979967711	6.62984872160587
O	7.87385863296916	3.69407218426924	7.29198220259600
N	7.87743151608509	2.42342525595435	7.55318051025160
O	8.39519057308500	2.03871538827724	8.59050380076133
O	7.34559649733576	1.66782182867616	6.72303010959252
N	4.92866157411276	5.38129850892142	6.77976998058091
O	3.89096364091891	5.71953398837546	7.33409434624748

O	5.77147551716911	6.18258844511977	6.34747825590494
N	11.60790914837893	2.55277616225352	6.62187692999683
N	14.51664043334204	6.02400215246895	6.67109519441208
O	12.12008278200228	3.47659593236172	7.34254392805377
O	11.24228526359843	1.49648378097802	7.06667559559986
O	15.19520977926669	6.91285176576355	7.16802576731810
O	14.97317402613190	4.94895360533431	6.26642073602986
N	8.40117923224773	15.04518521017375	-1.55764663510608
O	7.20048522471094	15.29769402340065	-1.32934625120633
O	8.95144787385220	15.40255503517519	-2.58742317480623
N	10.66383138321949	11.95489482539190	0.83315251180598
O	11.76537071073108	11.42945423304845	0.92052322524016
O	9.66697513575440	11.39366672159377	0.35961126344555
H	6.63857579816396	14.60973842777726	0.07949978078855
H	6.27921378613152	14.50630909889904	1.62529135441158
O	6.66467628032207	14.02249581052471	0.88040140721757
O	10.26365332279824	5.71984186131811	5.93812160714594
H	9.98611683846049	6.04715711129314	6.80473526408215
H	10.32538861673172	6.48559249054447	5.34323228599389
O	8.62401172714327	3.99138041117709	4.63505224221464
H	8.46420389300617	4.46614091327281	3.79972925217518
H	9.24342856755861	4.56158923791265	5.15256619225642

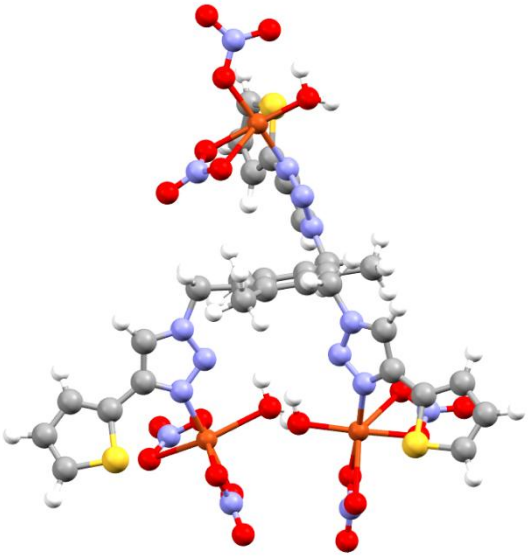

Figure B-7 *Cu(II)TC-Thio structure optimised with PBE0-D3(BJ)*

Table B-14-*XYZ atomic coordinates for Cu(II)- TC-Thio with both nitrate and water ligands using PBE0-D3(BJ) with a neutral charge and multiplicity of 4*

C	8.49971845113424	7.20085910678705	1.68710565909226
C	9.54275613261994	7.95744103828905	2.22531058421974
C	9.30843827918301	8.87061010041495	3.25622395122409
C	7.99578992909500	9.09651102758817	3.67971295041099
C	8.77621096067888	6.12595208579973	0.67532061094721
H	8.22185140812945	5.21662774515957	0.91330328405168
H	8.48530134992313	6.43566080913568	-0.33306375104970
H	9.82744358696749	5.84912804516184	0.64546293585364
C	10.45638546515083	9.59722762345199	3.89320771209732
H	11.36234506083096	8.99321333414927	3.89647359876432
H	10.24556212216389	9.84745360762923	4.93205578748823
H	10.68539118237271	10.53111292615484	3.37002937466828
C	10.92466394785501	7.84458640193975	1.65187891263685
H	10.89522440357020	7.60933266317855	0.58984916221403
H	11.46575762616366	8.78453503180200	1.75609367379930
N	11.74019743978558	6.80492407269195	2.28720190741451
N	11.42649768728305	6.31644758945305	3.45970558124369
N	12.36264085998489	5.46977723206890	3.78257357896463

C	*12.88696318439200*	*6.28114447630251*	*1.82450083856217*
H	*13.30432057815793*	*6.54600924134743*	*0.86737684199593*
C	*13.30004073013001*	*5.40439627474241*	*2.80269897966603*
C	*14.48694488812405*	*4.57861281740041*	*2.83510495982439*
C	*15.72679738974352*	*4.91867629754924*	*2.35831789651139*
H	*15.94270443077506*	*5.88576076623265*	*1.92234176728132*
C	*16.67708603782620*	*3.88601231268462*	*2.52410258314155*
H	*17.71347200543823*	*3.96179229276256*	*2.22296922498317*
C	*16.14443347364480*	*2.77816412975688*	*3.11860080801178*
H	*16.63487084167410*	*1.84911281438641*	*3.36939195824999*
S	*14.49045300936830*	*2.98144772076283*	*3.46943182926283*
C	*7.73324272190081*	*10.14334497254785*	*4.72740425424472*
H	*6.68106054367336*	*10.20373604270105*	*4.99170563794629*
N	*8.15348216109813*	*11.46620990181792*	*4.26322917281152*
N	*7.95847283078936*	*11.81539812521161*	*3.01566878988465*
N	*8.49255891287166*	*12.99235806761913*	*2.87232174140944*
C	*8.80075006058573*	*12.41957785615660*	*4.95524910545771*
H	*9.04854084474109*	*12.31814749949979*	*5.99854738459871*
C	*10.77618438835631*	*14.95152965131566*	*5.03548801781020*
H	*11.20243996264114*	*14.21416722870045*	*5.70362256757478*
C	*11.24351750598678*	*16.27996784980602*	*4.91002289487254*
H	*12.06392785925016*	*16.69016921661471*	*5.48385126316896*
C	*10.55161125700392*	*16.99331259957764*	*3.97446899000691*
H	*10.69163344148994*	*18.02067004433276*	*3.67234548052703*
S	*9.31765586673624*	*16.06128339168692*	*3.25829361018631*
C	*7.19267092931238*	*7.43971826044954*	*2.12474790945778*
C	*6.92738722983671*	*8.39265686096254*	*3.11397062264399*
C	*5.52827478261887*	*8.64297022198229*	*3.59896495766839*
H	*4.78003047750971*	*8.08693237003631*	*3.04143977446678*
H	*5.42427973547848*	*8.35569157577940*	*4.64887066025374*
H	*5.26710603482725*	*9.70088160694012*	*3.52122027391713*
C	*6.06670010868216*	*6.65441433952896*	*1.51500457450430*

H	6.36233634761507	6.19175173074881	0.57590225556615
H	5.19782071701208	7.27622090008097	1.30684377906505
N	5.61007017720239	5.58448739433078	2.40733758246770
N	6.41832315309083	5.09462448231321	3.30988934237940
N	5.76809189946635	4.15801692753970	3.94090554248795
C	4.41890778750146	4.96280720853296	2.42220773368278
H	3.62145928173942	5.21008931787541	1.74157033385446
C	4.51839953072720	4.02473939880456	3.42692457389826
C	3.53513994483373	3.06393653438588	3.87308958567149
C	2.17807779310116	3.24593690637534	3.93758296453622
H	1.69859291662245	4.18350196143266	3.68642941047105
C	1.49458399491197	2.09248774365036	4.38478648982194
H	0.42182416126216	2.03478430565000	4.51307167996913
C	2.34108498499733	1.05350083387110	4.64763185226116
H	2.09743886407569	0.06287414474074	5.00243385337944
S	3.96525446486614	1.46937297441465	4.34716652889320
H	8.29037034098322	9.95388592329465	5.64542011331077
C	9.03142250811729	13.42312410797278	4.04220131283416
C	9.73142874998200	14.67693876028449	4.19230185724686
Cu	12.22766714805067	4.72154689862243	5.62151832303607
Cu	6.69300981262858	3.62987682718552	5.63112392890139
Cu	8.77122733066567	13.63056382220512	1.01320269562345
O	11.61926422343367	2.83465799120835	5.25875669212872
O	12.90338109719941	6.32776280044129	6.51431749935980
O	10.67333505689077	13.08074905145233	1.13335231214287
O	9.25033387839777	14.41596131856593	-0.75204523559880
O	5.00954913670962	3.71325536816477	6.68135364673459
O	7.71233523549122	3.19732746737615	7.28271303188037
N	7.66213043989672	1.91824442639503	7.36065409317157
O	8.18860784948876	1.36149999478843	8.30093686789493
O	7.06769509517596	1.32165205448360	6.45669805064279
N	4.84280568546383	4.94381817672451	7.00453302003892

O	3.84653292439480	5.25370443866357	7.62707250416341
O	5.71014668065782	5.74988965141255	6.65879463695430
N	11.62415277759389	2.55268350801906	6.49696666493928
N	14.15828255401637	6.15883617101977	6.74889965887756
O	11.97209757486291	3.51400813348935	7.24366621054658
O	11.32606810295452	1.47299221652080	6.91560921333100
O	14.76989995310932	7.05354670997305	7.29545744363259
O	14.66391095119852	5.09213311025500	6.40245447072876
N	8.68158523109348	15.38809661530833	-1.35580136128068
O	7.57274259464575	15.79050498229170	-0.97430322777609
O	9.25544201834596	15.88746857978407	-2.29904503229776
N	10.70619908825246	11.89227449568802	0.64879446653008
O	11.76017615161289	11.29126743287750	0.64021184386908
O	9.64737328990736	11.42817904013987	0.21746022332762
H	6.89132008499699	14.75527760097653	0.11312750176757
H	6.39504523967268	14.27230626029692	1.53686031612495
O	6.85541418050949	13.98437448761453	0.73869409361535
O	10.05529538409813	5.57697446593307	5.77367834738920
H	9.79606242465312	5.98718542634811	6.60743834808912
H	10.08636058694360	6.28318676867021	5.10785379958239
O	8.43917240757103	3.73386299580915	4.67271384462509
H	8.28566909144132	4.16720364973255	3.81923087435149
H	9.04474098230786	4.34771023721040	5.15582955621056

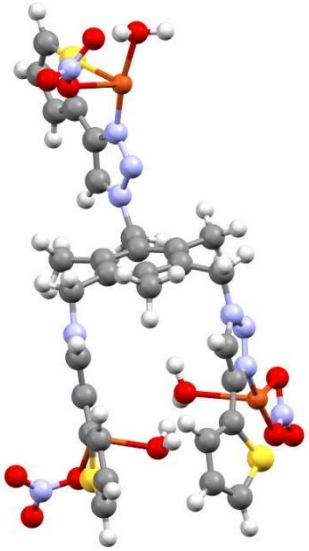

Figure B-8 *Cu(I) TC-Thio structure optimised with PBE-D3(BJ)*

Table B-15-*XYZ atomic coordinates for Cu(I)- TC-Thio with both nitrate and water ligands using PBE-D3(BJ) with a neutral charge and multiplicity of 3*

C	7.24942596986855	2.51859346812595	3.42792437880937
C	8.27104380351905	1.80049843816234	2.82736758543578
H	8.89776967054430	2.21318940603362	2.03691012504230
C	8.42512370077084	0.49981284625146	3.37615231754384
H	9.18453159599417	-0.20922716189920	3.04963704587199
C	7.52400845578060	0.23984412758981	4.38322087580696
H	7.41866716964668	-0.65936024682742	4.98480325780396
S	6.47616734795538	1.57771267666741	4.67201557769552
H	9.38819532114266	10.24930691129547	5.43827590629230
C	9.02787713917288	13.98169066109691	4.22482374625689
C	9.36543268662947	15.36298123662982	4.46718143388179
Cu	11.60926252524881	3.89025192785706	5.28678499020798
Cu	5.89806865712497	4.25036528453371	5.89262112445251
Cu	8.01286932249940	14.54898980201963	1.53457844692360
H	7.87667521323308	15.35740174121216	-0.69476722852877
O	12.21416987926628	3.36625952994252	7.07241276385932
O	9.93533894755842	14.24253452570748	0.11863859279505
O	8.07196748003502	5.36758943187894	6.61733716821005
O	5.41254100965997	3.62719034513235	7.64030063941529

H	*8.13579030013494*	*5.59766115949954*	*7.56275321477518*
N	*9.90576705867037*	*14.29390908388981*	*-1.14833963787725*
O	*10.79809898102593*	*13.76188489867741*	*-1.83208606296053*
H	*8.21742302333688*	*6.20469825911155*	*6.13829793615826*
N	*4.92422379291268*	*4.59565107032233*	*8.38445061349786*
O	*4.60668033292472*	*4.32601409594285*	*9.55053902114592*
O	*4.80346508877944*	*5.73244632000918*	*7.87863000213703*
O	*7.25867128527200*	*15.60778309184208*	*0.09216969052656*
N	*13.50394049611103*	*3.32657828968199*	*7.30048089274931*
O	*9.55821332897789*	*3.22702688129610*	*5.75275718364288*
H	*6.35978113669765*	*15.31887342273152*	*-0.14990363215156*
O	*13.87525222279103*	*2.98430976379610*	*8.43786926859534*
O	*14.29861588845710*	*3.62395269769667*	*6.38563145225179*
O	*8.93923798768200*	*14.90563219119800*	*-1.73489718764198*
H	*9.14032323322518*	*2.96696421691699*	*4.90833197992654*
H	*9.03353525486060*	*4.01561676741420*	*6.05986275866130*
C	*8.94946397733806*	*7.57620198504233*	*1.45197521562505*
C	*10.10161358474980*	*8.15197262153086*	*2.02292728690310*
C	*10.00191690367931*	*9.10322552664448*	*3.05707350415604*
C	*8.72527352051960*	*9.45688371773068*	*3.53340485144461*
C	*9.09535363989944*	*6.60438703135527*	*0.30855403246415*
H	*8.19181333274826*	*6.54027967086050*	*-0.30664322074373*
H	*9.91476329919434*	*6.89813557802853*	*-0.35960352170953*
H	*9.32265480933376*	*5.58658406665898*	*0.66070667003704*
C	*11.25305569788291*	*9.72441388050689*	*3.62887043576461*
H	*11.86511506164984*	*8.97439828124734*	*4.15265538400421*
H	*11.04437379947807*	*10.53301974169761*	*4.33451773870601*
H	*11.87586313317242*	*10.15472822838385*	*2.83150578210884*
C	*11.46465585921132*	*7.64783821461830*	*1.60043157160390*
H	*11.57849403726714*	*7.58425160744095*	*0.51231053830594*
H	*12.27393322056876*	*8.27724341125288*	*1.98172732155492*
N	*11.68503525635930*	*6.28479860735371*	*2.11958157821620*

N	*11.60795775674620*	*6.06279531596808*	*3.43867612860595*
N	*11.74013768572432*	*4.75504589403070*	*3.60147809068907*
C	*11.86966860629101*	*5.13730893310844*	*1.42458953184897*
H	*11.95339755848227*	*5.11606040051054*	*0.34425538407701*
C	*11.89917992095583*	*4.13428539100738*	*2.38365451319142*
C	*12.01701069671527*	*2.70306931469159*	*2.25679290076215*
C	*11.97930645989691*	*1.92815335256078*	*1.11146722233629*
H	*11.86844102116500*	*2.35208722557690*	*0.11381012684442*
C	*12.08192582035718*	*0.53827494669154*	*1.38238496401621*
H	*12.06767953173006*	*-0.23379053991939*	*0.61378802983999*
C	*12.19680404120731*	*0.26462514113617*	*2.72566380559803*
H	*12.28844924439826*	*-0.69823619597624*	*3.22120087469103*
S	*12.18452370509670*	*1.70808016558283*	*3.67413355076917*
C	*8.60165443158166*	*10.41573016637053*	*4.69345967064403*
H	*7.64240525527817*	*10.29716925000931*	*5.21011547937645*
N	*8.71288497210268*	*11.82862530228690*	*4.28877926350432*
N	*8.24380235493753*	*12.23232985553532*	*3.10596963408549*
N	*8.43472007792550*	*13.54437497191415*	*3.06418294849697*
C	*9.20524102169039*	*12.85676531011736*	*5.01924397709465*
H	*9.63642131615858*	*12.71948009411600*	*6.00421934572684*
C	*9.87117068400511*	*15.93097020071083*	*5.62332843701931*
H	*10.07576646305339*	*15.35479966207469*	*6.52531060534427*
C	*10.08210241318016*	*17.32918153188494*	*5.50516583780887*
H	*10.47113259990037*	*17.95570082076797*	*6.30704398356944*
C	*9.73918424281616*	*17.81544518642241*	*4.26471052688463*
H	*9.79172938585528*	*18.83514703696876*	*3.89223315576193*
S	*9.15546763134847*	*16.56487977719175*	*3.22810586550037*
C	*7.68089495074640*	*7.90698204845458*	*1.97778318659330*
C	*7.55663279333427*	*8.87495180454309*	*2.99683603139132*
C	*6.20919544064811*	*9.30470444793827*	*3.52537771902998*
H	*5.39365474291546*	*9.08247504547470*	*2.83099684803240*
H	*5.97021201502844*	*8.80253414184143*	*4.47597077289516*

H	6.18607173063716	10.38755202478523	3.70276611821054
C	6.47366026108055	7.09934940347648	1.54720117381821
H	6.49942670079349	6.81283087495728	0.49203833642910
H	5.52700370913541	7.61436199824632	1.72648054210198
N	6.42527424032910	5.84602489606345	2.32382415632619
N	5.97959984050804	5.87376999247433	3.58455223717633
N	6.22153921746258	4.67362148892843	4.08796240917339
C	6.95134764476000	4.63860523408998	2.00128550526110
H	7.34340626332008	4.40932512971514	1.01829379005664
C	6.82671511012890	3.87200562587351	3.14925890975957

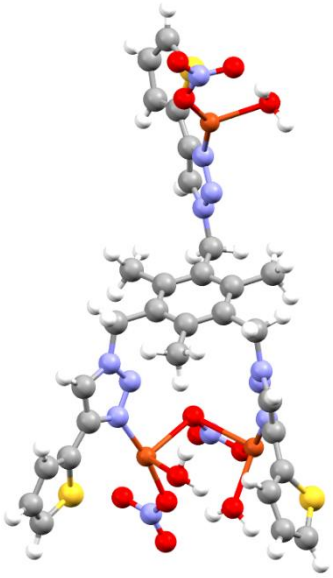

Figure B-9 *Cu(I) TC-Thio structure optimised with B3LYP-D3(BJ)*

Table B-16-*XYZ atomic coordinates for Cu(I)- TC-Thio with both nitrate and water ligands using B3LYP-D3(BJ) with a neutral charge and multiplicity of 3*

C	5.98164303712297	2.24239611868983	3.18382384293351
C	6.33440562472619	1.33011751147851	2.22222736176824
H	6.86663479242059	1.60458909371805	1.32223264485875
C	5.95237017811034	0.00366211961840	2.55269859645422
H	6.15150295037088	-0.85467790098544	1.92698845958956
C	5.31138488249373	-0.07506548566913	3.75730170885816
H	4.91982505322565	-0.94930794621426	4.25244820846140

S	5.15751200342972	1.46743131492325	4.49901036461845
H	9.08500603446806	10.77185193745275	5.59066329958707
C	9.51876875544574	14.13868442366595	3.65122453906622
C	10.13161827559428	15.44687407485133	3.66745953358824
Cu	11.09119252578881	3.82724916586429	5.25720372338468
Cu	6.84045017281848	3.77915271210633	6.08262890951408
Cu	8.47374543267617	14.47211558979567	0.87236898807713
H	6.54517637496395	15.52701594939191	-0.22625839844110
O	10.51690709121152	2.89117647747395	6.87074770691676
O	9.18490879630969	14.90089839944733	-0.93952928438843
O	8.19058617433146	1.83432315272777	5.96774510308159
O	6.88536825199280	3.59792410261032	8.02946802498104
H	7.76821437433384	1.00911149269695	6.23638408605535
N	8.59779433752187	15.55489207368418	-1.87071004995446
O	9.22481648647843	15.79593211196204	-2.90158494789927
H	8.95190494015017	1.98907282708508	6.56249031755169
N	6.59471226103069	4.63530781524746	8.74206541400027
O	6.62722916208424	4.51914633758156	9.97042652626085
O	6.29874665145625	5.69715191136149	8.17894507225522
O	6.40326719715121	15.26436683382527	0.70827713629742
N	10.80801393164385	3.36978593385199	8.04594758023970
O	9.67396314467557	2.64249169975986	3.80956013536712
H	5.76605980823818	14.53849210470012	0.69283602677443
O	10.34456836256451	2.78886492781248	9.02603904477154
O	11.52383617701664	4.36879278718076	8.12243361672551
O	7.41565270628048	15.93414480967114	-1.72609406442206
H	9.22226602848980	3.30065143062239	3.26589970261972
H	8.99113767680701	2.26859539461755	4.40337178740408
C	8.92085514354627	7.55354600939334	2.00128507337926
C	10.03692783701574	8.27139105844489	2.44820404140722
C	9.89353074053613	9.32687145572402	3.35851890833173
C	8.60741838589951	9.69405496645167	3.77481100335032

C	9.10333436010532	6.35799031409364	1.10092655264400
H	8.25927747102228	6.20738908285694	0.43288956919307
H	9.98845881364084	6.44331603745816	0.47590876987488
H	9.21314506059988	5.44621785180278	1.69633909333297
C	11.10666635807893	10.05488743126902	3.88395252321686
H	11.93928057293528	9.37431137949783	4.05053954922174
H	10.91060255741148	10.54356471375589	4.83370173440623
H	11.44120115114516	10.82595812777075	3.18428053842855
C	11.40874535932596	7.87403815563289	1.96591500088537
H	11.43856810629761	7.76231106179826	0.88420709472846
H	12.16523602185363	8.60417880572376	2.23182617781600
N	11.82097506799954	6.57501420137597	2.52596834493463
N	11.32888583805578	6.15471443048759	3.68174262925246
N	11.85397196466462	4.97338393237847	3.90626512055920
C	12.68031153715086	5.68085088434862	1.99576880991648
H	13.18799305030303	5.84438695445790	1.06193638526006
C	12.70593270741095	4.63367552440956	2.89419870763882
C	13.43544073216498	3.38662978980430	2.85885485072674
C	13.99952768438088	2.77084198010345	1.76988145037892
H	13.93854281377942	3.17487904731013	0.76902661946717
C	14.64493589678033	1.54971577344303	2.09702073610536
H	15.14041011862613	0.91774651917410	1.37377961350868
C	14.56595588065287	1.25183173772089	3.42793657990152
H	14.95989123199619	0.39348828462951	3.94837788825684
S	13.70868761636323	2.46024599956512	4.30218817426642
C	8.44345285577746	10.86234442550440	4.71722922038196
H	7.42544512745682	10.95841052655839	5.07617368681517
N	8.80207770591309	12.14203331551824	4.08348999041492
N	8.40068730644634	12.42235185065512	2.85129114010000
N	8.83727836386980	13.63227898311747	2.58093077419592
C	9.48993893949852	13.16423355894403	4.62838361715640
H	9.89349122044559	13.12788669487104	5.62437546975930

C	11.07087337766268	15.92144494377099	4.54982259289425
H	11.47381542406452	15.32628319399745	5.35732027244062
C	11.46253758261162	17.25741829506081	4.27668634585178
H	12.19440049404524	17.80069575512939	4.85746682238774
C	10.81927656316166	17.78547563751366	3.19305952356900
H	10.92311767475128	18.76798967804537	2.76126523694150
S	9.71875296455012	16.66014235941641	2.49695943585785
C	7.64168090624212	7.91017224794319	2.45959747581395
C	7.47253269628669	8.98964631866743	3.34005286661921
C	6.11492242040466	9.40578811068100	3.85617126114558
H	5.30085308570567	8.82407168970879	3.44168640874593
H	6.06240106113591	9.29540830253380	4.94118901295337
H	5.91521545624160	10.45314115240938	3.62294311553243
C	6.46769760409795	7.07854950877605	2.00813198011651
H	6.50631045342193	6.86802615975093	0.94334222785338
H	5.51389707710199	7.55545379332388	2.19934126010709
N	6.44019714164334	5.76507975475094	2.67602459184159
N	6.64151290546259	5.66920508257421	3.98282284844952
N	6.50842374889040	4.39869668637916	4.29128566393610
C	6.16409079072519	4.56618110318485	2.12557787895292
H	5.95812290535038	4.43946953141535	1.07786355520804
C	6.20543041385715	3.67192052629953	3.17367646660733

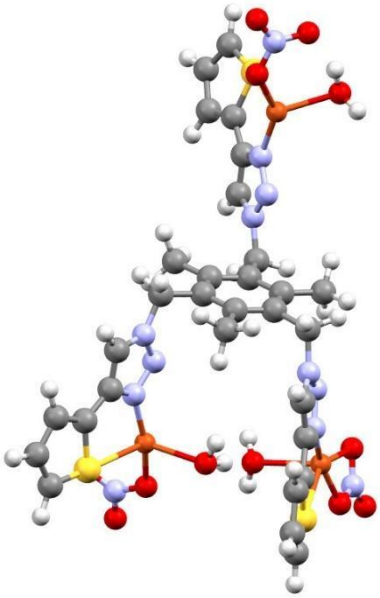

Figure B-10 *Cu(I) TC-Thio structure optimised with PBE0-D3(BJ)*

Table B-17-*XYZ atomic coordinates for Cu(I)- TC-Thio with both nitrate and water ligands using PBE0-D3(BJ) with a neutral charge and multiplicity of 3*

C	6.06542595300402	2.30088275340364	3.25203986040392
C	6.15652142722502	1.37700258914670	2.24312482824134
H	6.26467825559540	1.64865722662423	1.20077433595850
C	6.09237627843148	0.04497220133300	2.71297517994165
H	6.14357017132789	-0.82527154361993	2.07183159839378
C	5.95673566777183	-0.02678971303421	4.06870942264564
H	5.88030500141185	-0.90418041100426	4.69355231285115
S	5.90659754584788	1.52590061732810	4.78027170455609
H	9.33521895556375	10.41593435113937	5.49321635926395
C	9.52111003148094	13.92691299997782	3.79481525595325
C	10.02305045039265	15.27640406098053	3.87431039906382
Cu	11.46459724079227	3.78073177369631	5.25271833237986
Cu	5.65723621416314	4.14205077285666	6.03214339871970
Cu	8.49852865645574	14.38488534571751	1.06236459709146
H	6.73380700645557	15.72831306654578	0.10351680473359
O	11.32117307963221	3.02844639016012	7.04842355092960
O	9.22238658859410	14.84766913168637	-0.73687479262948
O	7.92353006608696	4.26330198366084	6.82850559057639
O	4.93383559814528	3.57272038747449	7.75822366929683

H	8.03260433798021	3.81962774238823	7.67789805793463
N	8.77131402537063	15.74612747132916	-1.50914916668946
O	9.39471244620334	16.01067984661700	-2.52564044507459
H	8.19692681772807	5.17586781858034	6.97930391838581
N	4.63613641580222	4.59036324210155	8.47083665117183
O	4.19508958101230	4.41019091767823	9.59615540068023
O	4.80619704669463	5.71363653300710	7.99095504760961
O	6.51189659516498	15.29219905833953	0.95252451736350
N	12.35758372372140	3.05863018939369	7.79617065002647
O	9.36754736834432	3.09450642659368	4.76576879725562
H	5.84516303238887	14.62863917843362	0.74539392330657
O	12.26753442476349	2.58490278113581	8.92273850359184
O	13.39643261930819	3.55415609992600	7.36657330220175
O	7.71793954146317	16.33822320676108	-1.22672167944405
H	9.08355328409209	3.49125805766315	3.93598016472593
H	8.80360357829529	3.49699624657462	5.45640981350055
C	8.97386727330157	7.39099940628927	1.78627441379975
C	10.11527165951165	8.05143871193351	2.24787441122652
C	10.01962085441997	9.07913093887516	3.19097926603918
C	8.75635405169589	9.46443860750841	3.64497743748909
C	9.11876751831587	6.23321438349235	0.84337992151967
H	8.26088062118941	6.11644915047988	0.18491317034237
H	9.99371154369127	6.33196496463916	0.20325060998381
H	9.23087075496838	5.29734582471344	1.40089190695867
C	11.26597279905823	9.74809848851736	3.69551569147501
H	12.01453110511721	9.01083146629668	3.99141918118427
H	11.08572126653385	10.38195085142851	4.55889659270827
H	11.71293823796467	10.37811129282573	2.92072233868480
C	11.46773870615101	7.63120397192312	1.74717115097434
H	11.48771579717629	7.53551848511044	0.66207625854999
H	12.23899089428377	8.34822925429838	2.01755165823565
N	11.86310823087502	6.32948825313571	2.28391067729088

N	11.46793841315398	5.95664884724393	3.48091463548156
N	11.98248267899653	4.77797711494527	3.69729475942781
C	12.64183883548170	5.40254678102753	1.70307205738858
H	13.05194818129899	5.52277394480065	0.71443553881115
C	12.72202069287550	4.38412043143273	2.62731089323316
C	13.40850337845418	3.11754047034879	2.56883497741889
C	14.30786196221973	2.68628986092496	1.62824495852626
H	14.61667986138320	3.29070101251897	0.78488445877049
C	14.78971001506084	1.38260920041650	1.88857872157777
H	15.50859920728101	0.86797004554361	1.26456223000970
C	14.25139336823636	0.84017588412558	3.01899030511973
H	14.43689149421468	-0.12970984180825	3.45608805825308
S	13.15386431516400	1.91220465550573	3.77085755462302
C	8.64041434650269	10.56103508997673	4.66697630189260
H	7.64299978005955	10.60765180207971	5.09600016172620
N	8.93693739505207	11.87831465834856	4.10697984639347
N	8.53799887730169	12.19567507181652	2.89411489139176
N	8.89316504327146	13.43445758018012	2.69400471708674
C	9.54815775409007	12.90630780919203	4.71780102184194
H	9.93728953748345	12.84175682852760	5.72003691470999
C	10.91880904014713	15.79896883188502	4.77019726646364
H	11.37895349939483	15.21208165162594	5.55478504460105
C	11.18044188801782	17.17045509178958	4.54426580355397
H	11.86199885409393	17.76219838239695	5.14121497644417
C	10.48233479200512	17.67155908568601	3.48409719565850
H	10.48801265619946	18.67529519048392	3.08589977067782
S	9.49609774600014	16.47879535040585	2.76132722732555
C	7.71274605679468	7.78694986899667	2.25676911144069
C	7.59390022540036	8.83412285045141	3.17926795145868
C	6.26243721429916	9.29936338025517	3.69922950173964
H	5.41902846704216	8.83236996478677	3.20215353218713
H	6.16183636525635	9.07853394027064	4.76521767008262

H	*6.15399624361921*	*10.37890823030996*	*3.57465573069378*
C	*6.49500673912868*	*7.04080642522313*	*1.78126455735459*
H	*6.56785571971067*	*6.76475544242582*	*0.73296527591727*
H	*5.58361283008009*	*7.62020817406131*	*1.88798295589990*
N	*6.30008759992911*	*5.79192533618379*	*2.51616625419598*
N	*6.06735691749238*	*5.81855846534021*	*3.81013865248955*
N	*5.95090171897229*	*4.57737855072725*	*4.19549378070800*
C	*6.34137196137175*	*4.53686592418677*	*2.04080912707113*
H	*6.52587359895027*	*4.31267719582685*	*1.00395116720715*
C	*6.11399838753702*	*3.73765456746221*	*3.13967289176170*

Table B-18- *Binding energies of the Cu_3-TC-Thio*			
	PBE	B3LYP	PBE0
	Binding energy (eV) per Cu	Binding energy (eV) per Cu	Binding energy (eV) per Cu
$[Cu_3(TC\text{-}Thio)(NO_3)_6(H_2O)_3]$	-4.9613	-5.2864	-5.4466
$[Cu_3(TC\text{-}Thio)(NO_3)_3(H_2O)_3]$	-2.1323	-1.4596	-1.2288

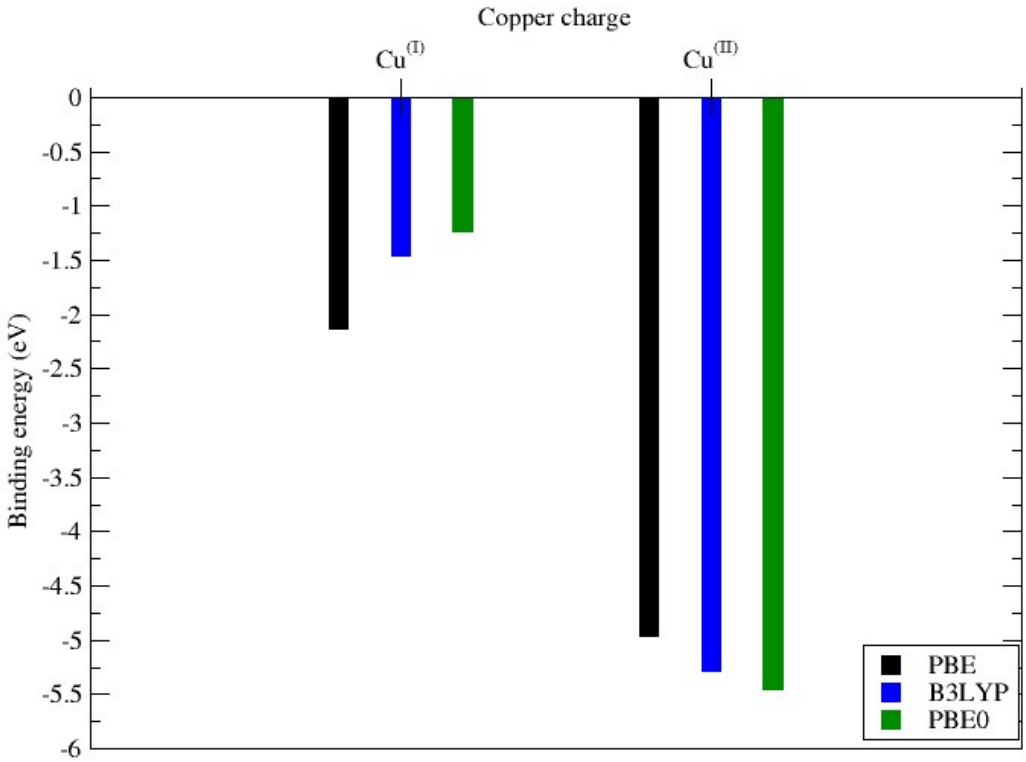

***Figure B-11**- Binding energies of the Cu_3-TC-Thio*

Appendix C

Table C-1 *XYZ atomic coordinates for Cu(II)-TC-1 with PBE0-D3(BJ) with a neutral charge and multiplicity of 4*

C	*1.61277509019483*	*2.25867183051856*	*-2.49872451621217*
C	*0.63134175441824*	*1.16021770693301*	*-2.20000654965898*
C	*0.96194379667061*	*-0.18822720432304*	*-2.40893593096106*
C	*0.05747304640722*	*-1.20316014770971*	*-2.07872827896472*
C	*-1.20321430861673*	*-0.85567655452120*	*-1.57429100081744*
C	*-1.56002634951825*	*0.48009556012785*	*-1.38132368958438*
C	*-0.62043074410834*	*1.47814950388933*	*-1.66799254153763*
C	*-0.94738811314444*	*2.90842622938029*	*-1.34365446092223*
N	*-1.11196749451276*	*3.12934799954049*	*0.09485006193221*
N	*-0.30912897488406*	*2.56443318264049*	*0.96847601978273*
N	*-0.69082188528243*	*2.99505430935448*	*2.13495215403045*
C	*-1.73666483780400*	*3.83695405803358*	*2.02406977743793*
C	*-2.01999459386112*	*3.92936707982647*	*0.68737197539932*
C	*-2.28939943720902*	*4.44406060458297*	*3.26231618140705*
N	*-1.81325638366493*	*3.66063762530679*	*4.41159028373186*
C	*-2.89815551592416*	*0.85212176770292*	*-0.81529948087573*
C	*-2.12681923885424*	*-1.95681705865120*	*-1.13676814337618*
N	*-1.78790879648262*	*-2.40985042106107*	*0.21585882049324*
N	*-1.43673251629503*	*-1.53922311783425*	*1.13450613632372*
N	*-1.19919192990006*	*-2.22764056676640*	*2.20663912714062*
C	*-1.38962027330981*	*-3.54500651613043*	*1.99656241625643*
C	*-1.77820030551010*	*-3.67402581207420*	*0.68846519781408*
C	*-1.16523756254433*	*-4.46652288936566*	*3.14179089999255*
N	*-0.33712736886854*	*-3.76225942907360*	*4.13569341810893*
C	*0.39358290698235*	*-2.66196785690946*	*-2.21337024112656*
C	*2.34914107909415*	*-0.52622551040229*	*-2.88259102771806*
N	*3.30159142371852*	*-0.38859090066428*	*-1.78019135260426*
N	*4.38526074043525*	*0.34055310076927*	*-1.91309913875600*
N	*4.98680556133622*	*0.29764635911453*	*-0.76191056626839*

C	4.30144351018166	-0.45451114743542	0.12142257835379
C	3.19219360877431	-0.90953995377936	-0.54005519955308
C	4.82391135320243	-0.56431794544021	1.50878949065794
N	6.18065131342708	0.00890236945690	1.53973027445463
H	2.48040046531182	1.91502528925289	-3.05249674852735
H	1.15266316053244	3.05099350892885	-3.09115193671272
H	1.97985749152990	2.70465234316864	-1.56963698586177
H	-0.17002947022025	3.58874773631838	-1.67928575998150
H	-1.88179041164937	3.23148932324103	-1.80224641913035
H	-2.50972973819462	2.96954348075202	4.67544356580335
H	2.36410855411332	-1.52625825264032	-0.23507281896203
H	-2.87021667338544	0.85192405410629	0.27877703661281
H	-3.21585934093141	1.84269249027981	-1.13725240945680
H	-3.68049251823287	0.16032367792426	-1.12079170583987
H	-3.16922985739180	-1.64846841763653	-1.12650104938964
H	-2.05337583322284	-2.83385084001890	-1.77547992736300
H	-2.76787950992820	4.46857414451245	0.13057000826748
H	6.88179161325804	-0.72567725285051	1.53613337460164
H	6.33534456445772	0.56250024438576	2.37647359854172
H	0.25420608011409	-3.18353424062687	-1.26415167997829
H	-0.25596997696690	-3.14570610907023	-2.94803013768775
H	1.41837181320832	-2.84695369471692	-2.51861686062019
H	2.42585028254108	-1.53898257236378	-3.26641918742511
H	2.70048560602418	0.13645391921952	-3.66899962816788
H	-2.02657046949931	-4.52342279894795	0.07437516493196
H	4.18756966984753	0.00863471088688	2.18497303666221
H	-1.62060136141414	4.25223341145489	5.21268888161246
H	4.82512204105942	-1.60126166079439	1.84760527636629
H	-3.37919484644685	4.48223322254109	3.22785040779264
H	-1.92434420285784	5.46812171803509	3.36213439665700
H	1.63997496552612	-0.19531367799041	3.28761838447963
H	1.60016271993153	-1.37606973298131	2.29801428892499
O	1.52321944767467	-1.16374085032062	3.23379105608706
O	7.04117157931059	2.11770749188480	-1.77462126278082

Cu	6.58570734300087	1.19127035513485	-0.04628699180809
Cu	-0.54802572706929	-1.72997305627532	4.00491244052157
Cu	-0.16755790199310	2.57277363257234	3.99285876141575
N	0.33609713250850	2.98808114421094	6.78917520061468
O	0.17956586217110	4.17326917909918	6.51222106389120
O	0.62271103188798	2.59941300210407	7.90952715382229
O	0.19667146653922	2.09918358629849	5.87500954488120
N	5.83774507737609	4.32689544766380	0.23776898028086
O	5.47921948795655	5.28177858644041	0.90960318497462
O	6.69306978203653	4.46903652115409	-0.66381748563726
O	5.34552263620873	3.18748313532181	0.44062544827020
N	-0.50194061539487	-1.74619187071578	6.82025897769493
O	-0.09397230191327	-1.41324296098205	7.92100128782447
O	-1.51675119571060	-2.41518507005047	6.65268128339280
O	0.17735879952150	-1.37623721446960	5.79753386849378
O	8.33857693905322	1.85227445226313	0.56754418060227
N	8.57445274657806	2.29495493984572	1.74991150832824
O	2.31559692833932	3.49501855641990	4.02302570954558
O	1.49588914951447	1.58378888632102	3.47478843588851
N	2.52157976957076	2.33916446383405	3.67494303117414
O	-3.09329268499732	-0.90929796731291	4.13017993497392
O	-1.26320696010701	0.19381339061730	3.85053027469748
N	-2.54665308062112	0.15552581250639	3.87333023017521
O	-3.16775070345543	1.18156611887359	3.63418166639964
O	3.62961088951006	1.86778163570545	3.50466111868181
O	9.69637757763239	2.71835529998118	1.97260956499333
O	7.68577022356785	2.28058126119939	2.59418466526362
H	6.92669899629123	3.06761821791299	-1.48729203774964
H	6.37331789288995	1.95590318585434	-2.45251173540530
O	2.51050164505356	3.74309397774089	0.57537696444833
H	3.42005797731684	3.41974963655108	0.67185380686807
H	1.93643995094215	2.98875164779917	0.74859221726015
H	-2.12172420122137	-4.71493302901609	3.60614042814807
H	-0.70216733126156	-5.39881940929734	2.81524934730141

H	*-0.57207513338469*	*-4.06473021055458*	*5.07486973222141*
H	*0.64666413301537*	*-3.96735020572172*	*3.98976258371357*

Table C-2 *XYZ atomic coordinates for Cu(I)-TC-1 with PBE0-D3(BJ) with a neutral charge and multiplicity of 3*

C	*0.58776524864190*	*2.82435006777453*	*-2.44820247910277*
C	*-0.09800221885163*	*1.53798784808172*	*-2.08750621972026*
C	*0.64583473969033*	*0.35187284876860*	*-2.16303388097221*
C	*0.04249076033081*	*-0.88406660815568*	*-1.93133188043318*
C	*-1.30004036176701*	*-0.92900465863831*	*-1.52315541953226*
C	*-2.02320088690879*	*0.25151091419988*	*-1.32973896153784*
C	*-1.42242034820059*	*1.48164613178047*	*-1.64778392235400*
C	*-2.18863199455240*	*2.75477265811247*	*-1.38945035879310*
N	*-1.91405795152675*	*3.26924855634181*	*-0.04533513670774*
N	*-0.68148686421479*	*3.58237122947280*	*0.29920940997387*
N	*-0.71100378251664*	*3.90746290515647*	*1.55614593302496*
C	*-1.96935757535315*	*3.80082917523156*	*2.04054257455691*
C	*-2.76141702693883*	*3.38793401771387*	*1.00012104804440*
C	*-2.22243606638980*	*4.09435263674330*	*3.48094487814648*
N	*-1.01519275531646*	*3.78318300695298*	*4.26092642282819*
C	*-3.41116475856582*	*0.25145879558006*	*-0.75440557397795*
C	*-1.89821149743574*	*-2.26920921785544*	*-1.19399676215416*
N	*-1.32133244644844*	*-2.81417768108875*	*0.03647469527898*
N	*-1.04472226539952*	*-2.02083450685176*	*1.05034605704446*
N	*-0.53889554119489*	*-2.76068312319352*	*1.99028994134484*
C	*-0.48746006152888*	*-4.04710357170976*	*1.59123021345471*
C	*-1.00111066850030*	*-4.09168861381340*	*0.31793897118281*
C	*0.11640517011725*	*-5.07560876899402*	*2.48727971960304*
N	*0.17947490805413*	*-4.56659962212261*	*3.86702459650983*
C	*0.85262088826478*	*-2.14467822214214*	*-2.03760876838045*
C	*2.14007062752101*	*0.44440419255945*	*-2.29402789459965*
N	*2.70334871500680*	*0.77707955564168*	*-0.98601683763275*
N	*4.10252630048774*	*0.78208362432208*	*-0.93015131488152*
N	*4.38886141702591*	*0.41953978459219*	*0.35020273465826*
C	*3.26492982191304*	*0.07933076811552*	*1.02685968260006*

C	2.20111939109927	0.23693246533209	0.20901648301758
C	3.44921055924597	-0.28198207851897	2.45951628180269
N	4.86558997107823	-0.65927974291985	2.66078983800258
H	0.98018207261879	2.76630914153496	-3.46684498250229
H	-0.06288232389831	3.69034654810143	-2.38882832744125
H	1.43309021765015	3.00661064537784	-1.78178199971007
H	-1.93607304266953	3.53710630616460	-2.10123206839940
H	-3.26323123366229	2.60469239844128	-1.44370472958348
H	-1.03200862218340	2.81924583253301	4.58667073410268
H	1.14640296473804	0.13754761616671	0.39487141752671
H	-3.46608158973693	0.90637250876793	0.11666394160290
H	-4.14627518950370	0.61153636408572	-1.47954629705127
H	-3.73694476910256	-0.72818997510779	-0.41982948997815
H	-2.97619106260014	-2.22770425910364	-1.06891352668127
H	-1.70148480873606	-3.00205812004812	-1.97472413082449
H	-3.81407156621521	3.17302090049900	0.92108262660114
H	4.98833523155075	-1.66171758210045	2.55057375334073
H	5.16889679497697	-0.42969227341287	3.60055348840741
H	1.45832507384625	-2.29126406957773	-1.13722625659671
H	0.23597851027241	-3.03103579978759	-2.16468311471202
H	1.53660138042847	-2.10790758261671	-2.88465886417867
H	2.57749293728760	-0.49123399016101	-2.65221955853829
H	2.44024714202467	1.22683051381121	-2.99213752933711
H	-1.14726723923450	-4.89154992697122	-0.38891557556216
H	3.24628566929264	0.58112741086654	3.09716983843439
H	-0.98174143726251	4.36436928744612	5.08923925426250
H	2.77558268255333	-1.08379561608711	2.76950494845948
H	-3.10042185628414	3.54448639541212	3.82793649575841
H	-2.43769575875693	5.15889205973528	3.60077395920129
H	2.81496407174344	2.47102851816461	4.77699962011626
O	9.38915156854428	0.69449706752097	3.14985025715917
H	1.83170278906570	1.51819558251812	5.46778693259373
O	6.94284208466985	1.01355595238470	-0.42350915840002
Cu	6.03734820968172	0.19931450593992	1.23147047794470

Cu	*0.22934507473879*	*-2.51100748389094*	*3.89616089460408*
Cu	*0.68116509235511*	*3.88671751961809*	*3.01960460274958*
H	*6.18317766027365*	*1.27641959561144*	*-0.97520615144882*
H	*7.40330727052249*	*1.82706606258594*	*-0.17959225779184*
O	*7.89499518643375*	*1.93182064236290*	*2.21213210795993*
O	*2.74411252755555*	*1.84746421798785*	*5.51675945280258*
H	*-0.66651292635677*	*-4.82204008506327*	*4.36683022768097*
H	*-0.44001660568271*	*-6.01333896562685*	*2.41977031436092*
H	*1.13698743557803*	*-5.28036444398021*	*2.15597968059923*
H	*0.94344651242660*	*-5.01439654312680*	*4.35834519317391*
N	*-0.26918778627248*	*-0.09719497060276*	*5.10244668306300*
O	*-0.04053466921641*	*1.06232478758594*	*5.47222457453349*
O	*-1.40600569048121*	*-0.55259014466522*	*5.05823606152952*
O	*0.71551611270047*	*-0.82093624328237*	*4.77107252350739*
O	*7.71486160817367*	*-0.21894862152138*	*2.16401882276383*
N	*8.35691778194770*	*0.83329815854021*	*2.52138366356549*
O	*2.98591753398195*	*3.87926963364607*	*1.21312661420401*
O	*2.59623485211884*	*3.67693557272375*	*3.33482486628604*
N	*3.40732763157371*	*3.63901574373920*	*2.33759030033862*
O	*4.57822181897441*	*3.36764873769975*	*2.56846569314235*
O	*-0.81367347566359*	*0.66213559601916*	*2.00262736252992*
H	*-1.01432588463042*	*-0.19268748883562*	*1.58273559523706*
H	*-1.66993340901692*	*1.07937559550786*	*2.13164396829877*

Table C-3 *XYZ atomic coordinates for Cu(II)- TC-* Benzothiazole *using PBE0-D3(BJ) with a neutral charge and multiplicity of 4*

C	*1.53089831222184*	*2.36412966122466*	*-3.90860450291327*
C	*0.74537046634029*	*1.08406667990264*	*-3.92488199339616*
C	*1.44042470326566*	*-0.13351249150427*	*-3.91524388349929*
C	*0.76387854425052*	*-1.35494964330865*	*-3.87306013346336*
C	*-0.63627255622913*	*-1.35248616085892*	*-3.93962765911620*
C	*-1.34806205130462*	*-0.15088936260378*	*-4.00578806184561*
C	*-0.65195752764046*	*1.06421815838357*	*-3.92833498957877*
C	*-1.43182219564707*	*2.32640235747383*	*-3.65439933532592*
N	*-1.55500224123073*	*2.47222976725616*	*-2.20011486840879*
N	*-0.48506162564582*	*2.80477324908793*	*-1.50036344722529*

N	*-0.79635997059673*	*2.65195242918741*	*-0.26175200978445*
C	*-2.07103280549574*	*2.21483865632603*	*-0.13826068079452*
C	*-2.57800104706957*	*2.09704673272120*	*-1.40674599724769*
C	*-2.47458645343370*	*1.89128155657135*	*1.20298581229153*
S	*-3.96161977234993*	*1.20788826424597*	*1.68937359242649*
C	*-3.37300306215652*	*1.13311694635863*	*3.31376719957286*
C	*-2.05828519168137*	*1.62846738840522*	*3.37340327757599*
N	*-1.58856340420982*	*2.05955327855526*	*2.15358592300453*
C	*-1.36823558948885*	*1.62905993841625*	*4.58443514948948*
C	*-2.01697250812640*	*1.15032191596146*	*5.70440553216014*
C	*-3.33252567994750*	*0.67784864034641*	*5.63838211794989*
C	*-4.02662688707701*	*0.66234422146295*	*4.44449649297912*
C	*-2.84283371189707*	*-0.15715428007040*	*-4.13894306557360*
C	*-1.39086348825764*	*-2.65586766360661*	*-3.86063547756030*
N	*-2.10362306515624*	*-2.77699176040201*	*-2.58547969385127*
N	*-3.42559580384858*	*-2.76467205516957*	*-2.55492754123347*
N	*-3.76013083205384*	*-2.78565019634530*	*-1.31060883075825*
C	*-2.66203249299147*	*-2.81148443957012*	*-0.51924400353495*
C	*-1.57209948459389*	*-2.80577014386354*	*-1.34950421806083*
C	*-2.92255360077294*	*-2.78515665461463*	*0.89595712058727*
S	*-1.77547760926038*	*-2.93386695090049*	*2.15008935983228*
C	*-3.05224786712057*	*-2.82914095362815*	*3.30808357594213*
C	*-4.28757698626980*	*-2.67732893302145*	*2.65290675682163*
N	*-4.17124428149497*	*-2.65307416864860*	*1.27948070001410*
C	*-5.45906027841940*	*-2.58607941264594*	*3.40389029077850*
C	*-5.36441616639679*	*-2.66324110017344*	*4.77823295335530*
C	*-4.12984360323717*	*-2.81666023614907*	*5.41816586250240*
C	*-2.95804479110035*	*-2.89532926012045*	*4.69239466635443*
C	*1.50854461661773*	*-2.65469929887662*	*-3.75265678739159*
C	*2.94013740503850*	*-0.09829144468513*	*-3.84926940536372*
N	*3.41392729482024*	*-0.14539441039766*	*-2.45764412279161*
N	*2.59064623750200*	*0.11068707590518*	*-1.45880003717923*
N	*3.28334253883381*	*0.01393238097738*	*-0.37812866571324*
C	*4.56740714669981*	*-0.30759751932896*	*-0.65986207869962*

C	4.66170241022133	-0.41006261138702	-2.02527311475707
C	5.41476364477274	-0.46092067085014	0.49503605288567
S	7.10321516778423	-0.70664073239055	0.51487363250920
C	7.07342147281472	-0.66731091412944	2.24346553181350
C	5.75833952956502	-0.46313194193242	2.69557440021449
N	4.84485783162889	-0.36732659607692	1.67292064376961
C	5.49930078247714	-0.35375741930001	4.06073763063528
C	6.55791946466088	-0.46979835386929	4.93695354525437
C	7.86258260812254	-0.68987752534231	4.47800247322571
C	8.13843646254677	-0.78718305542748	3.12805206693827
H	2.17622623928572	2.42584590689185	-4.78847000276045
H	0.90616498077101	3.25019951294331	-3.90523910796791
H	2.16935140664357	2.42310949472337	-3.02381790249311
H	-0.95579825311365	3.22596054590089	-4.03095375464619
H	-2.44228935833726	2.29992527835039	-4.04887560614499
H	-3.53501107085074	1.77333118033762	-1.78209638562131
H	-0.35022047499951	1.99139490973903	4.62642985723158
H	-1.49563522365675	1.13832979443122	6.65413657759985
H	-3.81321013331740	0.30603981015804	6.53508067959007
H	-5.03840416695889	0.28279303835632	4.38751519936957
H	-3.34080965413048	-0.09135829430242	-3.16837796764779
H	-3.19211993118636	0.67582318856991	-4.74712629415242
H	-3.20287625941221	-1.06597607752882	-4.61451538910778
H	-2.15215986365614	-2.74852473009399	-4.63285261258285
H	-0.73252076071341	-3.51548139710206	-3.94716239129599
H	-0.51394760525428	-2.78326912620552	-1.15083580840725
H	-6.41227065206372	-2.45292739379955	2.91202424414943
H	-6.26661898365312	-2.59714372009800	5.37452599463545
H	-4.09001574184772	-2.86689057848036	6.49957135590403
H	-1.99788155587416	-3.00618384730678	5.18071983760675
H	1.15081449537647	-3.24086712221394	-2.90404927297912
H	1.37622208855290	-3.26754592355238	-4.64836715771644
H	2.57590363541388	-2.51948023335101	-3.60516213082951
H	3.40196237513836	-0.93750411711672	-4.36401125394995

H	3.34126789042977	0.81117019715692	-4.29133129269425
H	5.47409455082546	-0.64834490183610	-2.69194975469822
H	4.49425327919658	-0.16306522013891	4.41128220100564
H	6.37733990092503	-0.38448970576542	6.00175365835604
H	8.67220182887564	-0.77655468674142	5.19260265938325
H	9.14793380881033	-0.94428606267566	2.76932005207266
Cu	0.18723486605317	2.79277980858625	1.47341233921198
Cu	2.84003664159028	-0.12638026576025	1.59362835132887
Cu	-5.43326661031505	-2.38917129965309	-0.30951981534051
N	1.87353188981604	-0.69894312470937	4.18818647520036
O	1.33087899629919	-1.43045058559457	5.00065285142601
O	1.94138601401729	0.51604644728131	4.31104582084040
O	2.41481526997765	-1.24948640326425	3.16005144288512
O	0.94453922774052	0.33249898834876	1.28587447547843
N	0.32350560055473	-0.60622782457167	0.65332241940502
O	0.90401863579519	-1.67166177557232	0.48799452456530
O	-0.80252911061344	-0.38312172034161	0.26055356423804
O	-7.24881588360059	-4.06615367472025	-0.03793799491256
O	-5.37385607762360	-0.07444119313965	-1.28470796625280
N	-7.77100836035891	-3.14136936349102	0.59026645048188
O	-8.87580212089422	-3.20172193138371	1.08644074699961
N	-6.06832446414717	-0.60956009131161	-2.15723315299458
O	-6.37631279588129	-1.84107909237265	-1.99299916625859
O	-7.08698937771419	-2.06141508144934	0.72182842022444
O	-6.46062630334328	-0.02817498605875	-3.14863180904549
O	0.80070272290774	3.51729293640947	3.21661917210666
O	1.82537501293469	3.36283095295654	0.51817570021340
N	0.28593114608715	4.68922672652777	3.31102668660644
O	0.49405955577365	5.33803183280589	4.31673152496187
N	2.96977327819680	2.95722583988670	0.91108004193470
O	3.03271641208594	2.19266721221534	1.88049846760473
O	-0.39531731231742	5.09363708494108	2.36632048028528
O	3.95401434777773	3.34038592661512	0.31101396178096

Table C-4 *XYZ atomic coordinates for Cu(I)- TC-* Benzothiazole *using PBE0-D3(BJ) with a neutral charge and multiplicity of 3*

C	*1.98885367611244*	*2.06036896840755*	*-4.04825445031497*
C	*1.08336338833794*	*0.86910852781847*	*-4.18639142108629*
C	*1.60095735668296*	*-0.43375670526414*	*-4.23142765447710*
C	*0.74290896773912*	*-1.54012165821145*	*-4.29576325608805*
C	*-0.63382683712803*	*-1.31712058992082*	*-4.36591298930645*
C	*-1.16722011402746*	*-0.02550310119151*	*-4.38861237731603*
C	*-0.30461523841126*	*1.06282139763877*	*-4.23240138796818*
C	*-0.86842233376410*	*2.42378439532083*	*-3.90835762516871*
N	*-1.13900669594111*	*2.50717350503339*	*-2.47161225779405*
N	*-0.27592121084159*	*3.10458651544627*	*-1.64799816510673*
N	*-0.69841151018483*	*2.93316499531453*	*-0.44034176393604*
C	*-1.84518411303955*	*2.20660803733856*	*-0.47063884212522*
C	*-2.13541350144005*	*1.92996770291460*	*-1.78496607379140*
C	*-2.53179428729541*	*1.86754652265669*	*0.74855908633221*
S	*-3.94112871611301*	*0.88092480594446*	*0.79133056526072*
C	*-4.00106686992395*	*1.05896877895726*	*2.50830431683704*
C	*-2.92971524254922*	*1.85777835229676*	*2.93649530235086*
N	*-2.11770917096942*	*2.29815479780018*	*1.91246533875813*
C	*-2.76590806631387*	*2.13941912122704*	*4.29019948550838*
C	*-3.67861502082379*	*1.61635323898636*	*5.18388156890780*
C	*-4.74431069939953*	*0.82100188659268*	*4.74740528440335*
C	*-4.91995955269093*	*0.53280787417073*	*3.40732831666728*
C	*-2.65293063313021*	*0.13548318392845*	*-4.53997732140549*
C	*-1.58524315751611*	*-2.46501178016963*	*-4.17398856662746*
N	*-2.00802652381461*	*-2.48200445087211*	*-2.76541411847516*
N	*-1.15080900119793*	*-2.12355891090682*	*-1.81856180498450*
N	*-1.77187773867948*	*-2.20340479214136*	*-0.69066050396618*
C	*-3.04833173467300*	*-2.62546236574396*	*-0.89505455575914*
C	*-3.20645372890949*	*-2.80254788254336*	*-2.24897957466528*
C	*-3.87436075305458*	*-2.78458603883167*	*0.27735953362785*
S	*-5.58603674413304*	*-2.99129578043062*	*0.28205201033505*
C	*-5.55930164478103*	*-2.98666403800933*	*2.01185674486364*
C	*-4.23546561350075*	*-2.82904138729950*	*2.46004978273590*

N	*-3.31094512261120*	*-2.71363258900337*	*1.45201108305665*
C	*-3.95977881236074*	*-2.79447659379748*	*3.82585254390793*
C	*-5.01135769195871*	*-2.90768756935772*	*4.71128707898767*
C	*-6.32727375161600*	*-3.05381781450527*	*4.25611479753571*
C	*-6.61875403047210*	*-3.09777250880556*	*2.90475774047964*
C	*1.23620148149647*	*-2.95750113756650*	*-4.22731423684676*
C	*3.07780817771190*	*-0.63801577118168*	*-4.01602152400047*
N	*3.38749127949624*	*-0.51316675657152*	*-2.59114187370772*
N	*2.78327879316055*	*-1.30994725955499*	*-1.72012994390540*
N	*3.14179715199131*	*-0.92547761559339*	*-0.54081385841993*
C	*3.98736821618802*	*0.13471653541671*	*-0.63886971885639*
C	*4.15166572870456*	*0.40364809302163*	*-1.97568963922635*
C	*4.43714677217902*	*0.73879261562067*	*0.59114147163666*
S	*5.55891834927057*	*2.04101006792844*	*0.71305272513169*
C	*5.36885765396473*	*2.01263377996791*	*2.43093115540393*
C	*4.46111375716645*	*0.99862655504238*	*2.78633456657176*
N	*3.95722208110631*	*0.29702932862639*	*1.71976710418171*
C	*4.13822617865684*	*0.79063740875770*	*4.12640377174043*
C	*4.72638272735658*	*1.59939620110847*	*5.07752594578888*
C	*5.62942843008596*	*2.60571952519560*	*4.71333519595606*
C	*5.96233554467505*	*2.82520574419678*	*3.38936872604853*
H	*3.01638170495319*	*1.84126846965565*	*-4.32341656088208*
H	*1.66428974305154*	*2.87834290629297*	*-4.69180547561719*
H	*1.99296662775487*	*2.43688465024066*	*-3.02164467631349*
H	*-0.17687350583924*	*3.23115686190231*	*-4.12607958981692*
H	*-1.79738550588092*	*2.64092607756141*	*-4.42856883818878*
H	*-2.94914136917697*	*1.40110889742545*	*-2.24963757382937*
H	*-1.93410630677385*	*2.75387052771795*	*4.61470115585340*
H	*-3.56792819984995*	*1.82339660666285*	*6.24162729786270*
H	*-5.44232861711321*	*0.41758209079812*	*5.47109710860440*
H	*-5.73977567694808*	*-0.08965211067192*	*3.07146808017277*
H	*-3.19890172772195*	*-0.23435874112305*	*-3.66786663850472*
H	*-2.95602092862590*	*1.16566336030611*	*-4.70382517796474*
H	*-3.00500927872354*	*-0.43982011566598*	*-5.39876109282597*

H	-2.49208128297242	-2.37069492089839	-4.76736161890625
H	-1.13749092455878	-3.42930346454857	-4.40075712180275
H	-4.03934979756730	-3.11586436256834	-2.85688175672051
H	-2.93832234328340	-2.66889072729930	4.16516758423992
H	-4.81911374754846	-2.87436947761807	5.77704427436537
H	-7.13448463377535	-3.13322650695767	4.97459762898916
H	-7.63745774325699	-3.21115005513148	2.55514621958971
H	0.89222689090349	-3.43247974985230	-3.30486607848112
H	0.85226421265623	-3.54451169989896	-5.06425507257512
H	2.31736533797608	-3.04294538424955	-4.24418695893570
H	3.41955714413108	-1.61441617586157	-4.34387436469460
H	3.68801642061424	0.09802228243077	-4.53124928180714
H	4.71474226304512	1.15053647147065	-2.51055752933149
H	3.43452967096559	0.01168278267934	4.39501944609761
H	4.48567302761150	1.45566355259924	6.12419745023551
H	6.07485746014058	3.22631877326536	5.48181531490965
H	6.65865694881929	3.60587818390191	3.10911695081730
Cu	-0.52036825954744	3.36537296421231	2.07374278148521
Cu	2.57571579645325	-1.31381660023669	1.36033213726838
Cu	-1.31954658863043	-1.93057405682231	1.26488342018240
N	1.99874016431044	4.42136260908958	2.27361462963037
O	2.21214358208179	3.48826461456229	1.50429678899311
O	2.87628690534363	5.18486464528086	2.65435364793930
O	0.50490592604378	0.90545170286332	3.35839555301786
O	2.05063167393675	-2.64706071139924	2.73960421460915
N	1.05855651713102	-3.39538340447542	2.49271737664144
O	0.49278686963583	-3.30127419426122	1.38853036706109
O	0.68237281671990	-4.18752705734467	3.34494976166406
O	-0.78572102513049	-0.70617350740024	2.76274481567006
O	0.66618062857464	0.08185228755774	1.37226893391804
N	0.14472134015250	0.10950361486178	2.49915928594567
O	0.80753594110162	4.61295972574391	2.70462944374423

Table C-5 *XYZ atomic coordinates for Cu(II)- TC-Pyridine structure using PBE0-D3(BJ) with a neutral charge and multiplicity of 4*

C	1.80072680667022	2.16794469397453	-2.84025355023605
C	1.03914168174667	0.87657944417740	-2.92390794569591
C	1.75166637909105	-0.33190152683923	-3.01634289539926
C	1.09140968375015	-1.56345238162857	-2.96679046150405
C	-0.30670292388774	-1.57325406439083	-2.88406664829623
C	-1.03872014052085	-0.38567087340053	-2.93043740028619
C	-0.35799014004070	0.83955634450589	-2.89382907520337
C	-1.16653904653781	2.09552924304350	-2.70864194676731
N	-1.51642248951576	2.28778454208648	-1.29778560651725
N	-0.57571697412141	2.56418815238846	-0.41507300485434
N	-1.16631425457514	2.64225568349695	0.73061887624513
C	-2.49340919709640	2.41757831169935	0.60810315198897
C	-2.73023528073310	2.18470921508506	-0.72332438588438
C	-3.29032911518648	2.48836152238528	1.81808473087855
N	-2.58855019332919	2.87067653846926	2.89849804417038
C	-3.19384224898682	2.95118632942500	4.07893150957984
C	-4.53811602436760	2.66413885172137	4.23314030983592
C	-5.26941483289612	2.28069766485601	3.12024452331498
C	-4.63865702781524	2.18565419968314	1.89138352662320
C	-2.53836704681863	-0.41715018814446	-2.98530179837284
C	-1.02636442060813	-2.85551564710855	-2.54502665368832
N	-1.53362426356198	-2.72830731626253	-1.17348673560755
N	-0.68560287536985	-2.42224005575173	-0.21031492957210
N	-1.40049611188570	-2.14621076751635	0.82639701472901
C	-2.71993057221376	-2.26888075019924	0.55263069615238
C	-2.81241520102636	-2.66056560516505	-0.75884468589739
C	-3.64954700372503	-1.90057492977483	1.60104950394956
N	-3.04578881968583	-1.43357091401980	2.70910484243636
C	-3.78659273524839	-1.04930056307400	3.74461733113440
C	-5.16837756934671	-1.11223398762496	3.71931439865009
C	-5.79511797060969	-1.58639215226269	2.57898580170688
C	-5.02625031193398	-1.98791618731623	1.49915609907825
C	1.82609169592786	-2.87366144007796	-2.97134949897175

C	3.25385352878439	-0.28107278033443	-3.11135385406754
N	3.90118795818105	-0.27713600771716	-1.79881551954730
N	3.81989485133342	-1.33639393220062	-1.01566485475246
N	4.46920966194435	-1.04124627936126	0.05804505748625
C	4.97374452011736	0.20940208939743	-0.00603887541810
C	4.60779775806638	0.71655028817015	-1.22755860343050
C	5.71528468268799	0.67969104208476	1.14731911903005
N	5.83605746451913	-0.24113188897235	2.12046433178471
C	6.49543831200221	0.06599381173028	3.23324729484563
C	7.06081039131111	1.31344474331153	3.42999995087124
C	6.93227044551007	2.26831899810485	2.43418457537064
C	6.25076693660959	1.94933527929718	1.27159049777862
H	2.48983377571138	2.28003515389014	-3.67997681208685
H	1.16182576380422	3.04438272424130	-2.83429028379175
H	2.39000474322660	2.21024759226370	-1.92102596823000
H	-0.64751245731689	2.99115735005532	-3.03378475542744
H	-2.11068312755545	2.06335110934349	-3.24555956019569
H	-3.62593480713914	1.97668973782914	-1.28400083787367
H	-2.99381841946666	-0.26771565891794	-2.00287379930231
H	-2.92457573009638	0.36198783492710	-3.64236170476407
H	-2.90890616515855	-1.36264234197822	-3.37516418336356
H	-1.88650570559169	-3.06161332644087	-3.17841884129677
H	-0.37413338512833	-3.72239542597340	-2.57650993419620
H	-3.64788326745373	-2.85992787923133	-1.40875362631888
H	1.75473816517290	-3.35602666920628	-1.99265194596145
H	1.40148329387379	-3.55555791174714	-3.71052610123481
H	2.88331663969376	-2.76993771098994	-3.19156237723756
H	3.65683406597168	-1.12543949995751	-3.66435112059072
H	3.59674177676806	0.61999136367790	-3.61148322350219
H	4.79105362121785	1.65858495913834	-1.71657816429287
Cu	-0.61438840466794	3.21473078718082	2.56119694702146
Cu	4.86101623741107	-1.98054831638670	1.76894504508131
Cu	-1.02048508609955	-1.40990795743345	2.61998027325887
H	-2.57749365680151	3.24928133914723	4.91791340276752

H	-4.99491915139623	2.73969125109783	5.21085399153291
H	-6.32325820657509	2.04641406812281	3.20895559182416
H	-5.17430854420894	1.87520563333378	1.00342960784238
H	6.57122406630409	-0.71502376216976	3.97860539811479
H	-6.87569152217828	-1.64298117883723	2.52733279202774
H	6.12833009115335	2.66882918298570	0.47218910946949
H	-5.47950003975599	-2.36461422425671	0.59112554762556
H	-3.25151483280301	-0.68255170260736	4.61065092397210
O	0.94375392127636	-1.57394126034704	2.60774558427584
N	-0.74085773029030	5.31632237352587	4.36934393174769
O	-0.23264238481601	4.13994095852860	4.25923365237383
N	1.69169947759290	4.20297478176495	1.46923079949613
O	0.87066301308446	5.09241192784948	1.26228793500584
O	-0.46968750728764	5.95793089210992	5.37053344139604
O	2.84388590336809	4.24630215774828	1.07068439043291
O	-1.47015998713864	5.73242879387404	3.47703422104712
O	1.32117487745061	3.17436905889673	2.13819665649965
N	5.10440095574946	-3.16314367882900	4.29221157968701
O	5.63846045298778	-3.81863242903293	5.17123059452825
N	4.23801124987790	-4.33812374963369	0.57527782919875
O	3.59558022969059	-5.30389953106833	0.20270188451892
O	3.97091704657547	-2.71123652915767	4.37659398890692
O	5.39713183987097	-4.12036887670214	0.22989012983873
O	3.67326969611043	-3.50560902970518	1.37170450718418
O	5.78517974601367	-2.93228472546836	3.22475452610447
N	-0.51840489760362	0.43905531258829	4.49083080063218
N	1.62700497457060	-0.70794258372465	1.95007280935389
O	2.77496139484962	-0.50005764572026	2.32889247371066
O	1.12553295984955	-0.13521155788191	0.99922338679355
O	-0.35887884322197	1.02724005672194	5.53513783718416
O	-0.34638345031998	0.95654558070730	3.37647255874016
O	-0.88409437586412	-0.78486357287570	4.50722571697356
H	-5.73400043196292	-0.78563933873634	4.58165134403852
H	7.58852716681662	1.52376122894808	4.35072149457340

H	*7.35896400524607*	*3.25605811456842*	*2.55988327721511*

Table C-6 *XYZ atomic coordinates for Cu(I)- TC-Pyridine structure using PBE0-D3(BJ) with a neutral charge and multiplicity of 3*

C	*2.24258321614870*	*1.94000723778580*	*-3.93827043574361*
C	*1.12614209622996*	*0.97558259280599*	*-3.64593246447327*
C	*1.34180208819068*	*-0.40570998556755*	*-3.58239239185710*
C	*0.27437238324930*	*-1.28595800289364*	*-3.34376660282032*
C	*-0.99995536421706*	*-0.76371504124551*	*-3.12435970209541*
C	*-1.24107988559616*	*0.61498311973785*	*-3.20020722345268*
C	*-0.16586324171383*	*1.47933014407362*	*-3.41700927315245*
C	*-0.35316683581623*	*2.96876250329003*	*-3.23946328784348*
N	*-0.37387256572248*	*3.31680383847410*	*-1.81509983828944*
N	*0.75961628361873*	*3.56862418542223*	*-1.16510123103035*
N	*0.46051948943046*	*3.73815102947129*	*0.08236415651912*
C	*-0.87310086348300*	*3.58502726870953*	*0.25844195203442*
C	*-1.42101576342700*	*3.32182743152645*	*-0.97534863354342*
C	*-1.47994830954193*	*3.68092501490050*	*1.57776586935559*
N	*-0.64476554212279*	*3.84932433594419*	*2.61429735889836*
C	*-1.13859566903842*	*3.95677648196075*	*3.84672673598486*
C	*-2.49392779610953*	*3.90601326598546*	*4.10854421821695*
C	*-3.36378893040120*	*3.71311145987625*	*3.04666986374170*
C	*-2.85331453715576*	*3.59847680562100*	*1.76677179366539*
C	*-2.64842392791418*	*1.11693389370566*	*-3.04159366543426*
C	*-2.07809094857065*	*-1.65556744323940*	*-2.56655358683658*
N	*-1.80816059851891*	*-1.86737594577163*	*-1.14096350915716*
N	*-1.81071988267609*	*-0.83587708467354*	*-0.31167889714461*
N	*-1.44351534940774*	*-1.28465496561945*	*0.84733382951745*
C	*-1.19589805463130*	*-2.61818497258945*	*0.77576216604903*
C	*-1.43410376062891*	*-2.99923066911641*	*-0.52229190705887*
C	*-0.77099084798816*	*-3.34066940800015*	*1.96681741897940*
N	*-0.66399807275024*	*-2.59274099611396*	*3.07088648535821*
C	*-0.28327272559191*	*-3.15374101263757*	*4.21025080875224*
C	*0.00861518918190*	*-4.51249005005319*	*4.32652497326640*
C	*-0.12144098338980*	*-5.22614986437930*	*3.16887475151517*
C	*-0.49882910529915*	*-4.71050917948306*	*1.96317084441242*

C	0.52509348222857	-2.76486693499450	-3.27963755714715
C	2.74317319578165	-0.95893897356696	-3.44814478984085
N	3.02832339851984	-1.00979328660453	-2.01122180925530
N	3.17067868790538	-2.15508884640709	-1.34426335723759
N	3.10316746041056	-1.87771796222847	-0.07779472039789
C	2.90119419363334	-0.54653344388424	0.07984596353857
C	2.86841548743078	0.01804840592687	-1.16847031927869
C	2.58484692718046	0.09017490560922	1.34704642676181
N	2.44196758733052	-0.68471802225717	2.43312769394084
C	2.02344368752458	-0.09787295084046	3.56331137308184
C	1.70214705165671	1.24633073722475	3.64282483885860
C	1.84129114602191	2.06795815173325	2.52307070182772
C	2.32546233190546	1.45173069715851	1.37892894504457
H	3.16841748954563	1.44442837726370	-4.21439377236684
H	1.96927154927027	2.58919992089454	-4.77312633547139
H	2.45468847116746	2.59091891589926	-3.08622572021636
H	0.45701717783989	3.54135266659457	-3.67943400380588
H	-1.28125237567961	3.33500830430599	-3.67065387024117
H	-2.43270418898599	3.15368833386343	-1.29879743705885
H	-2.99337646916284	1.03038184155660	-2.00845117910097
H	-2.76322879935915	2.15250795256854	-3.34965965651764
H	-3.33015044299102	0.53121861814850	-3.66065488720803
H	-3.06813618253571	-1.21737325948799	-2.64649419584715
H	-2.11557271130359	-2.63972839432493	-3.02496887116361
H	-1.36892096365925	-3.94552322250553	-1.03272108796929
H	0.95673302891198	-3.06034157523940	-2.31967226363716
H	-0.38243865312346	-3.34499052342354	-3.42713451172636
H	1.22589267460449	-3.07549222935172	-4.05485449394510
H	2.84679386129415	-1.97388868089206	-3.81988442888769
H	3.50263973393306	-0.34977398503937	-3.92912899342017
H	2.70143524562870	1.02514260200965	-1.50387729347623
Cu	1.34300494266621	3.93697923011660	2.26285550584215
Cu	2.78108846115448	-2.57398783309969	2.25566030429921
Cu	-1.28435481168644	-0.50026598077934	2.63240990669261

H	-0.41546171759424	4.08541675738258	4.64338503295601
H	-2.85073675132297	3.99999048098025	5.12482520807830
H	-4.43260980567406	3.65360400886362	3.21323989992426
H	-3.50846021211923	3.45283952034813	0.91755301175426
H	1.92377059758692	-0.74598729886979	4.42603067044599
H	1.32254986961790	1.62407422630476	4.58487401792397
H	2.46263326644290	2.02024964290875	0.46707762717866
H	-0.58565089601624	-5.29954053034879	1.05783568762253
H	-0.20656882398073	-2.49920500064360	5.07294159690490
H	0.31696214036529	-4.93749400576456	5.27333594952783
N	2.71667238440674	5.99594091494266	2.00482981228388
O	1.46959563818761	6.03740335649594	2.18923277991163
O	-2.76804198623722	1.14484173001207	5.81923768216010
O	-3.48988798680423	0.03592164794576	4.11780909040735
O	3.38313866739609	6.99147414347400	1.86433354885179
N	-2.58428697784865	0.59682800714322	4.73977237714943
O	3.21997461625944	4.83793817608058	1.97668820783836
O	-1.41155341014246	0.61023758579816	4.24122126732752
N	3.28292622047679	-5.00617525018033	3.43990105151755
O	3.36087408012366	-6.22671656317682	3.49752302903825
O	3.06841530873930	-4.47359109151827	2.29636233609142
O	3.40126991874092	-4.28528400203224	4.42760443410160

Table C-7 *XYZ atomic coordinates for Cu(II)- TC-Pyrimidine structure using PBE0-D3(BJ) with a neutral charge and multiplicity of 4*

C	1.94988226356492	2.17078353183254	-3.06538240330399
C	0.90408095095021	1.09391565145676	-3.04942586159999
C	1.31372492223912	-0.24185082447409	-2.98355589685518
C	0.38249212309089	-1.28200352361083	-2.91028231880603
C	-0.97837580835686	-0.96216435256490	-2.85647396659926
C	-1.41289804296841	0.36550303200649	-2.92801527753860
C	-0.46433383655214	1.38659098156805	-3.06150955487941
C	-0.92388212886766	2.81480410469625	-3.14178920152231
N	-1.16419912897713	3.35846881411767	-1.80243703046705
N	-0.36252606346157	3.01592108758670	-0.80994738553106
N	-0.80188842035407	3.62333162180109	0.23449248708022

C	-1.89095983897634	4.36492782617904	-0.05874225648722
C	-2.13357669784622	4.19943667629213	-1.39932767408646
C	-2.51833547925333	5.06745913179058	1.04517984767655
N	-1.93222792046292	4.83441927283179	2.23051668393767
C	-2.44306397949104	5.42955770742393	3.30311962338408
C	-3.53881912238301	6.26395075229351	3.19369849933076
C	-4.07285180996260	6.43876304794055	1.92815737724949
N	-3.56865246129914	5.84163204563461	0.84996737140537
C	-2.88140897190531	0.66672779124750	-2.82096641307986
C	-1.99040867903538	-2.05582008981697	-2.65433544377345
N	-1.94821490870916	-2.57112983654415	-1.28363355890686
N	-2.08429019178748	-1.74186045283281	-0.26422931982979
N	-1.99717229093960	-2.46275157754880	0.80154851889672
C	-1.80576050191874	-3.76253828441648	0.48664542796093
C	-1.77269862458660	-3.84160550592946	-0.88118854391535
C	-1.67597743750065	-4.69915336042672	1.58444210390120
N	-1.77515405099393	-4.12529966757197	2.79311710368293
C	-1.64822165141111	-4.90367809753242	3.86354894394143
C	-1.42318048473468	-6.25910473155062	3.72556696549752
C	-1.35510543482816	-6.75854382339490	2.43581593945777
N	-1.48326499277081	-5.98401963364567	1.36103189007867
C	0.84191161217196	-2.70794707065718	-2.82824538486617
C	2.78429321020136	-0.54387021828977	-2.93983185137398
N	3.32251632960394	-0.44596563702624	-1.57928645113340
N	2.68743995836983	-1.00385962772516	-0.56486308908583
N	3.41267244252068	-0.78159263916612	0.47878191497712
C	4.52002947449475	-0.08110432333308	0.15503980239845
C	4.46982803751874	0.14160583570386	-1.19613044775078
C	5.42704960214608	0.25775755129376	1.23341955868544
N	5.04403849188383	-0.21844381990748	2.42838063954101
C	5.81733644576698	0.04226536042502	3.47785950068069
C	6.97266830280376	0.78565922212730	3.33577656290700
C	7.28112297229466	1.23291499016677	2.06194676091077
N	6.51400904350498	0.96934574956416	1.00609436397680

H	2.53849876556370	2.13744911350165	-3.98679351338020
H	1.53684764466011	3.17022361509563	-2.97375377146322
H	2.64281398638793	2.04965025306319	-2.23046421552149
H	-0.19574379061278	3.45352655997154	-3.63625964249429
H	-1.85628235319462	2.91810021754373	-3.69008391711435
H	-2.89049162155572	4.58341858042255	-2.06271434501987
H	-3.28710320886418	0.26556105781386	-1.88947411421868
H	-3.10390404566447	1.72897681988976	-2.82805084198770
H	-3.43997418829589	0.21532740761193	-3.64491534036094
H	-3.00486916791354	-1.71223961679419	-2.83545239107132
H	-1.81883243267481	-2.91054398637564	-3.30507390179848
H	-1.63749604606175	-4.66231678897113	-1.56554029288990
H	1.17972666488230	-2.94717480330291	-1.81589787698200
H	0.05972906429257	-3.41500459162029	-3.09253824211014
H	1.67474206021865	-2.90225467261065	-3.50365426545186
H	3.01073814322086	-1.54453516123911	-3.29958522189653
H	3.36325382051518	0.15698870529401	-3.53660290180644
H	5.12423300641153	0.65374994689458	-1.88134282865572
Cu	-0.31799314990963	3.56917225134085	2.15296413163344
Cu	3.29363017436623	-1.27135001770713	2.39580124846715
Cu	-2.10235045262710	-2.12338499967626	2.76178812107059
N	0.72587599251472	4.15626561250600	4.62969948469978
O	-0.16655859332316	3.39356825708276	4.10176700156998
N	2.30379122057095	3.28203964410076	1.27266840935468
O	2.06505274365989	4.42211689296072	0.89470927726417
O	0.99231335627287	3.99005598606804	5.80653683291265
O	3.37326434246365	2.72274161975018	1.08069580019089
O	1.25260548097461	5.01082034387284	3.92678854222506
O	1.39749033578358	2.62717784369235	1.90274712224743
N	2.69732179285092	-0.66117156623246	4.88945185215473
O	2.54069593147473	-0.65919261812966	6.09165382572907
N	2.13790822218135	-3.58977885585625	1.95222929918287
O	1.36373410664919	-4.50581817178599	1.75766216690782
O	2.31072915637194	0.24030586564944	4.14331911471479

O	*3.36475281753841*	*-3.72947723842753*	*1.97104350671785*
O	*1.67465383438505*	*-2.41196737698718*	*2.14797903889459*
O	*3.31038911965880*	*-1.65106106366506*	*4.34184320369086*
N	*-1.47131392799254*	*-1.56523013389676*	*5.29937249023648*
N	*-1.71173061370399*	*0.59567223824192*	*2.28496736207878*
O	*-1.97526149768181*	*1.79505173365497*	*2.37558388807584*
O	*-2.61693429288451*	*-0.22225891041567*	*2.67035581818659*
O	*-1.53577829109054*	*-1.38247404511137*	*6.49823002763922*
O	*-0.49037996254242*	*-1.28537334244308*	*4.61369023296546*
O	*-2.48369083135108*	*-2.08774565357012*	*4.70105006505722*
O	*-0.65477574355816*	*0.17180033568065*	*1.85745400911204*
H	*5.50095913112475*	*-0.35742609990163*	*4.43356708990729*
H	*8.17390188202394*	*1.82155354009631*	*1.87763556009215*
H	*7.60562376173513*	*1.00363305445959*	*4.18453034427067*
H	*-1.19365026385162*	*-7.81607993410374*	*2.25442590696510*
H	*-1.31486931015169*	*-6.89850472324658*	*4.59037460569390*
H	*-1.73627952001509*	*-4.42523771426816*	*4.83076163912838*
H	*-1.96497854263743*	*5.22278671255588*	*4.25276044224811*
H	*-4.93514133919958*	*7.07798960374268*	*1.76906478817678*
H	*-3.95884259418814*	*6.75330458576588*	*4.06124481859402*

Table C-8 *XYZ atomic coordinates for Cu(I)- TC-Pyrimidine structure using PBE0-D3(BJ) with a neutral charge and multiplicity of 3*

C	*2.06200830494492*	*1.95389522636884*	*-3.67136458929564*
C	*0.97331117122861*	*0.92898389886664*	*-3.52038649088995*
C	*1.26512961018591*	*-0.42519865074440*	*-3.32739311803377*
C	*0.23609509466897*	*-1.37306515731178*	*-3.24734481939299*
C	*-1.08972993617288*	*-0.93885776563869*	*-3.28007352993727*
C	*-1.40811774844606*	*0.41133340453750*	*-3.46383306404306*
C	*-0.36852167717052*	*1.34105834724824*	*-3.56343353450718*
C	*-0.66311270199801*	*2.81932628605019*	*-3.51214688518007*
N	*-0.69792152076823*	*3.25999424819792*	*-2.11523188688212*
N	*0.34332749386246*	*3.88973056115573*	*-1.58546475339458*
N	*0.09122021418168*	*4.04165412786724*	*-0.32486725596060*
C	*-1.11823404871420*	*3.50754082643052*	*-0.02803964898339*
C	*-1.63640392415028*	*2.99732593591106*	*-1.18932777639258*

C	-1.60772487480293	3.55215150434494	1.34141163880625
N	-0.78354298921995	4.14346668403046	2.21179718488169
C	-1.18253989914320	4.20766428421772	3.47728800639806
C	-2.40125616541875	3.68737600408233	3.87402676470170
C	-3.17529312935459	3.08989998699320	2.89416485021455
N	-2.78681852346803	3.01828430456114	1.62321466723014
C	-2.85502828059083	0.81488991745764	-3.52384432503939
C	-2.16977055777625	-1.90752765608688	-2.88455731497081
N	-1.98773089035428	-2.26515403353145	-1.47287594920810
N	-1.57699140413336	-1.34870524721736	-0.62363547000782
N	-1.47647138795337	-1.95543586964741	0.53181064677853
C	-1.82671419964555	-3.27526617046217	0.43038989463290
C	-2.16451607855156	-3.46831952235279	-0.90040674076572
C	-1.73196285250759	-4.04502612897484	1.61669129981710
N	-1.28536457744912	-3.29734015943135	2.71118608793197
C	-1.15217538908097	-3.95345100021702	3.87880561392711
C	-1.44025003211241	-5.28149683075651	3.99780329931348
C	-1.88428482586342	-5.96080742143631	2.82746364856236
N	-2.02227308534331	-5.34690613469366	1.67338071095622
C	0.54261280475282	-2.83214495730790	-3.07264808123105
C	2.66644208847298	-0.85435456361913	-2.97191285193061
N	2.85285608468785	-0.69934838211974	-1.52717581664490
N	2.46005160763651	-1.66208293933098	-0.70304279320457
N	2.59870390606812	-1.20780821253566	0.50026515511670
C	3.07854440676419	0.05864452859851	0.46510545086022
C	3.24628148247128	0.39531561174270	-0.85428144353728
C	3.33143481709025	0.76117358876810	1.71328697640985
N	3.05708600289939	0.05883758543852	2.81873079416272
C	3.28718189996178	0.65193154552554	3.98568889471830
C	3.79250697531966	1.93817629303628	4.05217518660520
C	4.03937820833684	2.57614740904754	2.84906077655648
N	3.80878772025932	1.99611214145822	1.67362938874460
H	3.03715802193721	1.50809691250368	-3.84453339454328
H	1.85934853791617	2.60215682097426	-4.52595791861839

H	2.13830614236781	2.59911208646892	-2.79315165046193
H	0.10536024996456	3.41750802816874	-3.99178320695698
H	-1.61427270732525	3.08619183996590	-3.96322523637512
H	-2.56177646713309	2.49357130609480	-1.40531839894787
H	-3.35129430086972	0.67270764129257	-2.55926364835561
H	-2.99760143863962	1.85196773130457	-3.81419306292508
H	-3.39203843509914	0.20575064119896	-4.25335098725316
H	-3.16460199830197	-1.48436787064209	-2.99234268169551
H	-2.14686643757755	-2.83969724672009	-3.44658386154593
H	-2.48422262364198	-4.33150212466275	-1.45834135857463
H	0.74075268233721	-3.07672388844038	-2.02637205554453
H	-0.27880167270396	-3.45858095468362	-3.41349928371369
H	1.42168381828726	-3.12645510243863	-3.64526429585648
H	2.85519109059706	-1.89961872630788	-3.19475069396005
H	3.44150033105459	-0.26908266624431	-3.45695035440246
H	3.60543015661970	1.28794637853604	-1.33634468749449
Cu	1.04375647774539	4.78967147852893	1.25987327608392
Cu	2.37807819300524	-1.94586843545278	2.33724925692002
Cu	-0.87349650370397	-1.46504904685350	2.30114415009617
N	2.72688035708016	5.80300871105390	3.21375226842135
O	1.86422466233373	5.30231792483595	3.93191740474072
H	-4.13963985570295	2.65236600111842	3.13262271449026
H	-0.80077457966404	-3.36813912442122	4.72228116735745
O	3.70506509575951	6.38597556783490	3.66505225368682
H	-0.50130711167995	4.68131273829217	4.17437359832798
O	2.61530289530345	5.71194107917235	1.94268385964169
H	-2.72842401520197	3.73857836566667	4.90350361165869
N	2.30259768414230	-3.44804216095119	4.68026361769783
O	2.19825967896759	-4.46511163371829	5.35585170190721
H	3.05970829052564	0.07263773188148	4.87310447198428
O	-0.37053433033218	-0.61475457438998	4.06673203845739
O	2.52337566570026	-2.34493863688150	5.17515203309949
O	-0.31934586165259	0.47999941139021	2.24186728796152
H	-1.32862969014434	-5.79363905544446	4.94315274050673

O	*2.17500221567795*	*-3.55462012211468*	*3.41288984433482*
N	*-0.12761631601579*	*0.49138046182663*	*3.49554594900088*
H	*-2.12329099366318*	*-7.01932744871000*	*2.85631783453628*
H	*4.44232075791607*	*3.58330185515662*	*2.82083967488722*
H	*3.98274729326939*	*2.42198763645331*	*5.00034113503621*
O	*0.25441584694105*	*1.45870302083650*	*4.08936608849742*

Table C-9 *XYZ atomic coordinates for Cu(II)- TC-Carboxylate structure with O-Cu-O binding using PBE0-D3(BJ) with a neutral charge and multiplicity of 4*

C	*0.62614964903308*	*2.52988857690239*	*-2.39608447354061*
C	*0.21730649883402*	*1.13299549118990*	*-2.03614987672470*
C	*1.06988534543809*	*0.05873634615797*	*-2.32216752562351*
C	*0.69845241925998*	*-1.25289842063114*	*-2.01168141030176*
C	*-0.58185790712881*	*-1.48756159094341*	*-1.49287498739088*
C	*-1.41831355654179*	*-0.42461183532215*	*-1.13925898444097*
C	*-0.99771819345574*	*0.88639483421877*	*-1.39099502083004*
C	*-1.85368759946743*	*2.04202646396501*	*-0.94248028148656*
N	*-1.28282119282123*	*2.70371134163633*	*0.22725663595996*
N	*-1.21577052165523*	*2.05723042606166*	*1.39833294025361*
N	*-0.62573814451931*	*2.82692179951943*	*2.24574066068506*
C	*-0.29861628019239*	*3.98928347214712*	*1.62557312560740*
C	*-0.72495505911166*	*3.91249184251975*	*0.31854916514365*
C	*0.44027172360731*	*5.06526575074335*	*2.27004185775056*
O	*0.79469474580478*	*4.99101140214972*	*3.48456670237280*
C	*-2.74858664093201*	*-0.66780585886320*	*-0.48430840452850*
C	*-1.08411524259550*	*-2.89963342619024*	*-1.37249445792166*
N	*-1.09184462017095*	*-3.41509711544078*	*-0.00607211136732*
N	*-0.15178027732204*	*-3.07157073498158*	*0.88078365721091*
N	*-0.38790270085727*	*-3.70764786408979*	*1.97750775527699*
C	*-1.49195579382376*	*-4.47772110917277*	*1.80584597856630*
C	*-1.94926765807358*	*-4.29163836831863*	*0.52151911516320*
C	*-2.04867631314997*	*-5.33540722400249*	*2.84328412227337*
O	*-1.53869280127898*	*-5.39892093601042*	*3.99840542446223*
C	*1.65889796948586*	*-2.39036376310065*	*-2.22120383215546*
C	*2.39288396213904*	*0.33410909406664*	*-2.98385308431127*
N	*3.27300443970468*	*1.13883915654694*	*-2.14416810507928*

N	3.90524266009548	2.20338126887960	-2.65169166809407
N	4.56241993723402	2.76882515126999	-1.69962243856209
C	4.36959874044718	2.06024620954854	-0.55815107885104
C	3.53655412742015	1.00163072094412	-0.84250996766238
C	4.94305691790922	2.45125369968753	0.72143841307722
O	5.42494712603946	3.60743815014901	0.89981011774898
H	1.23510050201554	2.55100604732570	-3.29848935257854
H	-0.23410080965456	3.17110501636203	-2.57847843083522
H	1.21708582257348	2.99241855181969	-1.59933710493403
H	-1.95596767885570	2.80597350122610	-1.71076376321158
H	-2.85540621466741	1.72194398720116	-0.67114415823428
H	-0.66830760461221	4.60108644266087	-0.50756904629290
H	-2.78755188404900	-0.18019333145462	0.49248769273037
H	-3.56668764526031	-0.26200772097847	-1.08483202594025
H	-2.95699706549923	-1.72111949151950	-0.32397108406312
H	-2.11087502606516	-2.96987151511701	-1.72919116680764
H	-0.49319359961995	-3.58014137900425	-1.98234373160954
H	-2.78635456411786	-4.69652785181056	-0.02288260623460
H	1.42979396127512	-3.23564571081566	-1.57548255251456
H	1.65267543279384	-2.74667235493218	-3.25587786158553
H	2.67963418361141	-2.09077684315308	-1.98309326320125
H	2.91579651424439	-0.58193849514786	-3.24552052168340
H	2.26647803235695	0.90464120198859	-3.90418701065238
H	3.11731983075142	0.21704978661743	-0.23456259019594
Cu	5.73291073155404	3.09896907011656	2.80262769760974
Cu	-2.96636421235279	-6.71755603648313	4.46920869829342
Cu	1.81727170867784	6.67798846628244	3.22711460645965
N	3.65122510841075	7.97646691409886	1.82948556765159
O	3.91401046116236	6.77776244073208	1.73540981089008
O	4.27831629467271	8.85240989238390	1.27173648482923
O	2.65008778116912	8.31182531752112	2.56679631037302
N	5.17075268459560	5.26790537505700	4.14167694518853
O	5.17893874903046	6.37954169283242	4.65588480500415
O	6.23364927395682	4.84776505504753	3.57560690355864

O	*4.18553800961956*	*4.53496649226159*	*4.14476426722601*
N	*-3.43139057838974*	*-8.58651296853659*	*5.91769964300301*
O	*-3.64922507554900*	*-9.50847737407841*	*6.64791172373703*
O	*-4.03915970037525*	*-8.41384255007230*	*4.82102851474603*
O	*-2.56710054410908*	*-7.69174305234078*	*6.17741987176313*
O	*0.77883554835513*	*6.09209096273038*	*1.61028778896861*
O	*4.95204764227351*	*1.64437920547598*	*1.70110081157810*
O	*-3.07006578665774*	*-6.04692463560533*	*2.59756903807641*
O	*-4.48166121311566*	*-5.32942454804915*	*5.32013190822596*
H	*-5.23948845351216*	*-5.22766236685577*	*4.73270224763243*
H	*-4.85164071660848*	*-5.61380449133174*	*6.16391490937178*
O	*2.53888476732887*	*6.96479781588740*	*5.04741133791901*
H	*2.17529963366399*	*6.32949107638698*	*5.67766005651110*
H	*3.51021442234841*	*6.79173879281004*	*5.02205785617004*
O	*6.21169145109326*	*2.05622404023604*	*4.42178794498104*
H	*5.68763768146814*	*1.25146572056024*	*4.52901481858996*
H	*6.16317638471334*	*2.52438690042733*	*5.26533004680575*

Table C-10 *XYZ atomic coordinates for Cu(I)- TC-Carboxylate structure with O-Cu-O binding using PBE0-D3(BJ) with a neutral charge and multiplicity of 3*

C	*0.16859536100654*	*2.60905865539566*	*-2.22259895294446*
C	*-0.05849759331263*	*1.12627026816099*	*-2.22391193689145*
C	*0.99402545660812*	*0.27632556678434*	*-2.58733434348146*
C	*0.81402080439138*	*-1.10600406739661*	*-2.64913801620555*
C	*-0.45823152588867*	*-1.63713054983193*	*-2.38860905733714*
C	*-1.49513874101375*	*-0.81399021585137*	*-1.93393658555549*
C	*-1.27526705462685*	*0.56674154312669*	*-1.82737282511432*
C	*-2.30627529289107*	*1.43213082117202*	*-1.14526938033432*
N	*-1.86889928772043*	*1.73152951308247*	*0.21855507225882*
N	*-1.91675106810655*	*0.79294927889315*	*1.16410816800653*
N	*-1.33249250462344*	*1.26625957663045*	*2.21735571843414*
C	*-0.88425717775339*	*2.51855886034436*	*1.95751660501145*
C	*-1.23791732030495*	*2.82254909749405*	*0.66395824104637*
C	*-0.07168843694568*	*3.37193011347300*	*2.84880234782657*
O	*0.06775346597361*	*3.02108844980380*	*4.07162485978356*

C	-2.82430407444172	-1.37747706772429	-1.51260676087751
C	-0.67336861488950	-3.11957866563437	-2.51748590682201
N	-0.33150494238825	-3.81506472815098	-1.28121268050496
N	0.16261972168333	-5.05513513991751	-1.30909419193792
N	0.35842308511472	-5.43044267761650	-0.08510875245472
C	-0.01962719365027	-4.43247398081928	0.75115196821835
C	-0.46487237751507	-3.38522725033354	-0.02093691164033
C	0.08474163667293	-4.47925299709106	2.23627481731111
O	0.67237620774813	-5.41072458772703	2.78289277727167
C	1.98518366359824	-1.99841388221370	-2.95334725993763
C	2.36501553812015	0.87234135984531	-2.75530596440034
N	2.86341786493732	1.29790008473696	-1.44834869849417
N	3.57309584483317	2.42019425127694	-1.29597407892801
N	3.81932359813632	2.56487358249368	-0.03359604757191
C	3.26870161021837	1.52616379241748	0.64232379760709
C	2.65119019123518	0.70489484638819	-0.27028985149368
C	3.27414921128899	1.33632994196280	2.10532288356465
O	3.75328631795201	2.28017061643519	2.81997333231752
H	0.74762077313219	2.91092486039764	-3.09604100699789
H	-0.76167624198469	3.17109851229500	-2.25093167206529
H	0.72720857502049	2.93710162200991	-1.34169200331282
H	-2.46003663184195	2.38626147542467	-1.64422789877482
H	-3.27342960521657	0.94507072123697	-1.07292816337711
H	-1.08999093372754	3.70586022492969	0.06880218141596
H	-3.01139661218401	-1.16518407218226	-0.45749376068308
H	-3.64127592500843	-0.93087249172683	-2.08446021792007
H	-2.89260246791936	-2.45410524181355	-1.63759738564228
H	-1.70537714620092	-3.35322049553972	-2.77256852371099
H	-0.05298535720866	-3.55337005046115	-3.29759323204974
H	-0.82957073974853	-2.40700933783842	0.23811746789241
H	2.83638022269038	-1.75312058913736	-2.31494415448189
H	1.76864404851664	-3.04937888529031	-2.78607631813783

H	2.31380570081219	-1.88732129262470	-3.99044932860115
H	3.07265024594306	0.16609429930471	-3.18315790207319
H	2.36516842679983	1.75931634618673	-3.38672974947293
H	2.08441946015624	-0.20308860274369	-0.15681664123621
Cu	3.43767332435006	2.10550629784029	4.67754289421399
Cu	0.35511339226646	-2.11645726495706	3.77597765375429
Cu	1.41800667226676	4.14600685625647	4.84390964380450
H	3.24053831785616	5.33296011184893	4.16607583796294
O	2.91177752638031	5.35002880246401	5.10917016113573
H	3.61298355641780	4.98392098639001	5.66149703039872
O	3.22064381262506	5.01276513134829	2.49947880673675
H	2.02022662390560	1.61071883385925	6.52610697759298
O	2.96893745148233	1.89097793668640	6.53270141278641
H	3.46651391101543	1.18701473735838	6.96644771638755
O	0.42577087333626	1.14091051095231	6.03964913250598
H	-1.38706603587570	-0.33332679124790	5.06784072798084
H	-1.42259155845969	0.03648057641015	3.57154812044176
O	-1.53010332896622	-0.71601301679098	4.19637187594223
O	1.63672396396541	-0.90470179219838	4.59545557925673
O	0.44457772191030	4.37898699953609	2.34668636367730
O	2.79863227420951	0.27743522671162	2.53606570827084
O	-0.49594124662434	-3.49532413926587	2.81849465286807
H	3.55158038528476	4.09600557864704	2.43878788918946
H	2.26327503709296	4.90696663596764	2.34261572170888
H	0.11045588537308	1.75169937898962	5.34171160625824
H	-0.24367460102047	1.13116780255711	6.73241189363457
H	2.11774678151430	-0.38612989590337	3.90415756756977
H	1.18320809421640	-0.24882991549725	5.15943894941861

Table C-11 *XYZ atomic coordinates for Cu(II)- TC-Carboxylate structure with N-Cu-O binding using PBE0-D3(BJ) with a neutral charge and multiplicity of 4*

C	0.90899306227197	2.55268603410098	-1.95643229607737
C	0.40784677415261	1.14175098227540	-1.86166922373465
C	1.30149484225072	0.06109763570345	-1.89578815642417

C	0.83497330975229	-1.25459531237975	-1.79476273772457
C	-0.54362171939048	-1.47590591850045	-1.67179856697264
C	-1.44699763862545	-0.41124287879707	-1.61765528520340
C	-0.95584131152624	0.89600368288463	-1.68792204452616
C	-1.89036233814147	2.05501097066735	-1.47653905025384
N	-1.54048990119973	2.79449515996272	-0.25997767060387
N	-1.01509690864002	2.16667234400806	0.77573743753613
N	-0.78991656804616	3.07777626156910	1.66279261163193
C	-1.16569390835164	4.29565708587688	1.22344599310013
C	-1.66349578433053	4.11653576964800	-0.04043263641119
C	-0.89910522592646	5.44392936919817	2.13082190935026
O	-0.25607115247737	5.09865234726386	3.19276247142671
C	-2.91885412782526	-0.65223132467941	-1.44161554939725
C	-1.05150539439679	-2.87907094697818	-1.47269765596461
N	-1.46657047355038	-3.07367112660858	-0.08073068277780
N	-0.68177210997422	-2.65229005529992	0.89532803525765
N	-1.31667432069181	-2.90205747404957	1.98973262788060
C	-2.51079368630427	-3.48135210426373	1.74711889295832
C	-2.61254615769938	-3.60179094739303	0.38548785899804
C	-3.37566072480808	-3.75593262583623	2.92686441369398
O	-2.86737459998676	-3.32380370418402	4.03083145683951
C	1.76443172121538	-2.43642360798359	-1.78159781664565
C	2.77639625263761	0.35624006105221	-1.93374194738879
N	3.27852802396456	0.68524645507312	-0.59741812134769
N	3.82560369097332	1.86625888981077	-0.36381681599294
N	4.16008439704509	1.86225597886731	0.88393232917892
C	3.83809604888083	0.69132427520127	1.47183546589988
C	3.25419021377405	-0.08491501187978	0.50752121843673
C	4.18879703909951	0.53888377203344	2.90860574014299
O	4.75714241325904	1.58454415432486	3.39528534985394
H	1.74906946053448	2.64113303483562	-2.64348964413760
H	0.13823756737489	3.23269365922517	-2.31356649560290
H	1.24971682051702	2.92212419910821	-0.98397791528562
H	-1.85441697971954	2.77807204361625	-2.29195795281628

H	-2.92257164092795	1.73419830267094	-1.37000737963795
H	-2.05717396552839	4.79563142539685	-0.77813694868931
H	-3.23080726939036	-0.44047733012474	-0.41385379352472
H	-3.50817976600982	-0.01674986341950	-2.10293591757168
H	-3.20502344180620	-1.67635422923426	-1.66363230705644
H	-1.92164884350734	-3.10137581439920	-2.08728365629824
H	-0.29851990177940	-3.62872908010308	-1.69881998992158
H	-3.38369326003500	-3.98537659424133	-0.26176984640534
H	1.63659515196751	-3.01643271843095	-0.86432192350697
H	1.56083083206125	-3.10364891926851	-2.62245531343775
H	2.81340161002750	-2.16364275231194	-1.83987134069947
H	3.36509913702496	-0.47517247802338	-2.30967903562219
H	3.01161066273523	1.21834210506415	-2.55117591192251
H	2.84334002794618	-1.07977863587642	0.52785960815113
Cu	4.92702494594696	3.11871364274074	2.20034509115946
Cu	-1.12658469229896	-2.50240063840902	3.89231258979642
Cu	0.23657636793910	3.22562971584457	3.33234189338366
N	2.55079386649035	3.86070421577489	4.45560492981009
O	1.39977943131284	3.58755118161729	4.91560005377205
O	3.45689223235241	4.10888068171463	5.23711548511374
O	2.69996352663849	3.86033271318659	3.22820062259409
N	5.41790222304082	5.75404501637718	0.92767804696754
O	5.39218128200126	6.44331459046938	-0.07094234188623
O	5.70326662859604	6.21941720938371	2.03817724786758
O	5.14132006324856	4.51259421295261	0.80374817506360
N	0.53417953354373	-1.83462941830822	5.50520625912771
O	1.35082415311343	-1.47546253964749	6.30132829826585
O	-0.64669465499725	-2.16646057234174	5.82821184082825
O	0.76941421510228	-1.91240954054544	4.26116241188558
O	-1.26612961914592	6.57443547424340	1.85372241937708
O	3.94998184246778	-0.49349699964964	3.51613350129668
O	-4.44874773308399	-4.32455139546868	2.81128800566000
O	-1.64190579636143	-0.18739498380873	3.53065478841199
H	-2.09552816916076	-0.07506348009763	2.68486573036770

H	-2.25391128401965	0.15192046883324	4.19640404836611
O	0.62216902727285	1.28930935038461	3.47193356711345
H	-0.19591063709360	0.73396607576097	3.50661811317038
H	1.15607062850620	1.04824525679199	4.23889833270474
O	5.73129842604779	4.16134780167894	3.66387372995515
H	5.78515734620689	5.05926438126430	3.25652325032621
H	5.03766690746387	4.20775303408503	4.35534211874686

Table C-12 *XYZ atomic coordinates for Cu(I)- TC-Carboxylate structure with N-Cu-O binding using PBE0-D3(BJ) with a neutral charge and multiplicity of 3*

C	0.87326596230623	2.49069687047325	-2.47346463442329
C	0.34621908655193	1.11224696501766	-2.19969289805348
C	1.22305326479639	0.01784408705598	-2.14700549473654
C	0.73389863129644	-1.27876259957456	-1.96266584770508
C	-0.64122948312183	-1.45949397238009	-1.74985730437397
C	-1.51841900063386	-0.37115093680417	-1.72622177496140
C	-1.01309424628631	0.91622741633899	-1.95060208256832
C	-1.89899532619644	2.12262682673290	-1.73116161822995
N	-1.47592894745509	2.83723126263899	-0.54199926921332
N	-1.24645092875103	2.10703961599946	0.60190094080404
N	-0.61384665104986	2.98276998071814	1.43854671951282
C	-0.45218472359707	4.20131490730103	0.80371137799784
C	-1.00040727564452	4.08929616653794	-0.44209336799980
C	0.31682465802763	5.20640571177658	1.50190769941423
O	0.77899453839756	4.76032184110136	2.65810857238818
C	-2.97819931130261	-0.55085052028154	-1.41795196874295
C	-1.13793282499903	-2.83230914086462	-1.38061902691736
N	-1.25794979529694	-2.95536818782127	0.07431843110020
N	-0.24693327951720	-2.58991120854524	0.84694344729914
N	-0.62941203045170	-2.78344452520949	2.07007401653422
C	-1.88859411202639	-3.27365634114152	2.10592991355731
C	-2.30163006520505	-3.39047237909574	0.80197125895470
C	-2.54578473036931	-3.52659646758281	3.42889751176436
O	-1.84606287830364	-3.20868137636690	4.43041802473160

C	1.63959324534892	-2.47987708955849	-1.95650418517289
C	2.70283065420036	0.29766011222950	-2.07646054159253
N	3.05705812579219	0.62127104787613	-0.69178694778053
N	3.40299347086011	1.85824791686273	-0.35725493880842
N	3.53291044236478	1.87485932582572	0.93386145961934
C	3.27417324557772	0.64648476174671	1.44650756354527
C	2.96113804036672	-0.16872050200785	0.38915657385160
C	3.29788276823554	0.37995123210157	2.90978246144294
O	3.50555335347754	1.37222152359383	3.65492328457049
H	1.68159421434371	2.46879225956513	-3.20393520803544
H	0.10013630219338	3.14098068938613	-2.87679797429564
H	1.26415854718667	2.96460989148041	-1.56897844386451
H	-1.86302520973101	2.82851111933032	-2.56086920555069
H	-2.93866609809360	1.82666545515272	-1.60662605816142
H	-1.05709621007037	4.78855157460761	-1.26071497300525
H	-3.21616907571762	-0.15013649402104	-0.42846809959150
H	-3.60310699627240	-0.02596620455153	-2.14223396430800
H	-3.28816358394219	-1.59164177827981	-1.42978195732593
H	-2.11861272524182	-3.05578894334234	-1.79203244709707
H	-0.46267289305276	-3.61313860576293	-1.72083061426477
H	-3.22204455483100	-3.72562140628184	0.35385589176294
H	1.61228502984533	-2.98952991400261	-0.99043952190157
H	1.32517845179333	-3.20109286644743	-2.71469569021482
H	2.67593875023011	-2.23540706569838	-2.16742282020203
H	3.31889540565900	-0.53957527636817	-2.38934391619218
H	3.00204269865988	1.16008392884245	-2.66441004547869
H	2.67634133373590	-1.20557591020956	0.34195269173151
Cu	3.91965949329925	3.35757925865150	2.09859016451857
Cu	0.15859884625068	-2.37976912695030	3.79056350766514
Cu	0.37071999080663	2.87855951984119	3.05185103693852
H	-0.10449804525148	0.80482280916748	4.43935952474367
O	-0.10424246680267	1.00111188157981	3.49611469334223
H	-0.98122259131560	0.68831124878717	3.11572857224428
O	1.58294781944321	2.80946978452157	4.62699638675557

H	-3.09623542733853	0.61325804053997	2.66637860139769
O	-2.28148901359087	0.30769683840650	2.25535657465978
H	-2.08239774897190	0.95214139215798	1.51561836989083
O	3.34547805342195	5.07396148490511	2.97617293337279
H	6.42472496309398	2.78309175303281	2.98513851173757
H	5.99717158012051	4.08161426063166	3.66912045394450
O	6.01600111808198	3.63856158807705	2.81338983588956
O	1.52163875436257	-1.77117882666402	5.04369796900394
O	0.55322324057794	6.34244079532061	1.08788327367149
O	3.10879009026443	-0.79910600577958	3.26624623708237
O	-3.68848223652139	-4.00508456377250	3.42674038032179
H	1.94074989535708	3.66848567711484	4.87957690822638
H	2.35582878489362	5.11387754712248	2.85663421707128
H	3.70909723982568	5.86351008035468	2.56188324350424
H	2.36183702243899	2.24800292615036	4.34162773131699
H	2.20262591526286	-1.29055853902261	4.48669013045603
H	1.20427645820394	-1.15252660226754	5.70986474243094